Springer Link

Micro-endoscopy for Live Small Animal Fluorescent Imaging

Advanced Imaging and Bio Techniques for Convergence Science pp 153-186 | Cite as

- Bjorn Paulson (1)
- Jun Ki Kim (2) Email author (kim@amc.seoul.kr)

1. Biomedical Engineering Research Center, Asan Institute for Life Sciences, Asan Medical Center, , Seoul, Republic of Korea
2. Department of Convergence Medicine University of Ulsan College of Medicine, Asan Institute for Life Sciences, Asan Medical Center, , Seoul, Korea (Republic of)

Chapter
First Online: 09 April 2021

- 3 Downloads

Part of the Advances in Experimental Medicine and Biology book series (AEMB, volume 1310)

Abstract

Intravital microscopy has emerged as a powerful technique for the fluorescent visualization of cellular- and subcellular-level biological processes in vivo. However, the size of objective lenses used in standard microscopes currently makes it difficult to access internal organs with minimal invasiveness in small animal models, such as mice. Here we describe front- and side-view designs for small-diameter endoscopes based on gradient-index lenses, their construction, their integration into laser scanning confocal microscopy platforms, and their applications for in vivo imaging of fluorescent cells and microvasculature in various organs, including the kidney, bladder, heart, brain, and gastrointestinal tracts, with a focus on the new techniques developed for each imaging application. The combination of novel fluorescence techniques with these powerful imaging methods promises to continue providing novel insights into a variety of diseases.

Keywords

Intravital imaging Endoscope Microscopy Fluorescence Mouse imaging

Download chapter PDF

Introduction

Small animal disease models are widely used for the targeted observation of interactive cellular processes in the study of inflammatory disorders, cancers, neural processes, and infectious diseases. Mouse models, in particular, are highly valuable in vivo models of human disease, with similar cardiovascular and immune systems to those of humans, and recently a large variety of genetically engineered mouse models have become available at low cost (Jung et al. 2013). Of particular interest is the development of the many transgenic mouse strains expressing cells tagged with fluorescent proteins such as eGFP and RFP, which express fluorescence upon illumination of specific cell types. These mice allow for the cellular-level analysis of tissues and tumors on the basis of optical fluorescence techniques (Kim et al. 2012a).

In tandem with the development and analysis of these transgenic mouse models, many sophisticated diagnostic systems have been developed for the analysis of these transgenic mouse models. However, trade-offs exist between granularity of the available data in the spatial domain, granularity in the time domain, and spatial extent of the data. At the level of whole-body analysis, common radiological imaging modalities such as computed tomography and magnetic resonance imaging are available, as well as whole-body fluorescence imaging for mice, but due to their spatial extent, these do not provide data at cellular resolution. At the other extreme, in vitro culture and imaging systems (Rock et al. 2009; You et al. 2002) provide cellular resolution, but many elements that influence the development of pathologies at the cellular level are difficult or impossible to mimic in vitro, such as intercellular signaling cascades, innervation, cellular trafficking, and immune response. Ex vivo histology also provides information about cellular processes; however, the static and sacrificial nature of the imaging increases the cost to attain information about dynamic processes, including cellular trafficking and differentiation (Jung et al. 2013; Kim et al. 2012a, b; Miller 2002; Fan et al. 2010; Fujisaki et al. 2011).

The fluorescence micro-endoscopy technique has been introduced to overcome the limitations of these imaging modalities, combining the high cellular resolution (Ryu et al. 2018) and sensitivity of fluorescence microscopy to monitor epithelial pathologies in vivo, longitudinally, and with minimal invasiveness (Kim et al. 2012a, b; Ryu et al. 2018; Jun et al. 2018; Flusberg et al. 2005; Choi et al. 2014). To date, intravital fluorescence microscopy has been applied for the imaging of diverse cellular targets, from transplanted stem cells (Ryu et al. 2018) and tumor xenografts to immune response and individual neurons in vivo (Jung et al. 2013; Miller 2002; Fan et al. 2010; Fujisaki et al. 2011; Pittet and Weissleder 2011), and also to image cellular processes, including gene expression, cell activation, intercellular interactions, vascular changes, and cell trafficking (Kim et al. 2012a, b), to provide data and discoveries which cannot be easily acquired from other diagnostic modalities, and allows precise inference of the cellular mechanisms behind the pathologies under study (Kim et al. 2012a).

Recent advances in micro-optic and fiber-optic technologies have led to the commercialization of several micro-endoscopic probes from suppliers including Karl Storz (Becker et al. 2007), Mauna Kea Technologies (Hsiung et al. 2008), and Olympus (Dela Cruz et al. 2010), each with their own strengths and limitations. MicroProbe Objectives from Olympus are standard microscope objectives which offer an extension of the imaging plane into tissue via a long (20–25 mm), narrow diameter (1.3–3.5 mm) "stick," and offer high-quality correction for chromatic aberrations, at the expense of a fixed focal plane of the objective and a large overall footprint which restricts tissue access in larger animals (Dela Cruz et al. 2010). The Coloview® endo-microscope from Karl Storz is optimized for small animal colonoscopy, with probes of 10 cm length and narrow diameter (1.9 mm) suitable for tracking tumor progression in the colon on a macroscopic scale (Kim et al. 2012a). Finally, the Cellvizio® probe family by Mauna Kea offers exceptionally miniaturized front-facing probes based on a variety of technologies: microlenses, optical fiber bundles, and gradient index lenses, with diameters ranging from 0.3 to 1.8 mm, field depth from 10 to 60 microns, and resolutions down to 1.4 microns, for a variety of small animal experiments. Herein, we present an alternative, custom-built solution, rigid probes based on gradient index lenses which enable cellular resolution imaging of tissues, optical sectioning, and high stability (Köhler et al. 2018). A side-view extension prism allows a 90° rotation of the imaging path for side-view imaging of luminal organs at cellular resolution. Probes are available with diameters from 0.35 to 1 mm, and maybe fabricated for a range of lengths (20–100 mm) and numerical apertures (NA; 0.4–0.6) (Kim et al. 2012a).

Although several designs have been introduced for the development of flexible micro-endoscopes for human patients, including micro-endoscopes based on coherent fiber bundles (Göbel et al. 2004; Yang et al. 2005), scanning optical fibers (Wu et al. 2009; Lee et al. 2010; Kim et al. 2019), and micro-endoscopes based on chip-on-tip technology (Matz et al. 2017), the need for a flexible probe is less pronounced in small animal micro-endoscopy, since in the small animal disease model it is often more convenient to operate around curved organs than to navigate through their curves, especially in consideration of the fact that those curves are much sharper than in human anatomy. The remainder of this review will concern itself with rigid micro-endoscopic probes built on the recently developed gradient-index (GRIN, also referred to as "graded index") lenses (Kim et al. 2012a).

Geometry and Key Design Parameters for GRIN Probes

Before beginning the manufacture or acquisition of an optical probe, it is recommended to ascertain the optimal design based on the precise organs and tissues for which imaging is desired: the design will vary with practical considerations, such as the target tissue orientation and location relative to the point of entry, the size of the entry point, the desired field of view (FOV), and the desired resolution (Kim et al. 2012a).

Once requirements are specified, the geometry of a GRIN endoscope probe is defined primarily by the GRIN lenses which comprise the probe. These (typically three) lenses are commonly referred to as the coupling lens (CL), the imaging lens (IL), and the relay lens (RL). The CL and IL are high-numerical-aperture (NA) lenses that respectively collimate the input beam with respect to a microscope (or similar assembly) and convey the distal image into the probe. The relay lens (RL) is a longer lens of lower numerical aperture, which connects between the two to extend the beam path and probe length (Kim et al. 2012a).

The probe geometry is also determined by the viewing direction: whether the probe is to observe the target tissue in front or side view. The light propagation and schematic geometries of front-view and side-view GRIN probes are shown in Fig. 1 (Kim et al. 2012a; Jung and Schnitzer 2003). In addition to these three lenses, side-view GRIN micro-endoscopes have a prism mirror affixed to the distal end of the imaging lens. Normally, the front-view probe finds application in the imaging of convex organs or organs in large cavities that can touch the probe tip, such as the pancreas, lymph nodes, kidneys, bladder wall, liver, and heart. Tubular structures, as are found in the epithelium of gastrointestinal and respiratory tracts, are more suitable for imaging by the side-view probe (Kim et al. 2012a).

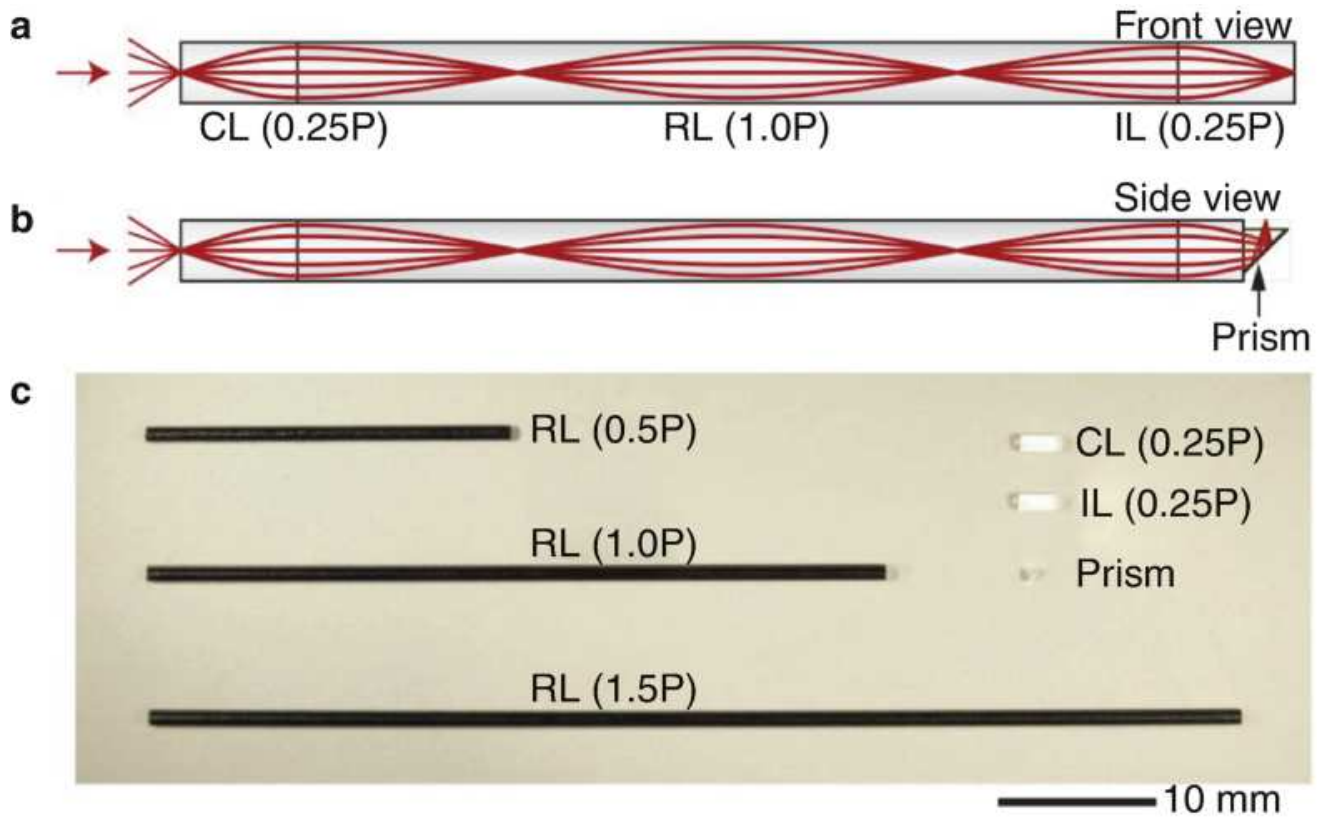

Fig. 1

Schematic and manifestation of gradient index (GRIN) optical probes. (**a**) front- and (**b**) side-view schematics and (**c**) photograph of micro-endoscope probes formed with GRIN collimating lenses (CL), relay lenses (RL), and imaging lenses (IL). The side-view micro-endoscope probe has a prism affixed to the distal end of the

imaging lens. Red lines denote a traced optical ray. Reproduced with permission from Kim et al. (2012a), © 2012 Springer Nature

For gradient index lenses, the length of the lenses is measured in pitch: In forward-view probes, the appropriate lengths for the coupling lens and the imaging lenses are measured in units of pitch: one pitch is the length at which a ray of light passing through the lens will trace out a full sinusoidal path due to the refractive index gradient. The appropriate lengths for the coupling lens and the imaging lenses are 0.25 pitch and 0.23–0.25 pitch, respectively. While the coupling lens serves to collimate the input beam, the imaging lens should focus on the object plane just past the distal end of the probe (Kim et al. 2012a).

For side-view probes, shortening the IL to a pitch of 0.16–0.17 will extend the working distance such that the object plane lies just past the distal end of the prism. This may be achieved either by ordering a custom IL or by polishing down an existing IL. The ideal prism is a glass or quartz cube with the distal end polished at 45° or to reflect light at the desired angle. A metal coating on the polished face results in a second surface mirror. Prisms with edge lengths less than the lens diameter will fit well in stainless steel sheaths or needles used for protecting the optical assembly (Kim et al. 2012a).

For GRIN probes of this design, the field of view (FOV) is proportional to the probe diameter multiplied by the ratio of the relay lens NA to the image lens NA, and thus the diameter should balance the desired FOV with experimental invasiveness. Commercially available GRIN lenses range in diameter from 0.35 to 2 mm but benefit from protective metal sheaths of an additional 0.20–0.30 mm in outer diameter. Although in practice, FOV is limited by GRIN NA to about one-fourth the diameter of the GRIN lens, compositing sequential images from a wider area may overcome this restriction (Kim et al. 2012a).

The length of the probe may be tailored to the application by extending the relay lens in multiples of half the relay lens pitch (Fig. 1c). (Odd multiples of half-pitch result in image inversion.) With increased pitch, optical aberrations (primarily chromatic and spherical) accumulate, resulting in degraded spatial resolution, and the limited stiffness of the probe results in a risk of probe damage due to bending. A length of 20–30 mm is suitable for imaging of the abdominal cavity in mice, as is a length of 60–100 mm for imaging of the gastrointestinal tract (Kim et al. 2012a).

The theoretical aberrations of the GRIN lenses have been calculated (Krishna and Sharma 1996; del Río et al. 2015; Bociort 1994); however, the spherical wavefront error depends on the ion-exchange chemistry of the GRIN fabrication process (Barretto et al. 2009). For this GRIN probe design and ignoring aberrations, the limit of spatial resolution for wavelength λ and imaging lens numerical aperture NA_I is given by $0.6\,\lambda/NA_I$ in the transverse direction and $1.1\,\lambda/NA_I^{\,2}$ in the axial direction (Kim et al. 2012a).

The imaging penetration depth by GRIN probes is limited to that of the optical modality, which is in turn bounded by scattering from tissue at the wavelengths used. For confocal fluorescence microscopy in the visible region, the optical penetration depth is restricted to about 100 μm in the majority of soft tissues. GRIN probes are also commonly used in a two-photon fluorescence modality for optogenetics, where they demonstrate penetration depths 2–3 times higher (Kobat et al. 2011), and with new light sources in the 1300 and 1800 nm infrared bands and three-photon processes, penetration depths be improved to the order of millimeters (Smith et al. 2009).

Thus, naive imaging with confocal fluorescent GRIN probes is limited to the dermis, epithelium, or mucosa. By physically injecting the probe into the target tissues, deeper features may be observed in the visible region, while minimizing trauma to surrounding regions (Barretto et al. 2011). Careful planning of surgeries and the incorporation of supplementary technologies such as needles and cannula (to be introduced later in this review) may also mechanically strengthen the probe while reducing surgical trauma (Kim et al. 2010a, 2012a; Barretto et al. 2011).

Fabrication of GRIN Probes

The fabrication of GRIN micro-endoscope probes from GRIN lenses requires some skill in optical polishing and assembly or maybe contracted from a commercial vendor such as GRINTECH GmbH. A suitably equipped laboratory should have two stereoscopes, tweezers, a UV light source and a hotplate for curing thermal epoxies, and a lapping surface and jig for the polishing of lenses. The fabrication process begins with the polishing of the GRIN lens. A lapping tool with an incorporated jig may be used to gently apply steady pressure to the lens while ensuring that the polishing is perpendicular to the axis of the lens.

Completed IL and CL lenses are gently adhered to relay lenses using transparent and nonfluorescent UV-curing optical polymer of matched refractive index, which minimizes back-reflections and aberrations at the surface between GRIN lenses. For mechanical stability as well as protection from stray light and moisture, the finalized assembles should be immobilized within a protective stainless steel sheath by heat-sensitive epoxies of high mechanical strength. In Fig. 2a, b, we show typical setups for the lapping and adherence of these processes, and in Fig. 2c–e, we demonstrate the assembly procedure for a front-view probe, with illustrations made at representative steps. Similar steps, with the addition of prism placement onto the IL and heat treatment of the sheathed probe, are depicted for the side-view probe in Fig. 2f–k (Kim et al. 2012a). The protective stainless steel sheaths are available in bulk as tubes of varying quality from a variety of high-gauge medical needle suppliers. A completed probe for side-view micro-endoscopy is shown in Fig. 2i.

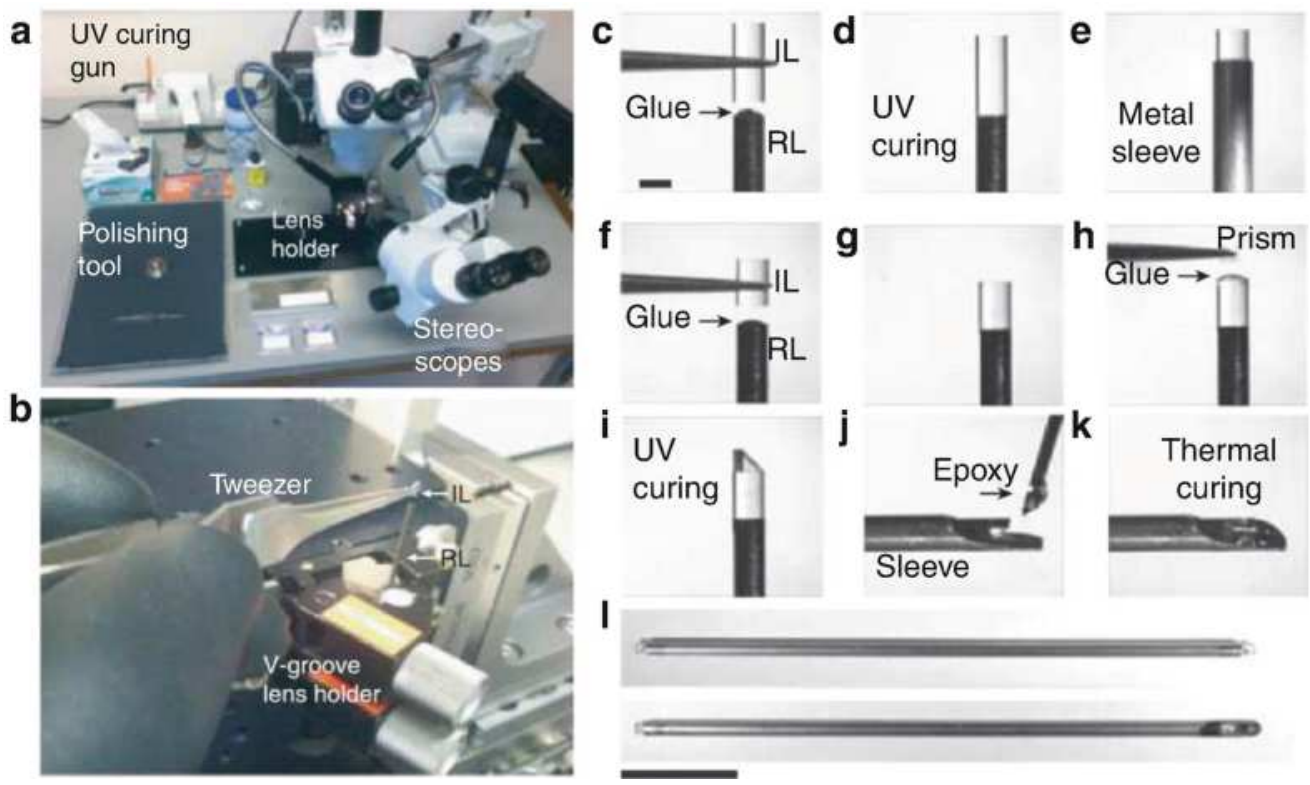

Fig. 2

Assembly of GRIN micro-endoscope probes. Reproduced with permission from Kim et al. (2012a), © 2012 Springer Nature

Imaging from the GRIN Endo-microscope Probes

For high-quality image capture, the manufactured GRIN optical probes should be integrated into a digital imaging system. High magnifications are not provided by the probe itself, and so it is easier to integrate the endo-microscopic probes with a preexisting or commodity microscope system than to develop a fully customized imaging solution. As shown in Fig. 3 for front-view probes, a mechanical probe mount and lens relay may be assembled to extend the image plane of a confocal microscope to the proximal end of the micro-endoscope probe.

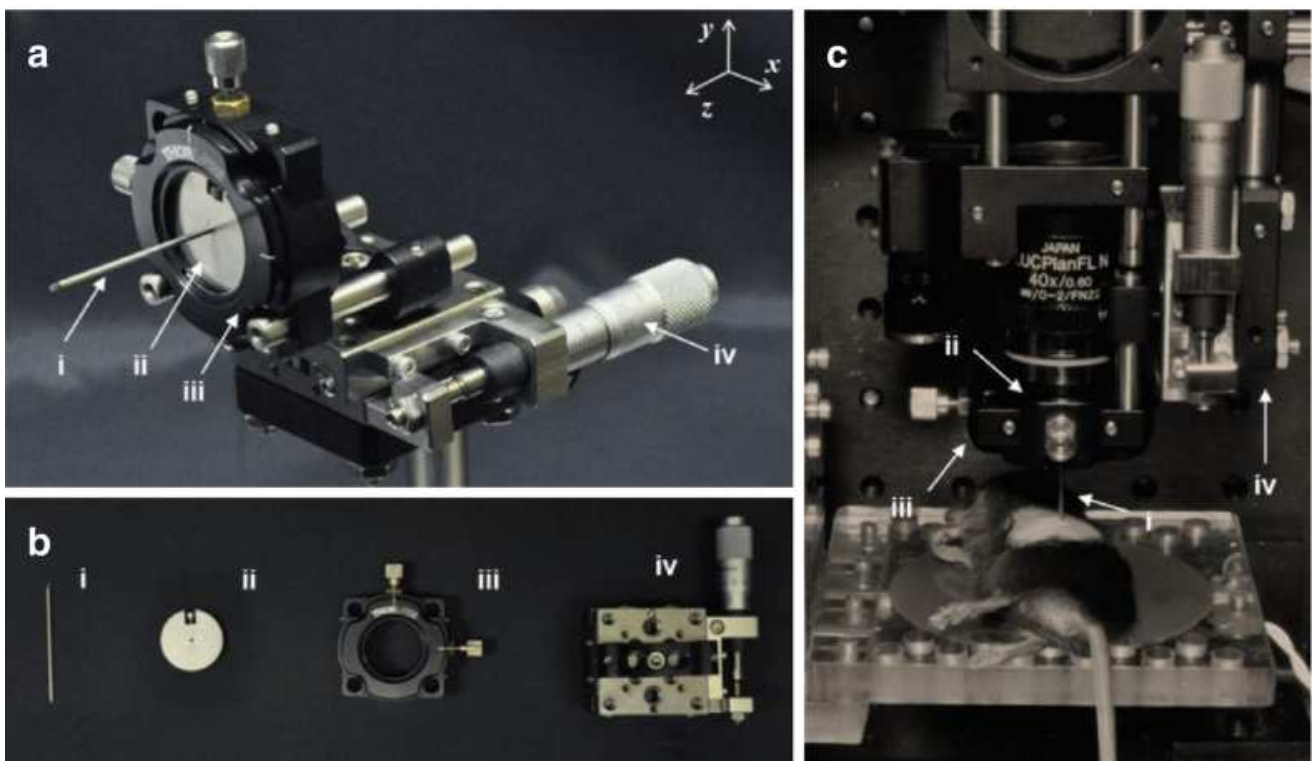

Fig. 3

Assembly for mounting a front-view probe to a confocal microscope. (**a**) Probe mount. (**b**) Individual components. (**c**) The complete assembly, applied for front-view imaging of a mouse model. Adapted with permission from Kim et al. (2012a), © 2012 Springer Nature

The mechanical mount should guarantee probe stability relative to an objective, as well as fine control of the probe position. Control of the probe is required with single-micron precision perpendicular to the beam path, while in the axial direction equivalent precision should be offered in movement of the microscope objective. For the side-view probe, the ability to rotate the probe 360° with 5° precision and to center the probe with respect to the axis of rotation are required (Kim et al. 2012a). These abilities may be combined into a unified probe mount and relay mount (Kohler et al. 2008).

Applications of GRIN Micro-endoscopes

A. Front-View GRIN Micro-endoscope Applications

Although miniature optical probes offer the benefit of being easily manufactured by the small laboratory, using tools and supplies currently on the market, they are more impressive for their many applications to minimally invasive, cellular resolution imaging in small animal disease models (Fan et al. 2010; Kim et al. 2010a). For the majority of in vivo organs, such as the kidneys (Fan et al. 2010), bladder, and heart, fluorescence cellular imaging is enabled by endo-microscopy systems which incorporate front-view endoscope probes. Side-view probes are well-suited for observing into the folds of the epithelium of tubular tissues as are commonly found in the gastrointestinal and respiratory tracts (Kim et al. 2010a), and will be discussed in the next section.

Longitudinal Renal Imaging with Forward-View GRIN Endoscopes

Through minimally invasive endoscopic microscopy methods, repeated imaging and longitudinal observation become feasible at the cellular scale. As an example of these possibilities, the authors report the observation of cellular motility and longitudinal cellular-resolution tracking of immune response in mouse models of renal transplantation (Kim et al. 2012a; Miyajima et al. 2011). As shown in Fig. 4, over a time-scale of 6 minutes, FoxP3-GFP$^+$ T cells (green) were observed to migrate from the recipient mouse into kidney tissues allotransplanted from a wild-type donor mouse (red autofluorescence). Quantitative analyses of dynamic processes, such as the counting and tracking of individual cells (“Track”) are demonstrated in these in vivo measurements (Kim et al. 2012a).

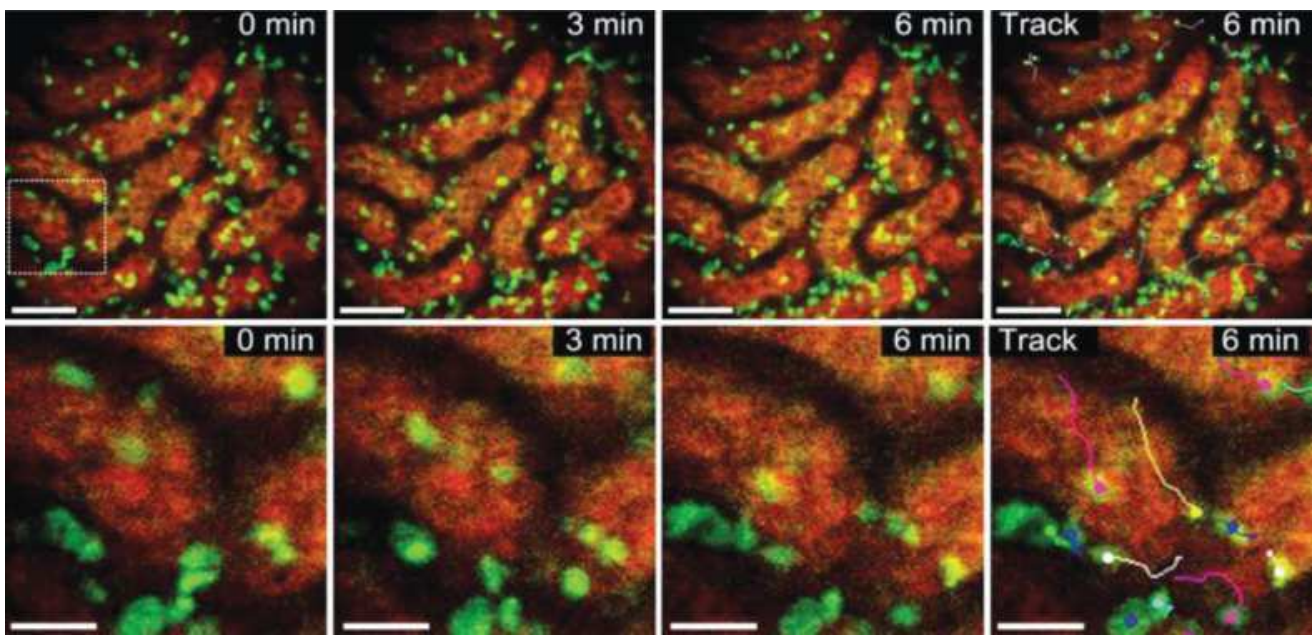

Fig. 4

Micro-endoscopic observations of immune motility in kidney graft allotransplanted from a wild-type donor into a transgenic mouse with FoxP3-GFP$^+$ fluorescent T cells. Green depicts FoxP3-GFP fluorescence while red is autofluorescent kidney capsules. (Bottom) Magnified images of the region shown in the box in the first pane. (Track) Overlaid tracks of individual T cells from time-series images taken every 20 s. Scale bars are 50 μm in the top panels and 20 μm in the lower panels. Reproduced with permission from Kim et al. (2012a), © 2012 Springer Nature

In Fig. 5, a BALB/C wild-type mouse was allografted with a donor kidney from a C57BL/6 mouse with a knock-in MHC class II gene which codes for an eGFP-tagged class II molecule. A front-view GRIN endo-microscope was used repeatedly to observe the fluorescent GFP antigen-presenting cells (APC) from the donor mouse. The renal tissues expressed relatively intense autofluorescence, which reveals kidney nephrons in the cortex. One day after transplantation, a large number of fluorescent dendritic donor APCs are seen (Fig. 5a). After 3 days, most dendritic GFP$^+$ cells had migrated to renal capsules, demonstrating the process of clearance (Fig. 5b). Such repeated imaging and longitudinal imaging would not be directly feasible in more highly invasive observational methods, such as fixed tissue histology.

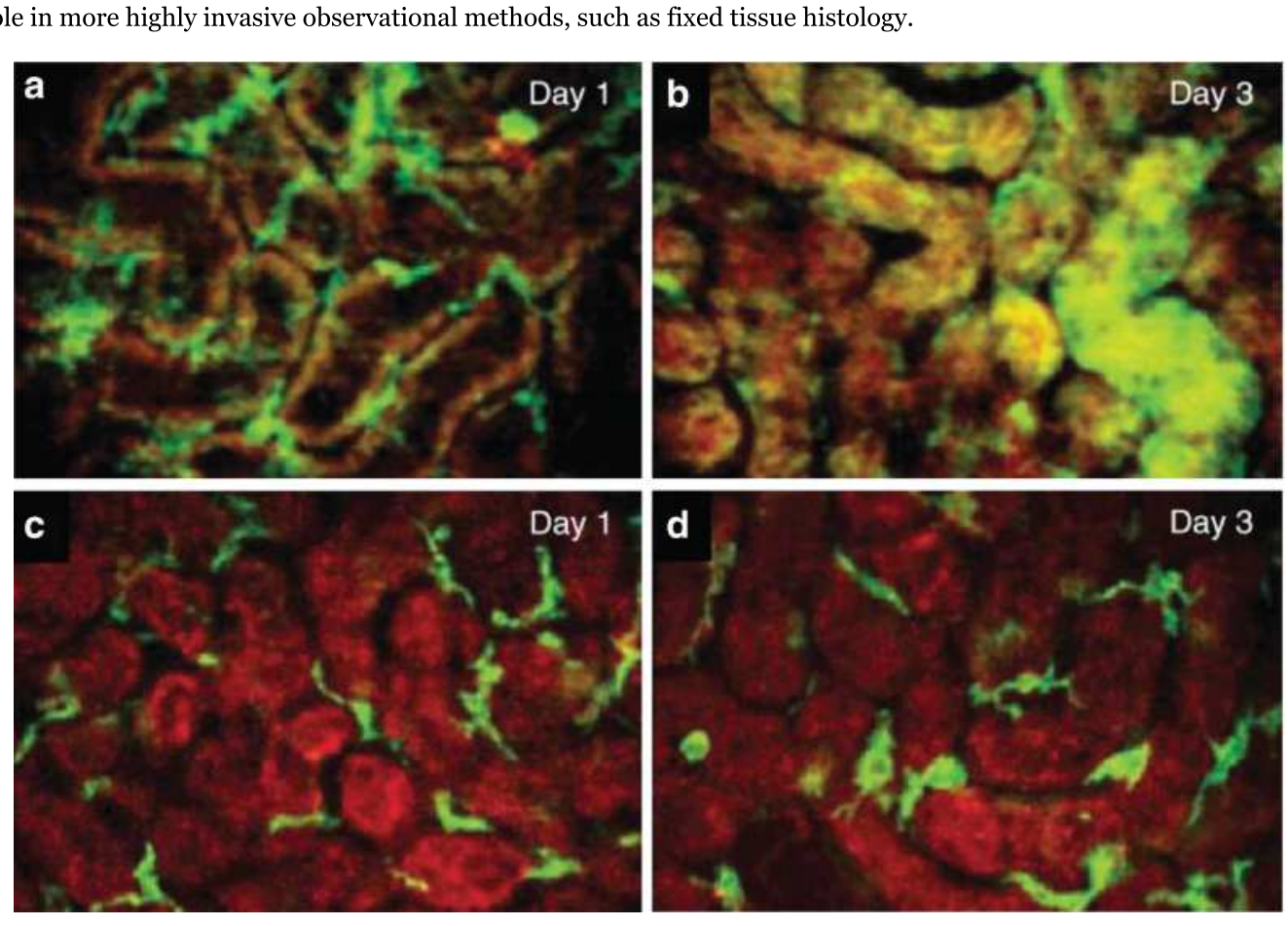

Fig. 5

Longitudinal observations of kidney allografts by front-view GRIN endo-microprobes. Fluorescent MHCII$^+$ cells are in green, while red expresses autofluorescence due to renal tubules. (**a**, **b**) Donor fluorescent cells in kidney graft (**a**) 1 and (**b**) 3 days following transplantation. (**c**, **d**) Controls following sham surgery. Scale bar, 100 μm. Reproduced with permission from Kim et al. (2012a), © 2012 Springer Nature

Synergistic GRIN Micro-endoscopy in Urologic Applications

Small-diameter endoscopic imaging has also been combined with intravital confocal microscopy to enable longitudinal observation of cellular migration in the bladder wall in mouse models of interstitial cystitis/bladder pain syndrome (IC/BPS). This section is adapted from a recently published study (Ryu et al. 2018) in which microscopic imaging was combined with intravital GRIN micro-cystoscopy to track the development of a preclinical stem-cell treatment of IC/BPS (Fig. 6).

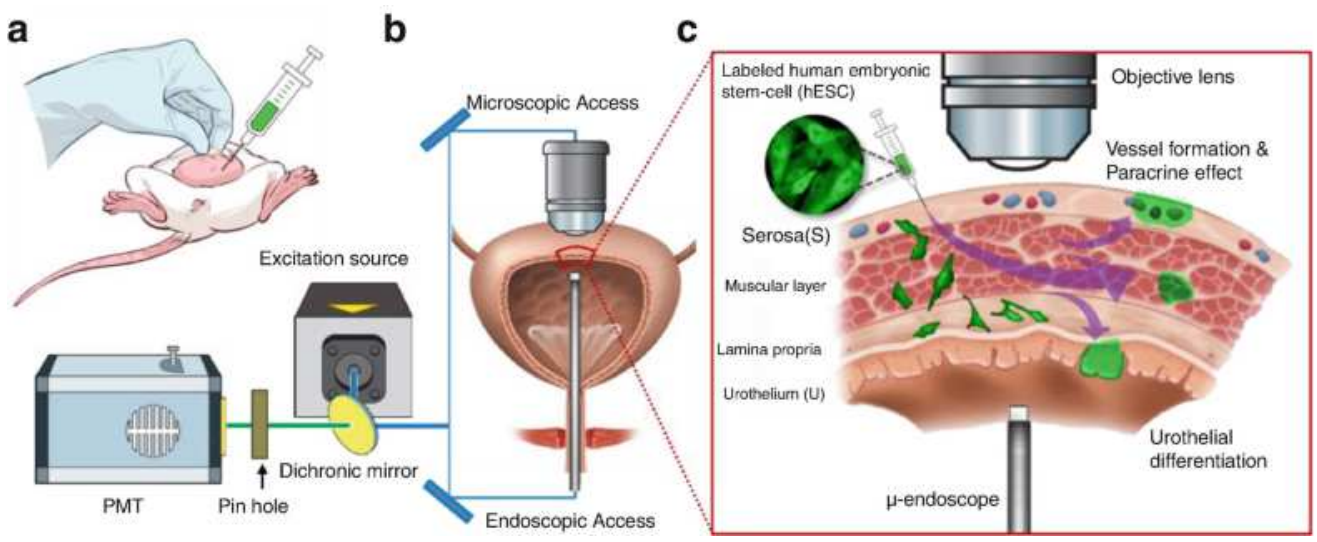

Fig. 6

Longitudinal synergy of microscope and micro-endoscope imaging of transplanted stem cells in a rat model of IC/BPS. (**a**) Injection of hESC-derived M-MSCs into the bladder wall. (**b**, **c**) Synergistic confocal monitoring of transplanted cell migration and observed repair of the denuded urothelial wall. Stem cells are observed to travel from the serosa to the lamina propria and urothelium, where they repair the urothelial wall. Reproduced under CC BY-NC 4.0 license from Ryu et al. (2018), © 2018 Ivyspring International Publishers

Interstitial cystitis/bladder pain syndrome (IC/BPS) is a bladder disorder characterized by chronic inflammation of the bladder epithelium (Propert et al. 2000), resulting in suprapubic pain that is intensified by bladder filling, resulting in urinary frequency, urinary urgency, and reduced quality of life. With unknown causes and no effective treatment (Oravisto 1975), stem cell therapy is one of the few potential treatments (Kim et al. 2016a, b; Song et al. 2015). However, cells did not engraft well in vivo, and undetermined issues remained in assessing their functional integration and the mechanism of treatment. A combination of intravital confocal microscopy and in vivo endo-microscopy was used to image the bladder wall following stem cell treatment, synergizing data from multiple imaging modalities to assess the longitudinal outcome of these treatments in a preclinical mouse model of IC/BPS (Ryu et al. 2018). Previous reports on MSCs have demonstrated beneficial effects on IC/BPS and ketamine-induced cystitis; however, the MSC cells from previous studies (Song et al. 2015; Kim et al. 2016b) were short-lived and were not able to directly repair damaged tissues. As they did not repair (Liang et al. 2014; Cosenza et al. 2018; Vonk et al. 2018; Wang et al. 2014), MSC-based therapies are still controversial issues (Ryu et al. 2018).

A mouse model of IC/BPS was established by instilling endotoxins into the bladders of female rats weekly for 5 weeks to induce realistic tissue inflammation and chronic urothelial damage (Stein et al. 1996; Birder and Andersson 2018), while a sham group was treated identically with phosphate-buffered saline (PBS). M-mesenchymal stem cells (M-MSCs) were derived from human embryonic stem cells (hESCs) and established with green fluorescence by transfection of a GFP expressing lentivirus (Kim et al. 2018). Compared to other stem cells, hESCs expanding many times and differentiating into therapeutic cells in vitro. They also exhibit high survival, engraftment, and functionality when transplanted in vivo (Kim et al. 2016c). Previous grafts have remained until 6 months post transplantation in an alternative animal model of IC/BPS (Kim et al. 2017).

Fluorescence was confirmed to be stable through long-term (5 week) cultivation and multi-lineage differentiation. M-MSCs were expanded for fewer than ten generations to make sure they maintained multipotency (Ryu et al. 2018; Kim et al. 2016c; Hong et al. 2015), and administered to the bladder urothelium 1 week after the final endotoxin instillation as a single injection from a variety of doses (0.1, 0.25, 0.5, and 1×10^6 cells) via a lower abdominal incision (Ryu et al. 2018; Song et al. 2015, 2014; Kim et al. 2016b, 2017), following confirmation of negligible autofluorescence (Ryu et al. 2018).

Living rat models of IC/BPS were surveyed before transplantation and at regular intervals for up to 42 days post transplantation by in situ confocal microscopy and observation with a micro-endoscopic optical probe. A continuous 488 nm laser was used with a scanning galvanometric system to excite GFP for both microscopy and endoscopy, and the signal was detected by filtered photo-multiplicative detectors to quantify emitted light while avoiding most sources of noise. The video capture rate was 30 fps. In situ microscopy was performed via a short incision in the abdomen which exposed the bladder, enabling observation 40× objective lenses mounted on a standard confocal microscope. For micro-endoscopic observation, a probe with 1.2 mm diameter and 5.5 cm length was prepared by affixing GRIN lenses together inside a protective tube, using the procedure above (Kim et al. 2012a). The probe was inserted through the urethra in a consistent manner and focused to a consistent depth within the bladder wall (Fig. 7).

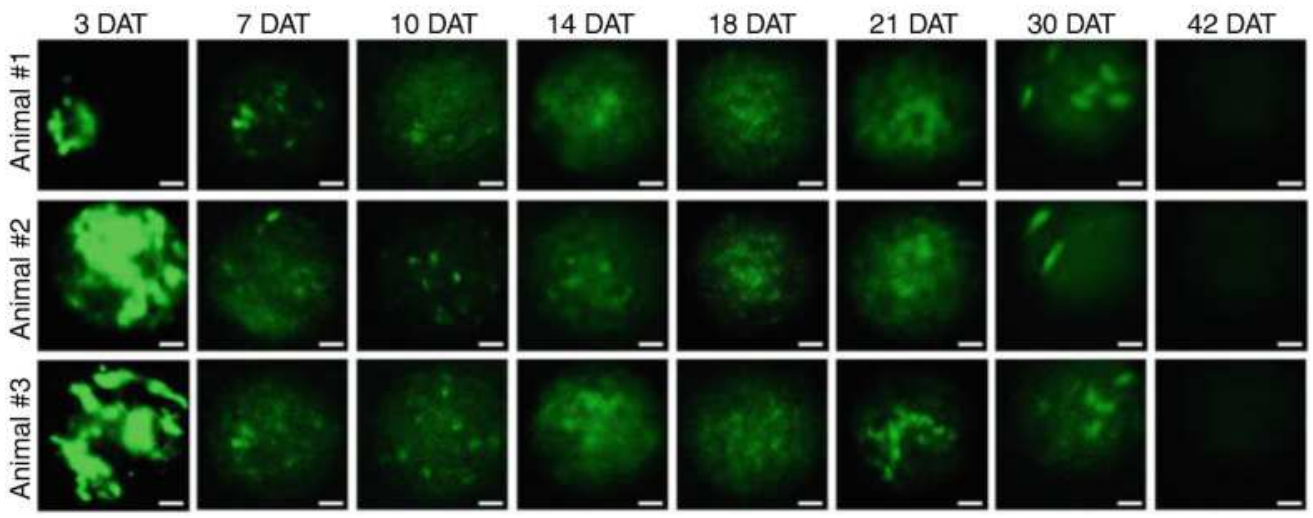

Fig. 7

Longitudinal GRIN probe micro-cystoscopy of engrafted fluorescent stem cells (M-MSCs) in living rats from 3 to 42 days after M-MSC injection (DAT). Microendographs were captured using a 40× objective. Scale bar is 50 μm. Reproduced under CC BY-NC 4.0 license from Ryu et al. (2018), © 2018 Ivyspring International Publishers

Fluorescence intensity and the focus of the observed fluorescence were recorded in the urothelium by micro-cystoscopy (Fig. 7) and by confocal intravital microscopy (Fig. 8) beginning 3 days after M-MSC transplantation (DAT) and over a 42-day period. Both fluorescence intensity and focus varied over time, and the combination of images from cystoscopy and intravital microscopy allowed survival, migration, and differentiation of the transplanted stem cells to be inferred, with worsening focus indicating migration of cells away from the focal plane and into the lamina propria, while decreased intensity indicated a combination of apoptosis and cellular diffusion across the entire bladder wall. Detailed examination of intravital micro-endoscopic images showed engraftment of M-MSCs into blood vessels of the bladder wall, and subsequent differentiation of MSCs into epithelial, stromal, and perivascular cells appropriate for rebuilding the bladder wall was verified by immunostaining.

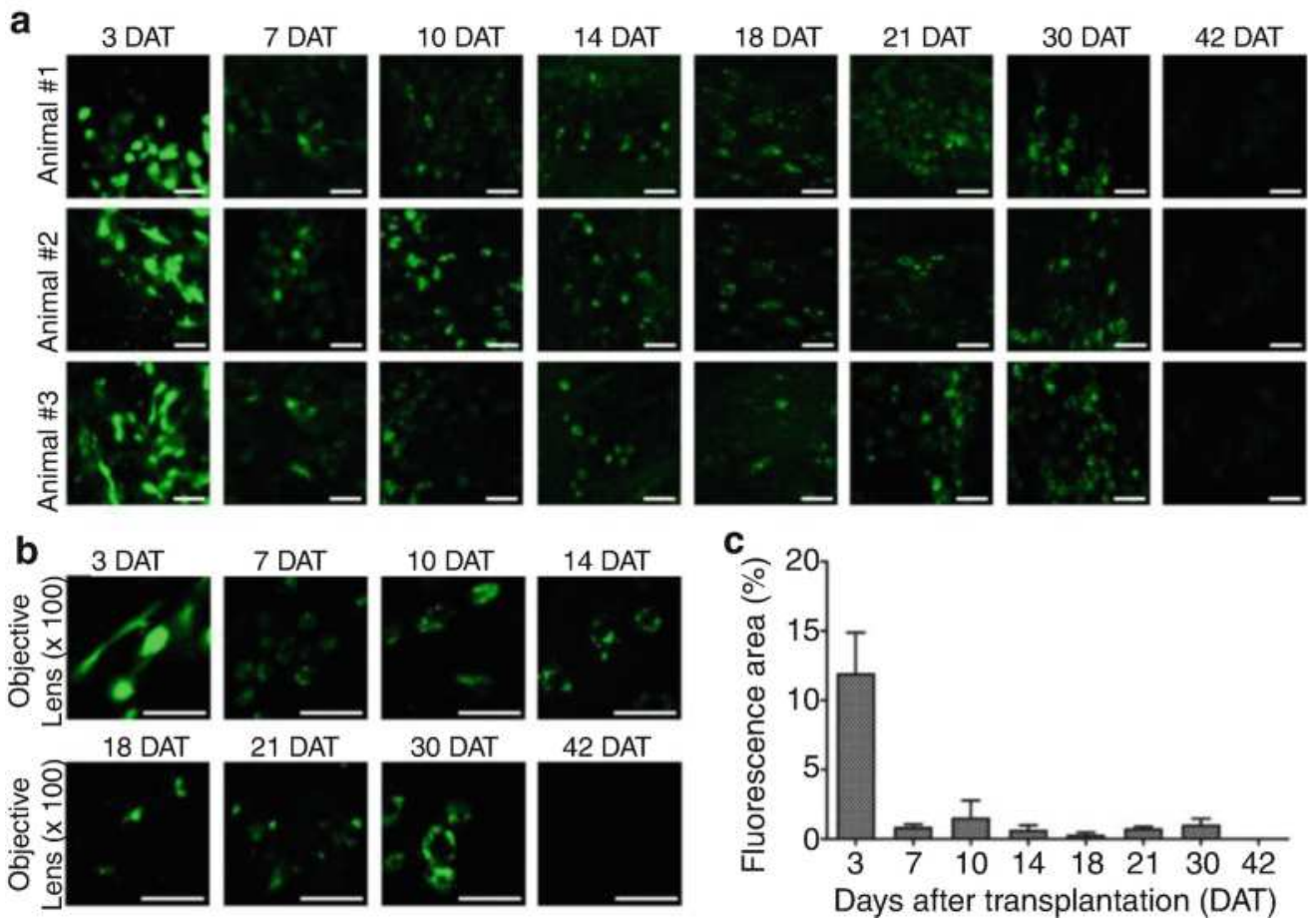

Fig. 8

Intravital microscopy of transplanted stem cells in living rats reveals engraftment from 3 to 42 days after M-MSC injection (DAT). (**a**, **b**) Fluorescent micrographs capture changes in intensity, focus, and morphology over time (**a**, ×40; **b**, ×100; scale bar: 50 μm). (**c**) Fluorescence as a percentage of confocal micrograph area. Reproduced under CC BY-NC 4.0 license from Ryu et al. (2018), © 2018 Ivyspring International Publishers

Further synthesis of these intravital imaging results with cystometric evaluation demonstrated that although the observed intensity decrease likely included some stem cell apoptosis, therapeutic efficacy as measured by improved bladder voiding parameters indicated that healing of the bladder wall was not limited to the injection site. Careful immunostaining demonstrated that the success of a small, single-point inoculation of stem cells in decreasing the symptoms of IC/BPS in the rat model and the result was also due to severance of the WNT and IGF signaling pathways (Ryu et al. 2018). In summary, the synthesis of two different intravital imaging techniques allowed accelerated longitudinal tracking of cellular migration, differentiation, and pathogenesis from a preclinical model of advanced stem cell therapy for pathologies of the bladder wall.

Stabilization of Forward GRIN Micro-endoscopes for Cardiac Applications

As seen in the renal imaging with front-view probes, the resolution of endo-microscope probes for cellular time-lapse visualization is often affected by autonomous tissue motion due to the breathing and heartbeats of experimental mice. In cardiac applications, in particular, despite high interest in cellular processes for healing cardiac tissue in mouse models of the heart, the study of cardiac tissue in vivo by microscopy and endo-microscopy has been limited by autonomous tissue

movement. Herein is described the development of a minimally invasive tool for immobilizing endoscopes relative to moving tissue, which offers the potential to observe and probe the cellular processes connecting cardiovascular and immune functions in vivo, and thereby markedly accelerate the development and testing of new therapeutic and preventive strategies for cardiac pathologies (Jung et al. 2013).

While the autonomous healing of heart tissue is limited in humans, several cellular processes are known to affect heart health. In humans, the formation of arterial plaques is driven by immune cell infiltration and inflammation (Woollard and Geissmann 2010), and immune cell recruitment is crucial in many processes related to myocardial infarction, including phagocytosis, myofibroblast accumulation, angiogenesis, and collagen deposit (Nahrendorf et al. 2010). Immune cell behavior is also a significant consideration in potential regenerative therapies for atherosclerosis, including stem cell treatments and cellular reprogramming (Jung et al. 2013; Anversa et al. 2006; Chien et al. 2008; Ieda et al. 2010). The present paradigm for cellular observation of cardiac tissues is primarily fixed-tissue histology, which provides only static imagery of completed tissue processes, rather than the cellular movement and interactions which characterize living heart tissue.

Seeing this problem, many research groups have developed means of extracting cellular information from the beating mouse hearts and proxy tissues. Relatively low-movement mouse embryos have been examined, and histology and transplantation procedures have been optimized for minimal tissue trauma (Li et al. 2012; Eriksson 2011; Lucitti et al. 2007). Highly disruptive open heart vasculature imaging (Chilian et al. 1986) and microscopy have been made possible to some extent by image registration (Greenberg and Kerr 2009; Schroeder et al. 2010), temporal gating (Lee et al. 2012; Wiesmann et al. 2003), and motion-dampening windows, glue, and even centimeter-wide suction rings (Looney et al. 2011). Despite these advances, the high invasiveness of open surgery and the resultant visual debris have complicated experimental imaging (Jung et al. 2013).

The requirements for stabilizing cardiac tissue for cellular-level imaging are at first daunting: tissue moving on a range of 1–2 mm must be restricted to sub-micron deviations relative to the imaging system, while also avoiding tissue damage (Looney et al. 2011). In Fig. 9, we present a suction system that achieves minimally invasive imaging, holding tissues with suction pressure from a narrow tube at nondestructive pressures of 50 to 100 mm Hg. The suction tube was manufactured from two concentric stainless steel tubes of 1.8 mm and 2.9 mm diameter, separated by a 0.45-mm gap. A 20-mm-long gradient index probe was designed as described at the beginning of this chapter, with a protective sheath diameter of 1.25 mm and 1× magnification. As depicted in Figs. 9 and 10, a small, self-sealing incision in the rubber tubing facilitated insertion of the probe into the suction tube, and the tube was joined to a micro-diaphragm pump by way of a vacuum gauge, a liquid trap, and a flow valve. Suction tubes of 1.8 mm and 2.7 mm diameters fit around the endo-microscope probe and were sufficiently narrow to be put through a minimally invasive incision made in the center of the intercostal space (Jung et al. 2013). A longer, flexible suction tube allows resilience to torque and a small tilt angle under translation. Fluorescent dyes and GFP-expressing transgenic mouse models were used to image the blood vessels and monocytes, respectively (Jung et al. 2013). To improve the uniformity and noninvasiveness of the suction tube, an O-ring was formed out of UV epoxy at the tube's distal end. The assembled probe was connected to a video-rate laser-scanning fluorescence confocal microscopy system (Kim et al. 2010a; Veilleux et al. 2008) using optical relays as described above. The GRIN probe had a resolution of 1 μm in the focal plane and 10 μm perpendicular to it, an optical penetration depth near 100 μm, and a 250 μm FOV (Kim et al. 2008). As with other micro-endoscopes of this design, the focal plane of the probe can be shifted noninvasively by translating the objective lens (Barretto et al. 2009; Kim et al. 2008).

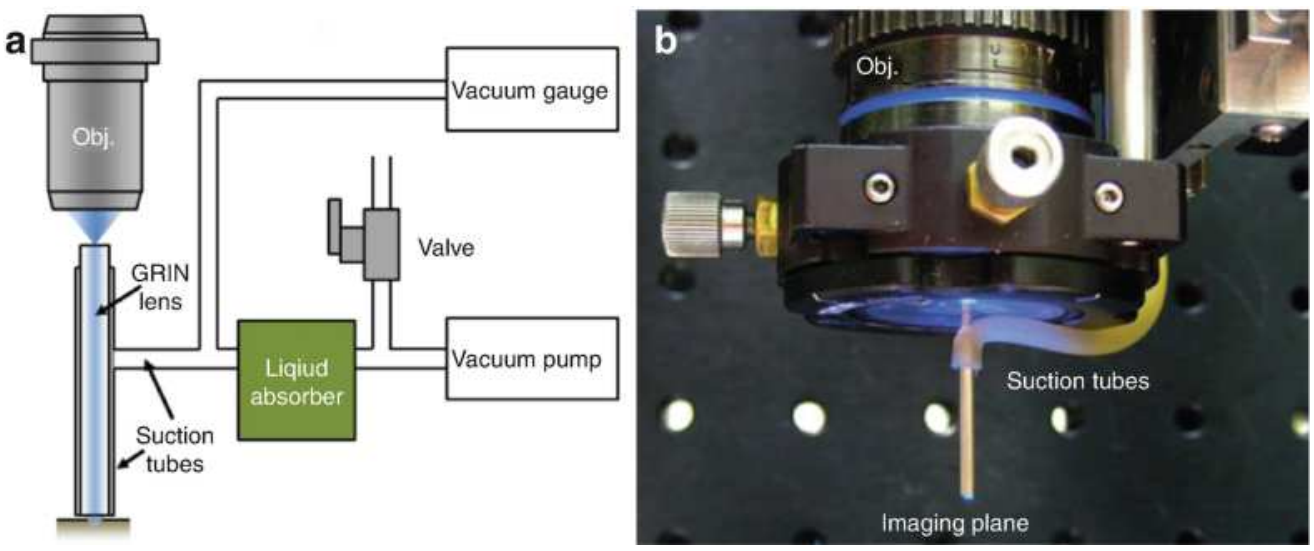

Fig. 9

Schematic and implementation of suction stabilization system for GRIN micro-endoscopes. (**a**) Schematic of the vacuum system, showing liquid absorption system. (**b**) The suction system can be designed to fit flexibly around existing GRIN micro-endoscope setups. Drawn with reference to Jung et al. (2013)

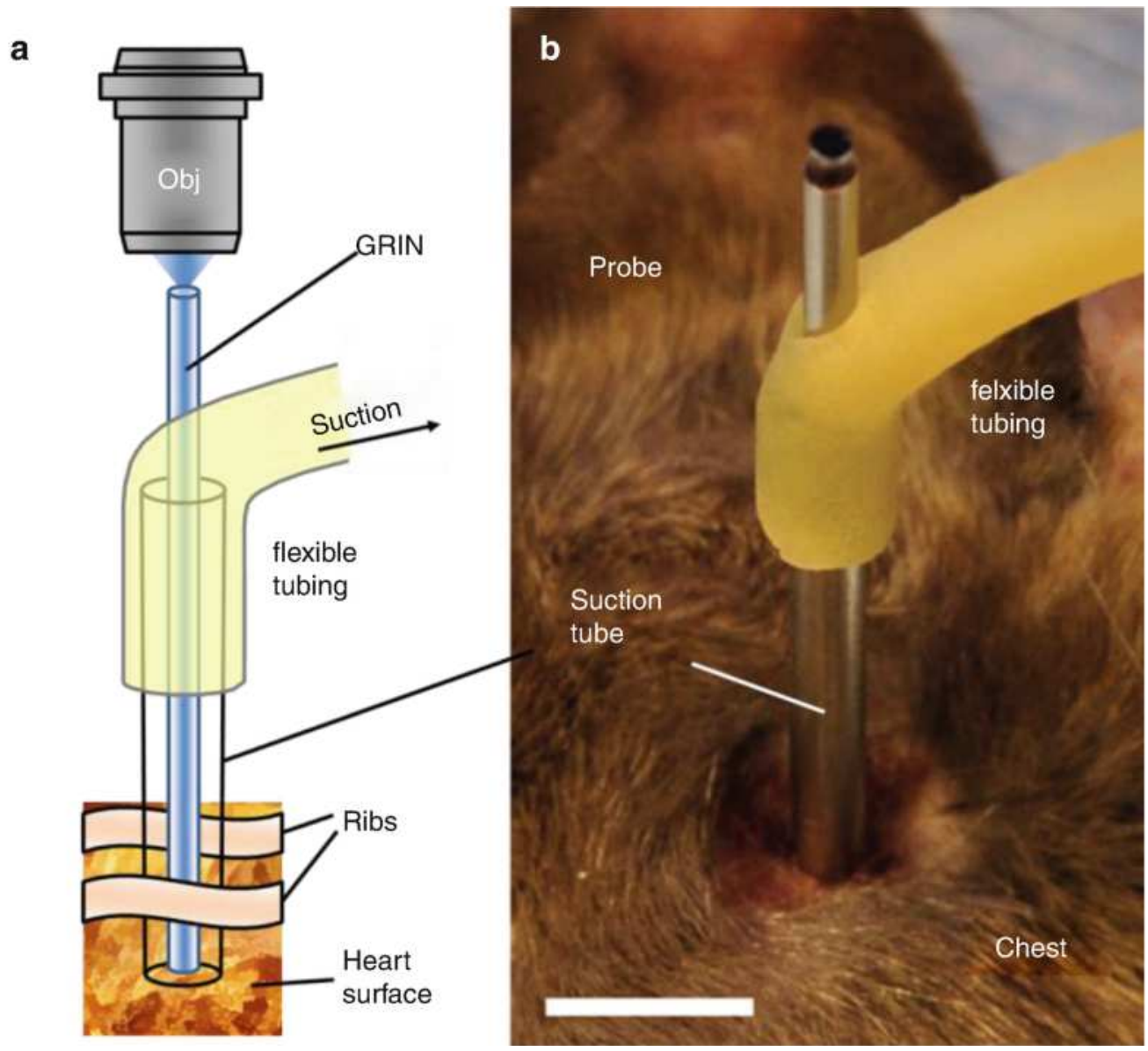

Fig. 10

Motion-stabilization effect of the suction system for cellular endo-microscopy. (**a**) Schematic of the system in use. Lateral motion of cardiac tissue is reduced relative to the probe with suction, and blood flow is maintained in the renal capsule despite suction. (**b**) Image of the system in practice. Scale bars, 50 μm. Image drawn with reference to Jung et al. (2013)

Anesthetized mice 8- to 10-weeks old were translated on a three-axis stage to align the point of tissue incision with the endo-microscopy platform. The mouse was raised onto the endoscope to achieve a slight tissue pressure without suction before suction was gradually applied, and suction of the tissue was confirmed by slightly lowering the animal stage. Horizontal motion of the stage suction was applied translation of the micro-endoscope probe relative to the stabilized tissue for mosaic imaging.

The relative motion of the probe to the cardiac tissue was quantified by a cross-correlation algorithm (Guizar-Sicairos et al. 2008) and can be seen in Fig. 10b. It was found that leaving a loose connection between the suction and the heart at 50 mm Hg did not cease blood flow while reducing tissue movement to less than 10 μm peak-to-peak. This physical correction for tissue motion enabled further noise correction by image registration, which increased the signal to noise ratio and made possible automated mosaicking (Kim et al. 2010a). As shown in Fig. 10c, application of suction up to 150 mm Hg resulted in no disparity in blood flow, as measured by motion tracking of fluorescently tagged red blood cells and polystyrene beads, and under suction, there was negligible reduction in blood pressure or heart rates, as tracked by a CODA monitor and mouse tail cuff. Furthermore, despite repeated observation over several weeks, there was no sign of tissue damage to the heart: no immune reaction was induced, demonstrating that the suction endo-microscopic imaging procedure is less invasive than open in situ microscopy, utilizing a standard objective or a small objective glued to the pericardium. The minimally invasive nature of suction endo-microscopy enables repeated nonfatal and time-lapse imaging, in contrast to prior techniques, and may be easily combined with commercially obtained microscope platforms (Jung et al. 2013; Kim et al. 2012a).

The suction-assisted micro-endoscope enabled a number of novel observations, including the microvasculature and active immune surveillance of the heart. Of particular interest, rolling monocytes were observed patrolling coronary venules in addition to flowing monocytes. Following an induced infarction, an increase in the frequency of flowing monocytes was seen within 30 min and corresponded with a transient decrease in the observation of circulating monocytes in peripheral vessels. The magnitude of this change suggests monocytes are recruited from the vascular pool and then released from the spleen in the first 60 min after infarction, faster than previously believed (Jung et al. 2013; Swirski et al. 2009).

Side-View GRIN Micro-endoscope Applications

Unlike front-view endoscopes, which are useful for the imaging of organs in cavities and on the rounded surfaces of organs, the side-view micro-endoscope probes based on GRIN lenses are principally applicable to the noninvasive observation of the epithelium of tubular organs in the gastrointestinal tract and airways through natural orifices (Kim et al. 2010a). We survey applications to the colon, esophagus, and trachea which are enabled by the narrow probe diameter, but also look at the application of these probes to minimally invasive injection in the murine brain.

Small Animal Colonoscopy Application

The colon is a particularly relevant target for imaging based on the side-view optical probe, as the probe allows noninvasive imaging of early colorectal tumor formation deep in the crypt bottom. Figure 11 shows endo-micrographs of fluorescently tagged cells and vasculature in the colon of a genetically modified mouse model exhibiting spontaneous carcinogenesis. By knocking out the adenomatous polyposis coli (APC) gene with an adenoviral factor and activating a linked reporter gene for GFP, the formation of fluorescent intestinal tumors can be tracked over several weeks (Kim et al. 2010a). Blood vessels may be observed simultaneously by injection of indocyanine green or tetramethylrhodamine dextran into the bloodstream. In Fig. 11a, early-stage neoplasia is observed with diameters of 50–150 μm after a period of 4 weeks. Observed 2 weeks later, the same neoplasia showed high blood vessel perfusion, with polyp diameters of 200–400 μm (Fig. 11b) (Kim et al. 2012a).

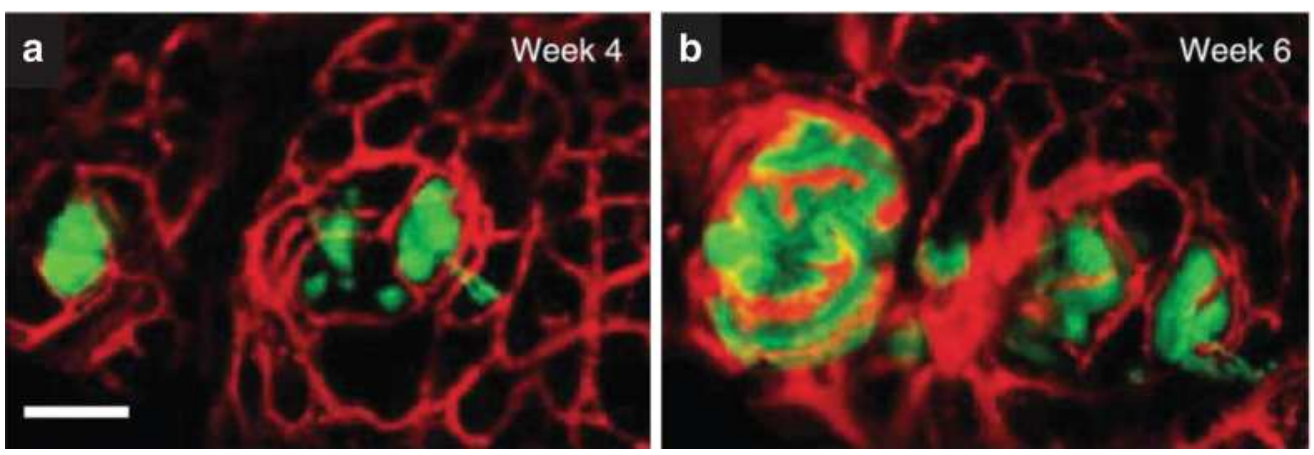

Fig. 11

Time-lapse cellular-level tracking of early colorectal tumor formation in side view. (**a**) Neoplasia expressing GFP in mice 4 weeks after inactivation of *APC* (**b**) The same region shows tumor development and blood vessel perfusion 2 weeks later. Scale bar, 100 μm. Reproduced with permission from Kim et al. (2012a), © 2012 Springer Nature

The procedure for side-view imaging of the colon makes use of a horizontal mount and relay mechanism which connects the 1× magnification GRIN endo-microscope probe to a 40× confocal microscope, while allowing probe rotation. Mice are prepared for observation by fasting and a gentle stool removal procedure following anesthetization. Mice are placed on their backs on a translation stage, so that the point of entry may be viewed when the probe is oriented for ventral observation. By gradual translation, the anus is moved around the distal end of the probe. The probe may be scored for return to consistent locations within the colon, and scanning may be performed to produce image mosaics at 100–200 μm/s. Figure 12a–c depict fluorescently tagged cells in the mucosa of the colon, as well as vasculature visualized by intravenous injection of FITC-dextran. Digital stitching allows a large set of images to be presented as a composite image (Fig. 12d) or as a fly-through rendering (Fig. 12e) (Kim et al. 2010a). The procedure may be adapted for the upper gastrointestinal tract (Kim et al. 2012a; Jun et al. 2018).

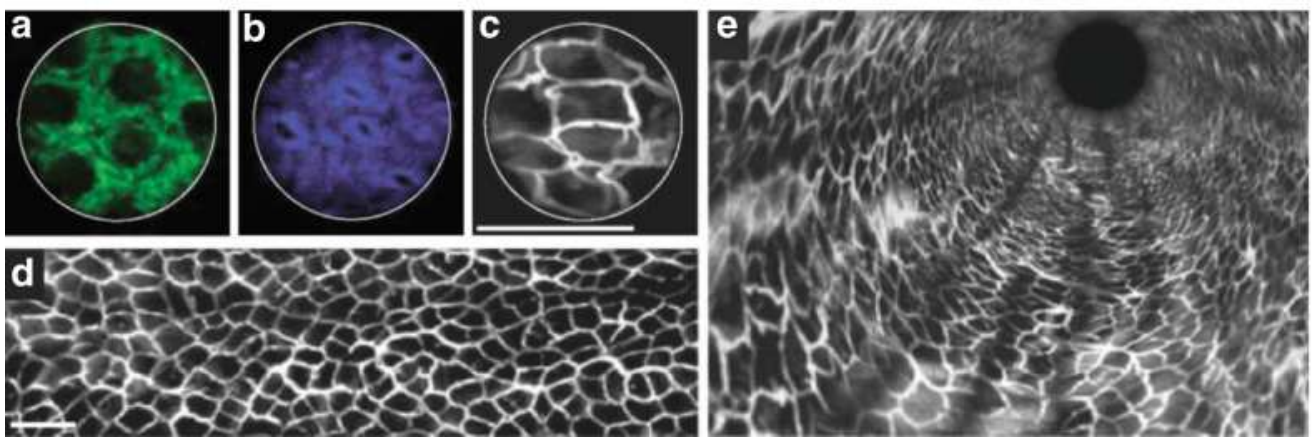

Fig. 12

Potential presentations and imaging targets for side-view microprobes in the descending colon of mice. (**a**–**c**) Images from a single probe field of view (**a**) $MHCII^+$, GFP^+ cells (**b**) stained epithelial cells (**c**) vasculature (**d**, **e**) Composite synthesized from many single-FOV images. (**d**) Unwrapped colon wall (**e**) fly-through presentation. Scale bars, 200 μm. Reproduced with permission from Kim et al. (2012a), © 2012 Springer Nature

Applications to the Upper Digestive Tract for Small Animal Diseased Model

While frequent use is made of mouse models for the study of colorectal cancer, mouse models may also be applied to the simulation of a variety of disorders in the upper digestive tract. Although cancers and related inflammation disorders are common in the esophagus, esophageal passages are also the frequent target of gastrointestinal stenting for the correction of strictures. The pressure induced by these stents on the luminal wall, in turn, may induce a proliferative cellular response (Jun et al. 2017; Werner et al. 2007) which results in complications of restenosis. Here we survey an application of the side-view micro-endoscope to evaluate the safety of a novel self-expanding metal stent (SEMS), observing the proliferation of fibroblast cells and epithelial cell migration over time in a minimally invasive manner. The application of side-view GRIN micro-endoscope probes to the upper digestive tract is interesting for the novel considerations they bring to endo-microscopy in the mouse model. In particular, care must be taken to prevent asphyxiation when accessing target tissue by way of the mouth. Restenosis is not just a concern for the esophagus, but also for the urethra and trachea (Kim et al. 2009, 2007; Park et al. 2012; Song et al. 2003). The results are significant for understanding the cellular processes underlying restenosis in human patients and for motivating new clinical strategies for the mitigation of stent complications (Jun et al. 2018).

Fibroblast cells are the primary imaging target for restenosis, as stent-induced proliferative cellular response is characterized by reepithelialization and fibroplasia (Jun et al. 2017), which are modulated by fibroblasts' creation of extracellular matrix and production of collagen (Taylor et al. 2010; Okada et al. 1997; Polyak and Weinberg 2009; Park et al. 2014; Leask and Abraham 2004; Frangogiannis 2006; Lindley and Briegel 2010). Although rat, rabbit, and pig models of human restenosis are available (Jun et al. 2017; Zhu et al. 2017; Feng et al. 2016; Kim et al. 2010b, 2013a; Wang et al. 2015), deeper studies are possible in mice due to their low cost and additional transgenic varieties. Mice were bred expressing fibroblast-specific protein-1 labeled with GFP (Jun et al. 2018; Iwano et al. 2002).

Self-expanding stents for mice were manufactured from threaded nitinol filament with radiopaque markers to assist in stent placement at each end. SEMS were placed under fluoroscopic guidance in ten mice with a pusher catheter (Fig. 13a–c), while ten mice underwent a sham procedure as controls. Fluorescence micro-endoscopic observations were performed concurrently with fluoroscopy prior to and 2, 4, 6, and 8 weeks after stent placement. Two mice died during the study, one due to breathing difficulties during endoscopy and one due to stent migration (Jun et al. 2018).

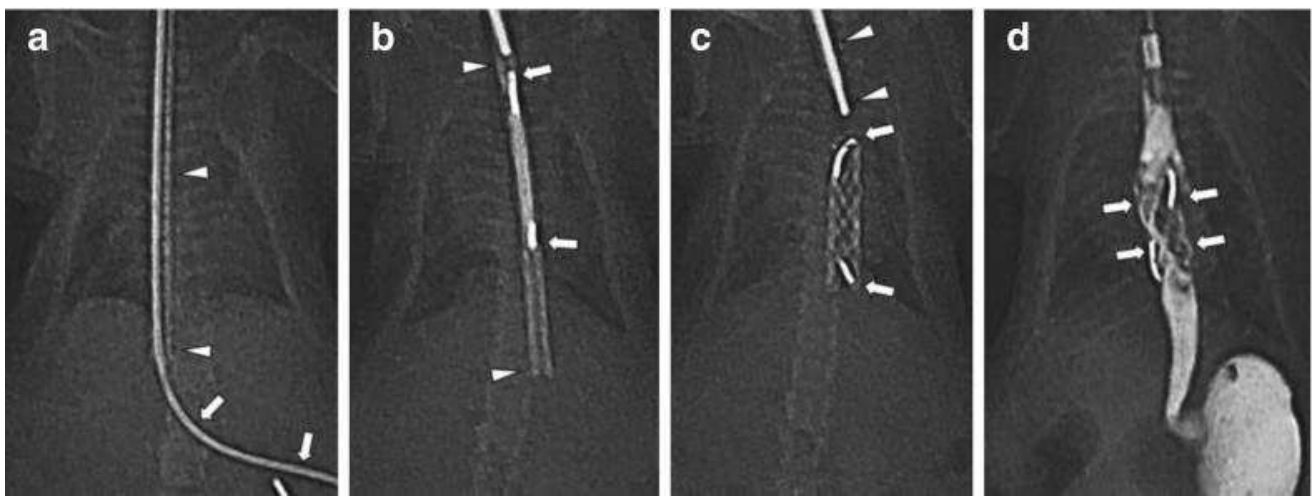

Fig. 13

(**a**, **b**, **c**) Radiographs and esophagography of stent insertion in a mouse model of the proliferative cellular response. (**a**) Guidewire (arrows) and sheath (arrowheads) placement. (**b**) Stent delivery. (**c**) Stent placement. (**d**) Esophagograph captured 8 weeks after stent placement depicting a filling defect (arrows) caused by restenosis. Reprinted from J. Vasc. Interv. Radiol. 29, Jun et al. "In Vivo Fluorescence Microendoscopic Monitoring of Stent-Induced Fibroblast Cell Proliferation in an Esophageal Mouse Model," pages 1756–1763, Copyright 2018, with permission from the Society of Interventional Radiology (SIR)

As shown in Fig. 14, for fluorescence micro-endoscopic imaging, anesthetized mice were immobilized on a homeostasis-maintaining three-axis translation stage. To ensure a clear airway while facilitating endoscope insertion, the tongue of the mouse was gently pulled out. After insertion of the endoscope into the mid-thoracic esophagus, fluorescence images were captured at 30 Hz using a laser scanning confocal system, including a 488-nm excitation laser and photo-multiplicative detector tubes. Frames were subsequently averaged and filtered to reduce shot noise, and a background normalization procedure was applied to reduce noise from background tissue (Tyack et al. 2014), enabling automated cell counting (Al-Khazraji et al. 2011) and comparison of fluorescence intensities, as a marker of fibroblast health (Jun et al. 2018).

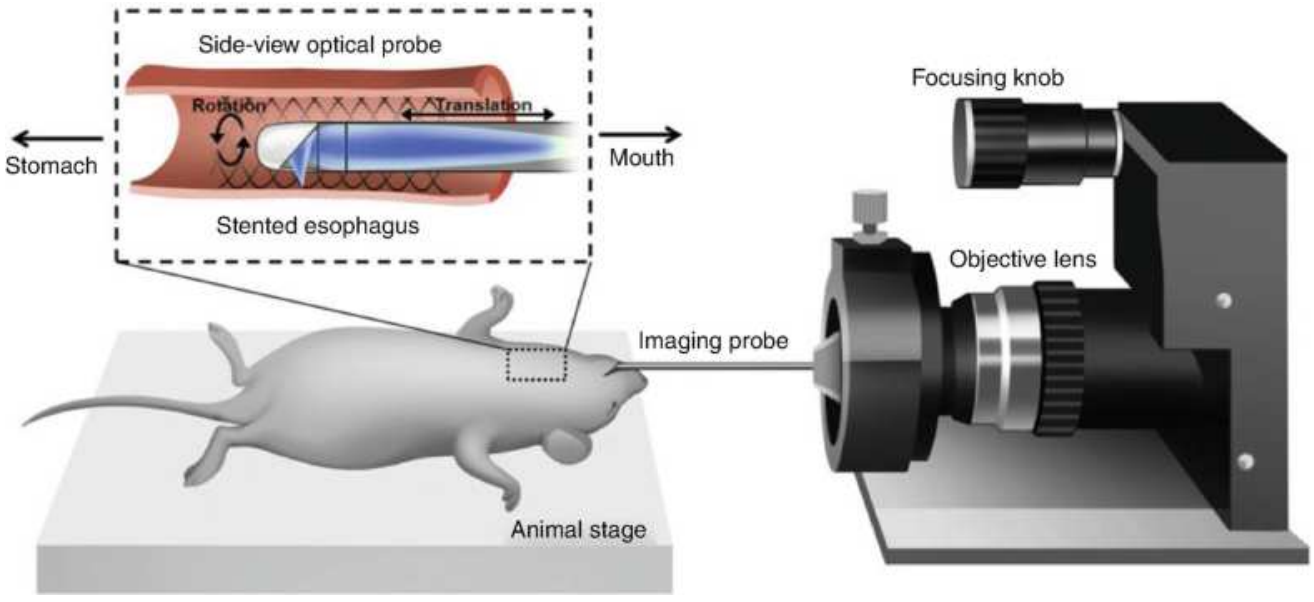

Fig. 14

Application of esophageal fluorescence endo-microscopy to track the cellular response to stenting in vivo. Reprinted from J. Vasc. Interv. Radiol. 29, Jun et al. "In Vivo Fluorescence Microendoscopic Monitoring of Stent-Induced Fibroblast Cell Proliferation in an Esophageal Mouse Model," pages 1756–1763, Copyright 2018, with permission from the Society of Interventional Radiology (SIR)

As a result of this imaging procedure, it was possible to capture time-lapse fluorescence micrographs of the GFP fibroblasts, as shown in Fig. 15. In the stenting group, the fibroblast cell density increased immediately, peaking in the first measurement after stent placement before declining gradually (Fig. 15a). The average fibroblast GFP count (Fig. 15b) and average fluorescence intensity (Fig. 15c) were both significantly higher after stenting than in the control group, indicating higher fibroblast health (Jun et al. 2018).

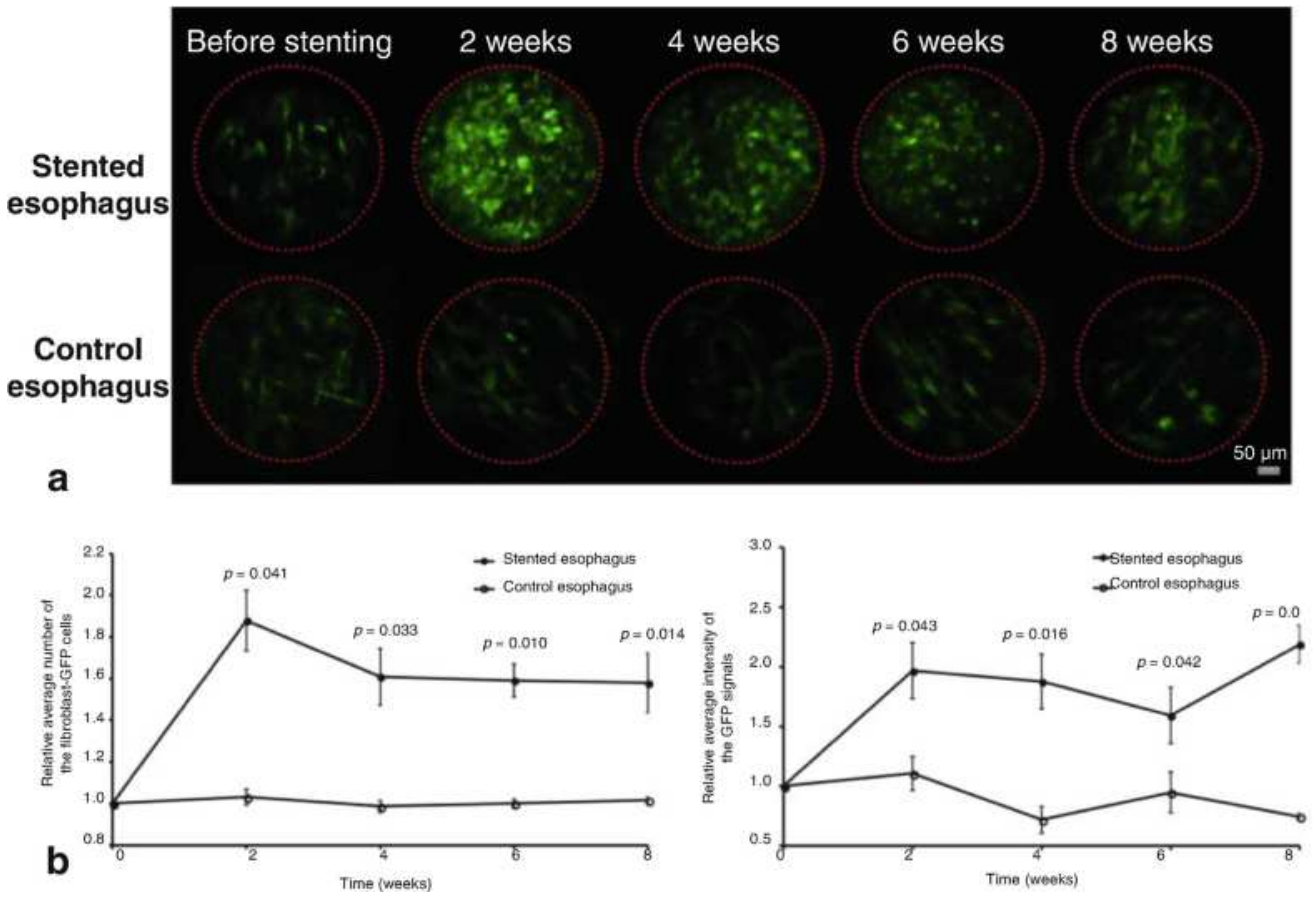

Fig. 15

Fluorescent fibroblasts proliferate in stented mouse esophagi as compared to a control, as shown by longitudinal side-view micro-endoscopy. (**a**) Representative endo-micrographs in vivo before and after stenting. (**b**) Averaged fibroblast counts (**c**) Averaged fibroblast fluorescence intensity. Reprinted from J. Vasc. Interv. Radiol. 29, Jun et al. "In Vivo Fluorescence Microendoscopic Monitoring of Stent-Induced Fibroblast Cell Proliferation in an Esophageal Mouse Model," pages 1756–1763, Copyright 2018, with permission from the Society of Interventional Radiology (SIR)

These results are consistent with the standard explanation of a wound-healing process occurring over the first 4 weeks. Within a short period, fibroblasts and epithelial cells migrate to the inflamed tissue, where they undergo highly proliferative cellular responses. Fibroblasts in this situation transform into myofibroblasts, resulting in decreased fluorescence while the lesion becomes a collagen-dense scar (Jun et al. 2018).

Concurrent esophagography and subsequent histology supported the conclusion of the fluorescence monitoring, with a correlated decrease in the luminal diameter after stenting, and increases in tissue hyperplasia, granulation tissue, epithelial tissue, and submucosal fibrosis as measured ex vivo after 8 weeks. In histological samples, markers for fibroblasts, connective tissues, and mesenchymal cells were also increased in the stenting group. These results demonstrate that the inferences made by fluorescence micro-endoscopy are useful for the time-domain monitoring of stent-induced cellular processes in vivo (Jun et al. 2018).

In conclusion, by using minimally invasive micro-endoscopy, insight was gained into the number and behavior of fibroblast GFP cells in a mouse model of restenosis. In vivo imaging allowed increased statistical power from a smaller number of animals, by controlling for statistical errors from individual variability through repeated measurement (Kim et al. 2012b; Choi et al. 2014) and supporting radiographic observations and final histological measurements. Gradient-index-based fluorescence micro-endoscopy permits the investigation of cellular and molecular progression of gastrointestinal tract diseases in living small animal models (Jun et al. 2018).

Small-Diameter Endoscopes Enable Respiratory Imaging

Although intravital fluorescence microscopy is a powerful tool for the study of cellular changes during the progression of diseases, mechanistic studies of lung diseases in the airway epithelium of small animal models are limited by probe size and difficulty in accessing the respiratory epithelium without either obstructing breathing or collapsing lungs. In the following section, we summarize the application of a miniature side-view confocal probe to obtain fluorescence cellular-resolution images of the trachea from live transgenic fluorescent reporter mice in vivo. Fluorescent reporters specific to cell types were used to give insight into the cell biology of airway diseases, and a custom small-diameter confocal micro-endoscope was designed to allow simultaneous intubation and observation during repeated in vivo endotracheal observations over 3 weeks following a sulfur dioxide-induced injury. In vivo side-view endo-microscopy offers a minimally invasive method for the investigation of regenerating airways in small animal models of respiratory diseases.

With the recent growth in the accessibility of tools for genetic manipulation and a similarity in cellular organization to the human airway, mice present an ideal model to observe the process of airway regeneration after epithelial damage. In particular, we were interested in observing the processes by which basal stem cells self-renew and differentiate into Clara cells and ciliated cells (Rock et al. 2009), resulting in rapid healing of the airway epithelium after trauma (Rock et al. 2010). A strain of transgenic reporter mice was bred for fluorescence in each of these three major cell types. The CK5-nGFP, B1-EGFP, and FoxJ1-EGFP reporter strains allow visualization of GFP basal, ciliated, and Clara cells, respectively (Fig. 16) (Kim et al. 2012b).

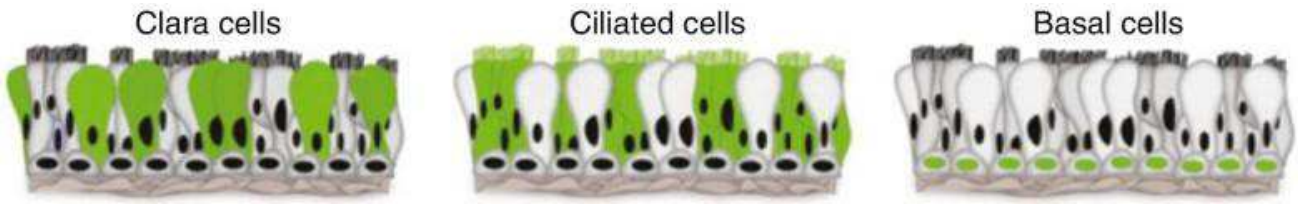

Fig. 16

Sketch of the ciliated, basal, and Clara cells of the tracheal epithelium. Reprinted from Kim et al. (2012b) with permission of the American Thoracic Society. Copyright © 2019 American Thoracic Society

As a model of airway injury and regeneration, we applied SO_2 inhalation, which is widely used due to its induction of rapid sloughing of cells from the suprabasal epithelium in the murine trachea (Kavet and Brain 1974). The practicality of longitudinal endoscopy was verified by the application of doxycycline to induce the generation of GFP^+ Clara cells in the CK5-nGFP mouse model over a 10-day period (Kim et al. 2012b).

Direct imaging and time-lapse visualization are much better suited than ex vivo histology to understanding the regeneration of the epithelium. Imaging of the respiratory system in vivo has been reported by a variety of methods, including open surgery (Kimura et al. 2009), surgical window implantation (Looney et al. 2011), and fluorescence fiber-optic bronchoscopy (Cortez-Retamozo et al. 2008). Our group had previously observed dendrites in the upper airway through a wider, 1.25-mm-diameter side-view GRIN micro-endoscope (Kim et al. 2010a). However, the large probe diameter mandated tracheostomy and ruled out longitudinal imaging. Thus, size remained a barrier to the minimal invasiveness of tracheal imaging (Kim et al. 2012b).

In response to this limitation, GRIN lenses of only 0.35 mm diameter were used to fabricate a new probe with a total outer diameter of 0.61 mm. This thin and semirigid probe of length 62 mm was protected in a metal sheath, integrated on a rotating mount, and pushed into the murine airway via an intubation cannula (OD, 1.0 mm; ID, 0.7 mm) so as to not block the flow of air (Fig. 17a) (Kim et al. 2012b).

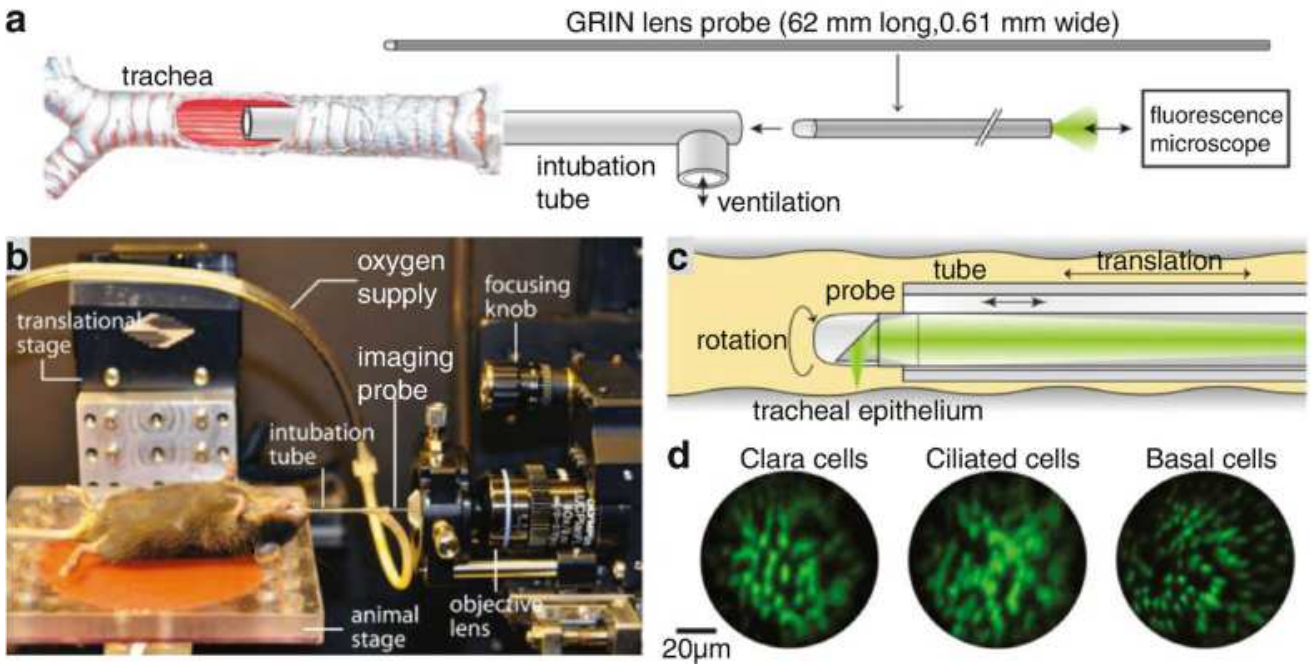

Fig. 17

In vivo GRIN fluorescence endo-microscopy of the trachea. (**a**) Preparation of the GRIN lens imaging through an intubation tube. (**b**) Actual imaging setup. (**c**) Side-view imaging of the tracheal epithelium. (**d**) Resultant in vivo endo-micrographs, showing Clara, ciliated, and basal cells in their respective GFP^+ mouse models. Scale bar, 20 μm. Reprinted from Kim et al. (2012b) with permission of the American Thoracic Society. Copyright © 2019 American Thoracic Society

By adjusting the position of the confocal microscope's objective, the endoscope's focal plane was easily controlled (Kim et al. 2008) (Fig. 17b). Translation of the mouse parallel to the tube and rotation of the probe allowed visualization of an area larger than that of the optical system's native field of view, which was limited to about 6400 μm^2 (Fig. 17c).

Fluorescence images were acquired with an identical image processing workflow to the esophageal imaging described above, with the exception of an image registration algorithm (Zitová and Flusser 2003), which corrected for artifacts of the motion due to respiration (Kim et al. 2012b).

Anesthetized mice were intubated with an endotracheal cannula and connected to an oxygen supply prior to imaging, as shown in Fig. 20. A paraffin film sealed the tube while the narrow-diameter optical probe was pushed in. Imaging sessions lasted approximately 40 minutes, concluding with the slow removal of the micro-endoscope and cannula, and the resumption of autonomous breathing. During in vivo application, the captured images discerned individual cell nuclei, thanks to local confinement of GFP.

Following creation and verification of a new dual-reporter fluorescent Clara cell mouse line, in vivo observation prior to SO_2 inhalation injury revealed uniformly dense Clara cells in the tracheal epithelium (Fig. 18a). One day after exposure, fluorescent Clara cells were completely lost (Fig. 18b). Immunofluorescence of concurrently harvested tissue sections revealed an absence of Clara and ciliated cells while some basal stem cells appeared healthy (Fig. 18c) (Rawlins et al. 2009). One week later and 2 weeks later, fluorescent Clara cells had regenerated, and their population was increasing (Fig. 18d), although the speed of recovery varied between animals (Fig. 18e and f) (Kim et al. 2012b).

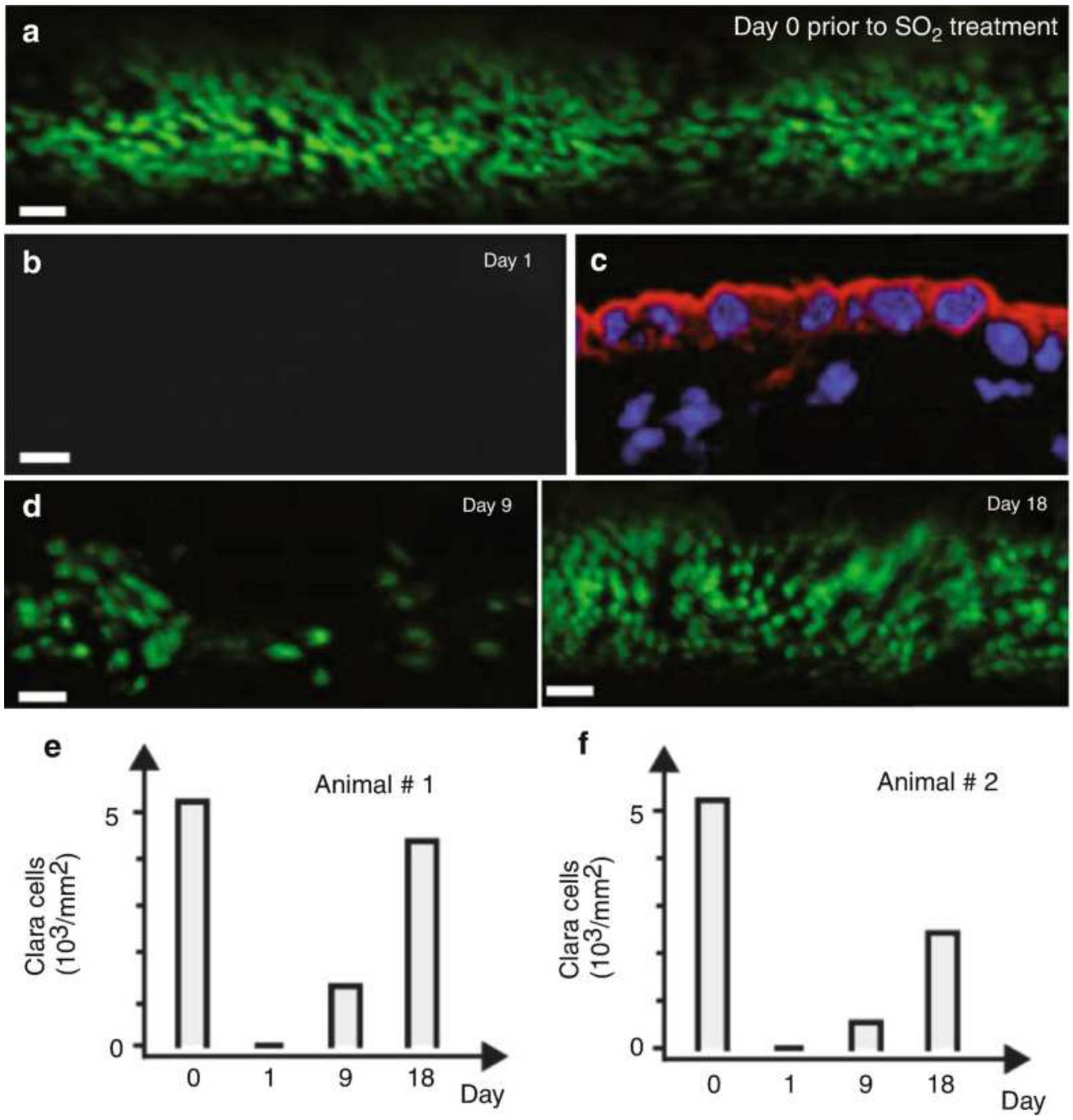

Fig. 18

Micro-endoscopic imaging of Clara cells in vivo following SO_2 injury to the mouse trachea. (**a**) A composite image of the tracheal epithelium pre-injury. (**b**) Complete depletion of Clara cells one day after injury. (**c**) Immunofluorescence of a section obtained one day after exposure reveals basal stem cells. (**d**) Later in vivo images show recovery of Clara cell population. Scale bars, 20 μm. (**e**–**f**) Clara cell densities from two different mice. Reprinted from Kim et al. (2012b) with permission of the American Thoracic Society. Copyright © 2019 American Thoracic Society

Provided cell-type-specific fluorescent reporters from the tracheal epithelium, gradient index micro-endoscopy probes of sufficient miniaturization provide visualization in vivo, over time, and with minimal invasiveness, at the resolution of individual cells. Side-view design enabled the positioning of the target tissue at short focal distances compared to the typical bronchoscopes (Cortez-Retamozo et al. 2008; Thiberville et al. 2007), but an autonomous movement of the respiratory system challenges the imaging system. Through the micro-endoscope imaging system, Clara cell depletion and recovery were observable in live mice, saving much time and resources over orthodox histological measurement, while reducing errors due to animal variation (Kavet and Brain 1974; Rawlins et al. 2009). The minimally invasive, in vivo observation of cellular processes using fluorescent epithelial reporters in the airway will likely find applications in murine models of asthma and cancer (Kim et al. 2012b).

Small Animal Brain Applications for Minimum Traumatic Injury

A number of significant pathologies involve the brain, including neurodegeneration, stroke, cerebral infection, cerebral inflammation, and metastasis of brain tumors. While clinical treatment of these pathologies is necessarily noninvasive, using radiological brain imaging modalities, the small animal researcher is frequently interested in mechanisms that require cellular-level resolution and prefers techniques less invasive than histology or brain needle biopsy (Feiden et al. 1991; Tilgner et al. 2005). While in situ fluorescence microscopy (Helmchen and Denk 2005) may permit cellular-resolution longitudinal observation of the mouse cerebral cortex via a transparent cranial window (Holtmaat et al. 2009) or thinned skull (Yang et al. 2010), side-view micro-endoscope probes (Kim et al. 2010a) are ideal for observing columns of fluorescent cerebral tissue at imaging depths below the 500–750 μm limit of surface imaging (Kim et al. 2013b). Here is reviewed a narrow 350-μm-diameter side-view micro-endoscope probe and needle-based package which achieves high-resolution, large-volume imaging deep into the small animal brain while minimizing trauma and therefore behavioral side effects. The probe may be inserted into the murine brain via a hole drilled in the cranium (Kim et al. 2013b), or when strengthened with a 22-gauge needle may be directly injected through the murine skull.

The optical probe and needle package were based on standard GRIN endo-microscopic probes, designed with GRIN rod lenses of diameter 350 μm, fashioned into side view probes by attachment of a 0.16-pitch imaging lens and a right-angle prism with 250 μm edges (Kim et al. 2013b). Adding a 22-gauge needle (610 μm diameter) as a protective sheath, as shown in Fig. 19, made it possible for the probe to penetrate the mouse skull without craniotomy.

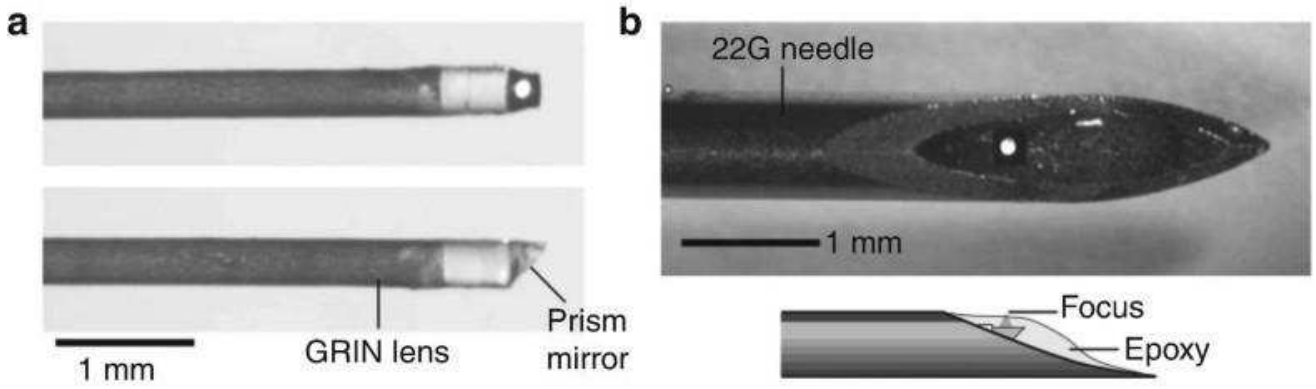

Fig. 19

Photographs of the (**a**) miniaturized and (**b**) stiffened needle side-view probes. Reprinted with permission from Kim et al. (2013c). © 2013 The Optical Society

The optical probe was coupled into a confocal microscope as described above and mounted as shown in Fig. 20, including a translating objective (40×, NA = 0.6) for adjusting the probe working distance from 0 to 100 μm and a rotational stage for panoramic imaging (Kim et al. 2013b).

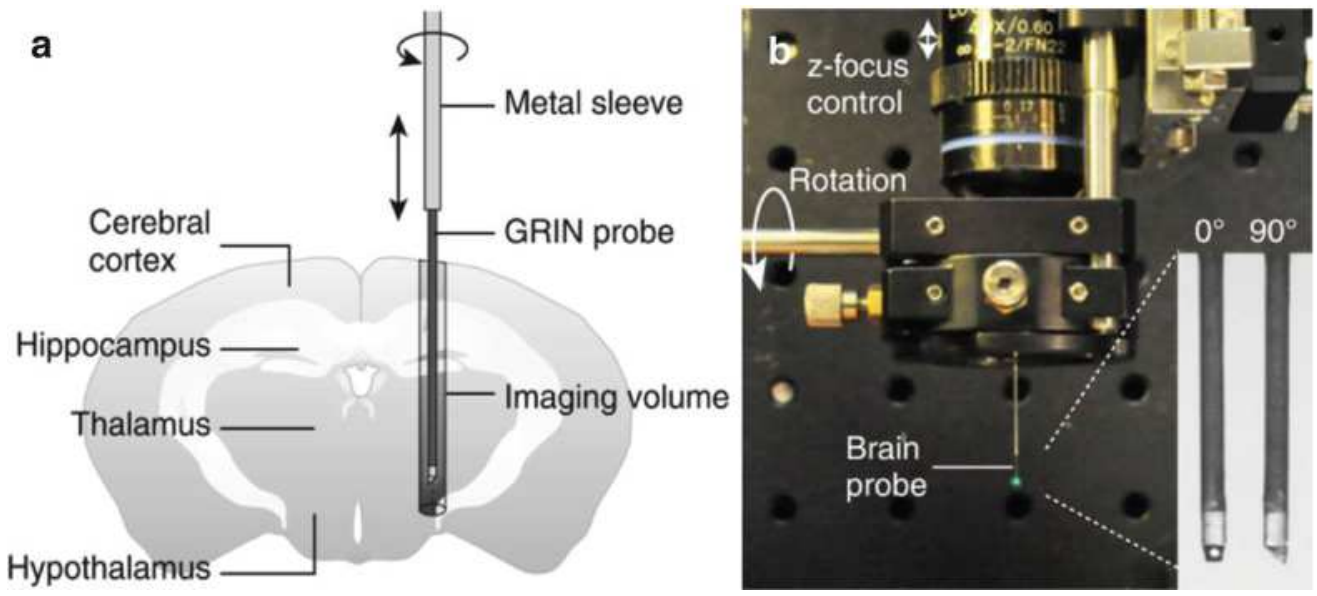

Fig. 20

Small-diameter side-view GRIN endo-microscope probes. (**a**) Application of the probe for deep brain observation. (**b**) The intravital microscopy setup. Reprinted under CC BY 4.0 license from Kim et al. (2013b). Copyright © 2013 SPIE

As in the preparation of stainless steel prisms, the probe was immobilized relative to the needle by a heat-sensitive epoxy; uniquely, in this application, it is ideal for the epoxy to cover the distal probe tip so as to prevent collection of debris during insertion. The FOV of the 350 μm diameter probe was approximately 90 μm; however, inserting and rotating the needle enabled observation of a much larger tissue area (Kim et al. 2013b, c).

Mouse models were prepared to replicate neuronal degeneration due to intoxication, ischemic stroke, and metastasized melanoma in the brain. Two neural degeneration models (n = 5 each) were created by chronic treatment of methyl-mercury and trimethyltin hydroxide, which are known to cause apoptosis in the cerebellum granule cells (Nagashima et al. 1995; Hara et al. 1997), into Thy1-YFP^{+} mice, which express yellow fluorescent protein in neuronal cells (Kleinfeld et al. 1998). Injections were performed intraperitoneally every 2 days for 30 days. Cerebral ischemia was modeled by blocking the middle cerebral artery for 1 hour in mice expressing green fluorescent protein in MHC-class-II (Arumugam et al. 2006). Metastatic cancer models were established by craniotomy followed by in situ injection of 2×10^{6} B16 melanoma cells modified to express RFP (Kim et al. 2013c). Groups were prepared with and without overexpressed p53 genes, which limits metastasis in melanoma (Kim et al. 2013c; Chudnovsky et al. 2005).

Imaging was performed on anesthetized mice after initial preparation, which consisted of hair removal followed optionally by drill craniotomy (Kim et al. 2013b), after which mice were placed in a homeostasis-maintaining stereotaxic mount on a translational stage. Tissue was moistened with saline, and the stage was raised such that the probe was gradually inserted into the brain. Smooth, low-trauma penetration was facilitated by the sharp distal edge of the prism (or needle), the narrow probe diameter, and the application of force along the probe axis (Kandel 2000). Axial and rotational scanning of the imager were achieved by moving the staged mouse vertically and rotating the probe as described earlier in the chapter (Kim et al. 2013b, c). The setup for this procedure is shown in Fig. 20 (Kim et al. 2013b).

Through axial and rotational composites of a series of images, it becomes possible to used gradient-index-lens-based confocal micro-endoscopes to capture in vivo panoramic and cylindrical sections of fluorescent tissue, including all the layers in the cerebral cortex at cellular resolution, as demonstrated in Fig. 21.

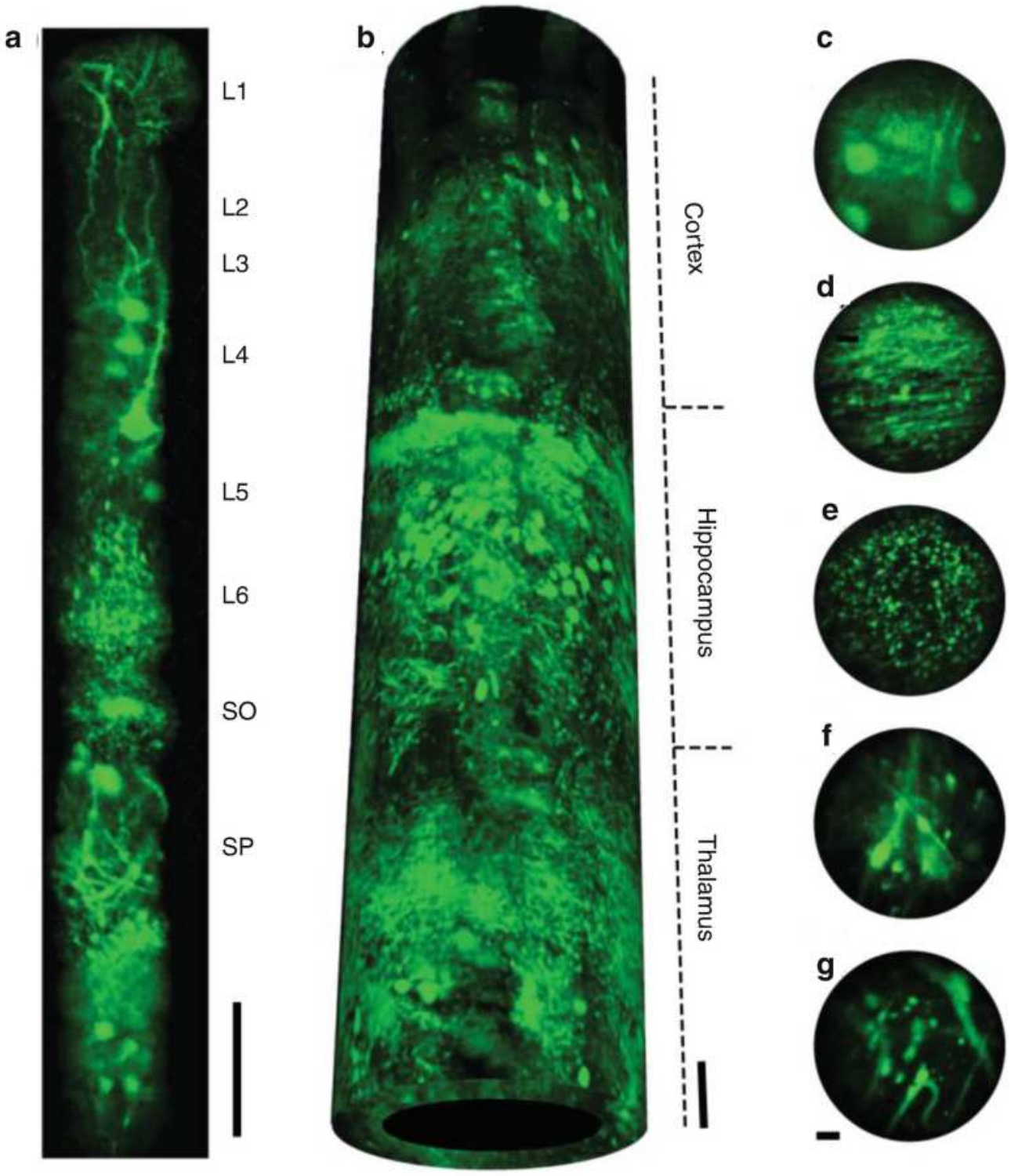

Fig. 21

In vivo composite images of the murine brain captured with a 350-μm side-view probe from Thy1-GFP mouse. (**a**) A composite of neurons and neural cells along a cross-section of the cerebral cortex and hippocampus. (**b**) Cylindrical rendering of captured wide-area deep-brain neuronal images. Scale bars: 100 μm (**c**–**g**) Varieties of cells observed from across the optical section. Reprinted under CC BY 4.0 license from Kim et al. (2013b). Copyright © 2013 SPIE

In Fig. 21a, vertically (axially) scanning the probe during insertion revealed a deep view of the axon structure in the brain tissue encircling the inserted probe, showing the layers of the cortex, and striatum. Adding rotation to the axial translation allowed reconstruction of a cylinder of the brain from the cortex to the thalamus. Individual neurons were observed clearly in the olfactory bulb, hippocampus, thalamus, hypothalamus, midbrain, and medulla, indicating that clear visualization is possible across the entire brain (Kim et al. 2013b).

The resulting side-view GRIN micro-endoscope probes are well suited for optical biopsy. In the murine models of neuronal degeneration, observation by intracerebral endoscopy was performed prior to, after 15 days, and after 30 days of chemical treatment in each model (Fig. 22). The time-lapse endo-micrographs exposed a significant decline in fluorescent granule cell density over time in both treatment groups relative to the control animals (Fig. 22b–e). Behavioral impairment, as measured on mice exempted from endoscopy by the NSS (Beni-Adani et al. 2001), showed onset of symptoms at between 23 and 25 days of treatment (Fig. 22f), demonstrating that in animals, significant cell loss must occur before behavioral deficits are detectable (Kim et al. 2013c).

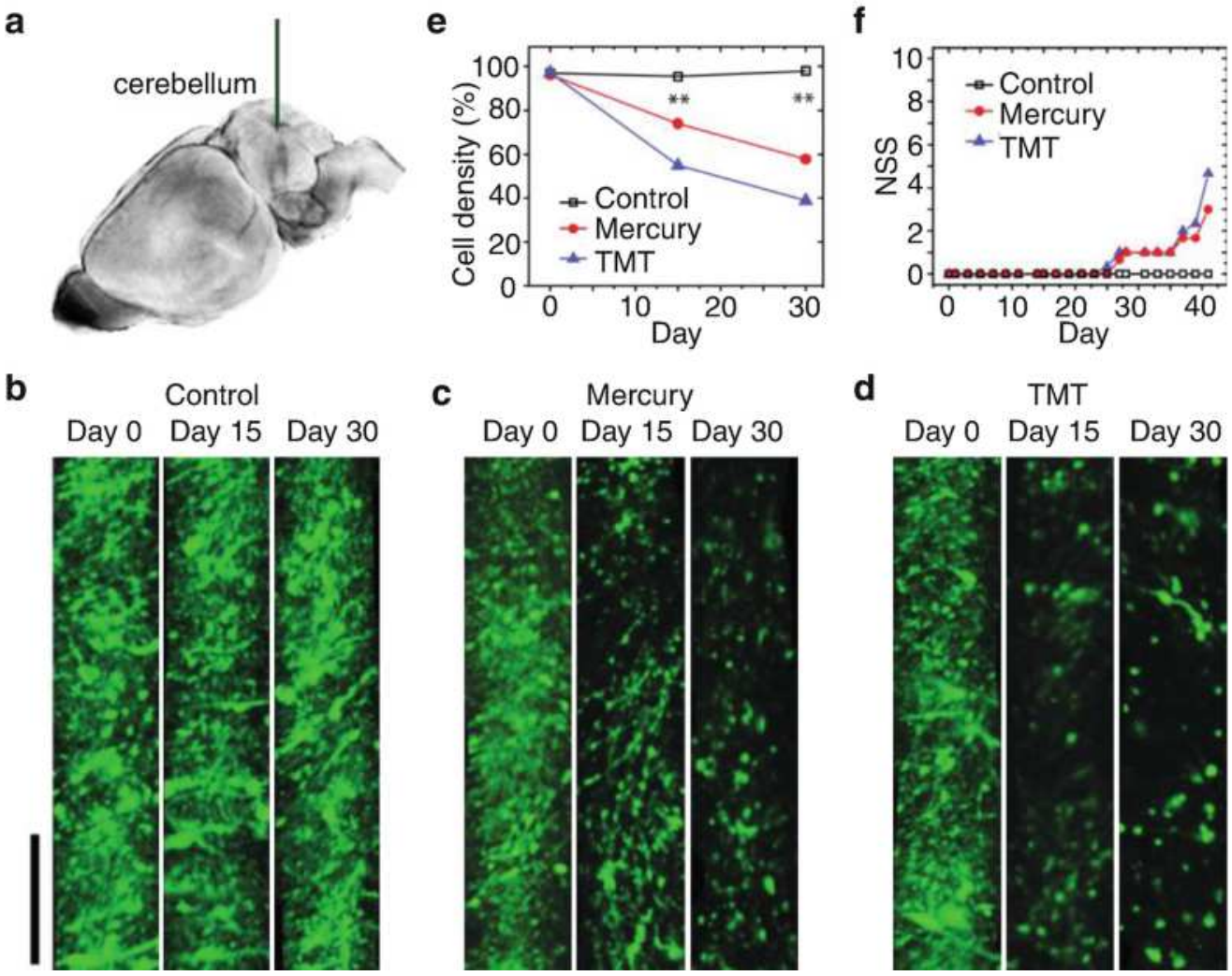

Fig. 22

Longitudinal observation of neuron apoptosis in mouse models of neurodegeneration due to intoxication. (**a**) Schematic of the 22-gauge probe's route through the cerebellum. (**b**, **c**, **d**) Wide-area composite images of fluorescent neurons at days 0, 15, and 30 in mice (**b**) unexposed (**c**) exposed to methyl mercury. (**d**) exposed to trimethyltin hydroxide. (**e**) Cell densities measured in the three cohorts. (**f**) Average neurological severity scores assessed for each cohort (n = 5 each). Reprinted with permission from Kim et al. (2013c). © 2013 The Optical Society

Similar optical biopsy was applied to the direct imaging of inflammatory cellular response in deep ischemic sites in vivo. One, two, and three days after a surgically induced stroke, the density of inflammation-linked MHC-Class-II-GFP$^+$ fluorescent T cells was observed to increase linearly with time up to 70,000 cells per mm^3 at depths of 1–1.5 mm into the ischemic hemisphere, but not at the symmetric point in the unaffected hemisphere, in agreement with prior findings (Gelderblom et al. 2009). Thus, minimally invasive endoscopic optical biopsy shows promise as a method for understanding the dynamics of inflammation in stroke through optical biopsy, as well as the preclinical assessment of strategies and drugs for the treatment of stroke (Kim et al. 2013c; Storkebaum et al. 2011).

Finally, optical biopsy with GRIN probe was applied to a metastatic melanoma model in the mouse brain, demonstrating a change in cell roundness in the metastasizing, low-p53 variant cells compared to the high-p53 cell variant. While the low-p53 variant proliferated in deep brain tissues, the high-p53 variant disappeared over a period of 3 days (Kim et al. 2013b).

Although tissue damage is unavoidably caused by inserting and removing GRIN microprobes from the brain, the 350-μm diameter optical probe is much less invasive than a similar probe of 1250 μm diameter, as shown in Fig. 23. On the left, brain tissue is shown after one pass of a 350-μm diameter probe. Histology reveals that the wound closed itself due to tissue pressure, in comparison to the clearly hemorrhaging, open wound visible after a single insertion of a 1250-μm probe, as seen on the right (Kim et al. 2013b).

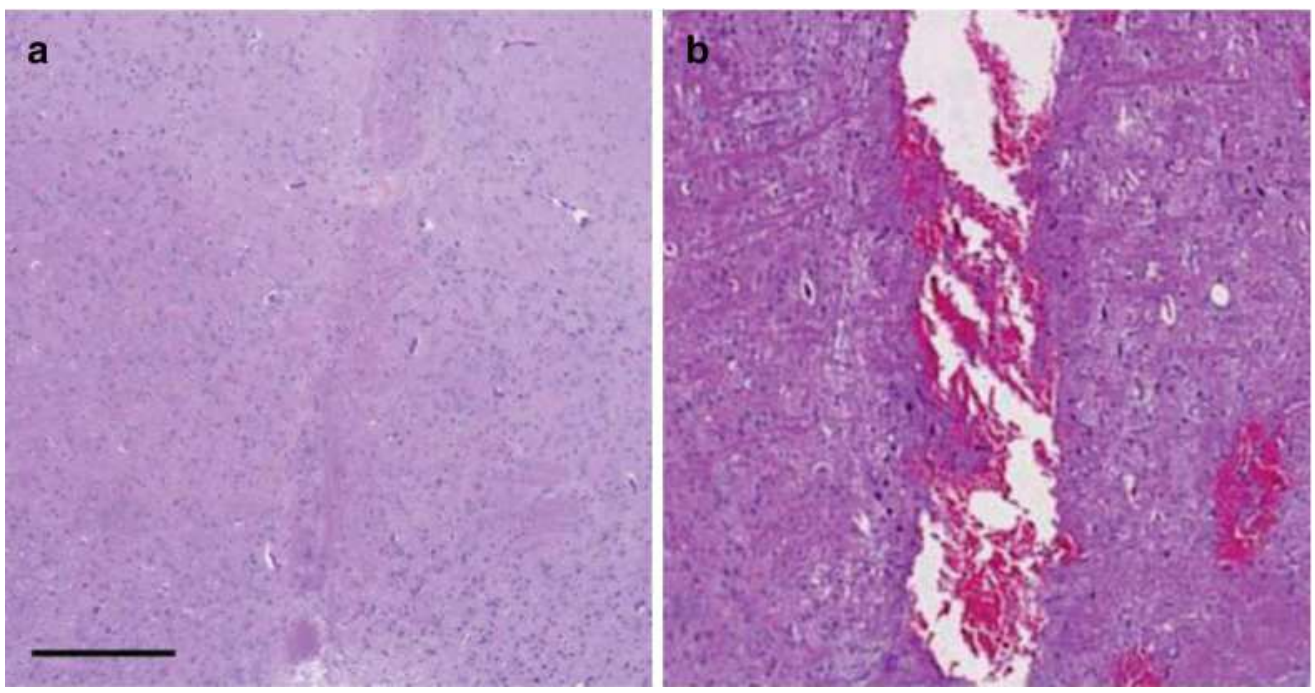

Fig. 23

Trauma received during probe insertion, via stained histology of cerebral tissue (**a**) 350-μm-diameter probe and (**b**) 1250-μm probe. Scale bar: 500 μm. Reprinted under CC BY 4.0 license from Kim et al. (2013b). Copyright © 2013 SPIE

Further histological and behavioral observations with needle-sheathed probes indicated apoptotic tissue damage due to the needle-sheathed probe heals over the course of a 2-week period, and that the impact of needle insertion into the thalamus or cerebrum on mouse behavior is negligible. Insertion into the cerebellum caused impairment in all mice, but behavior was restored after a 1-week period (Kim et al. 2013c).

In conclusion, the introduction of ultrathin side-view micro-endoscopy probes based on GRIN lenses has resulted in cellular resolution imaging of the brains of living mouse models of neurological disease at depths of more than 10 mm. The probes are minimally invasive and can be inserted with minimal trauma and, for some applications, without causing changes to behavioral patterns. These optical probes allow the researcher to quantify the density of active neurons and immune infiltration longitudinally and in vivo. Further observations of the cellular-level dynamics of the deep brain are promising for the unraveling of disease mechanisms, for developing diagnostic technologies, and for the treatment of neurodegeneration (Kim et al. 2013b, c; Fuhrmann et al. 2010). Further extensions to the imaging method include switching to near-infrared multiphoton excitation for increased imaging depth and developing protocols for the observation of other models based on other animals frequently used in neuroscience and pharmaceutical research.

Conclusion and Future Perspectives

The present review has demonstrated the design, fabrication, and myriad possibilities for the extension and application of endo-microscopic probes based on GRIN lenses. The probes are adaptable, and during the fabrication process may be optimized for front or side views, narrowed for minimal invasiveness, or reinforced for mechanical strength. Suction and gating techniques may be used to correct for large-amplitude autonomous tissue motion, while the combination with other diagnostic techniques and imaging systems may be used to reveal more detail about the behavior of tissues both at the cellular level and at the level of whole organs.

While we have tried to give a representative sampling of the applications of the GRIN micro-endoscope, our breadth has necessarily been limited. Nonfluorescent imaging modalities applying GRIN lens micro-endoscopes have not been discussed, nor have two-photon, three-photon, lifetime, or near-infrared microscopy been discussed. We hope that, when combined with the present techniques, these avenues may serve up a multitude of discoveries for the enterprising researcher, enabling them to approach important the deep unsolved questions concerning cellular-resolution phenomena deep in model animals that concern biology, medicine, and biomedical engineering.

Funding

This work was supported by the National Research Foundation of Korea (NRF) (2019R1A2C2084122, 2020R1F1A1074033) and MRC grant (2018R1A5A2020732) by the Ministry of Science & ICT (MSIT), and by a grant of the Korea Health Technology R&D Project through the Korea Health Industry Development Institute (KHIDI), funded by the Ministry of Health and Welfare, Republic of Korea (HI18C2391). This work was also supported by grant number 2021IP0017 from the Asan Institute for Life Sciences, Asan Medical Center, Seoul, Korea.

Notes

Acknowledgments

We thank Mark Myunghwan Choi and Woei-Ming Lee for technical assistance in microscopy; R. Colvin, C. Chase, H. Ploegh, R. Kucherlapati, K. Hung, Thomas Graf, Klaus Ley, and Adam Glick for generous gifts of transgenic mice and mouse models; Dr. Barry Stipp for providing antibodies; and C. Lin, D. Cote, L. Kaplan, M. Ferrari, and G.Y. Koh for discussions which contributed to previous versions of the component manuscripts.

References

Al-Khazraji BK, Medeiros PJ, Novielli NM, Jackson DN (2011) An automated cell-counting algorithm for fluorescently-stained cells in migration assays. Biol Proced Online 13:9
PubMed (http://www.ncbi.nlm.nih.gov/entrez/query.fcgi?cmd=Retrieve&db=PubMed&dopt=Abstract&list_uids=22011343)
PubMedCentral (http://www.ncbi.nlm.nih.gov/pmc/articles/PMC3214125)
CrossRef (https://doi.org/10.1186/1480-9222-13-9)
Google Scholar (http://scholar.google.com/scholar_lookup?title=An%20automated%20cell-counting%20algorithm%20for%20fluorescently-stained%20cells%20in%20migration%20assays&author=BK.%20Al-Khazraji&author=PJ.%20Medeiros&author=NM.%20Novielli&author=DN.%20Jackson&journal=Biol%20Proced%20Online&volume=13&pages=9&publication_year=2011)

Anversa P, Kajstura J, Leri A, Bolli R (2006) Life and death of cardiac stem cells: a paradigm shift in cardiac biology. Circulation 113:1451–1463
PubMed (http://www.ncbi.nlm.nih.gov/entrez/query.fcgi?cmd=Retrieve&db=PubMed&dopt=Abstract&list_uids=16549650)
CrossRef (https://doi.org/10.1161/CIRCULATIONAHA.105.595181)

PubMedCentral (http://www.ncbi.nlm.nih.gov/pmc/articles/PMC16549650)
Google Scholar (http://scholar.google.com/scholar_lookup?title=Life%20and%20death%20of%20cardiac%20stem%20cells%3A%20a%20paradigm%20shift%20in%20cardiac%20biology&author=P.%20Anversa&author=J.%20Kajstura&author=A.%20Leri&author=R.%20Bolli&journal=Circulation&volume=113&pages=1451-1463&publication_year=2006)

Arumugam TV et al (2006) Gamma secretase–mediated Notch signaling worsens brain damage and functional outcome in ischemic stroke. Nat Med 12:621–623
PubMed (http://www.ncbi.nlm.nih.gov/entrez/query.fcgi?cmd=Retrieve&db=PubMed&dopt=Abstract&list_uids=16680150)
CrossRef (https://doi.org/10.1038/nm1403)
PubMedCentral (http://www.ncbi.nlm.nih.gov/pmc/articles/PMC16680150)
Google Scholar (http://scholar.google.com/scholar_lookup?title=Gamma%20secretase%E2%80%93mediated%20Notch%20signaling%20worsens%20brain%20damage%20and%20functional%20outcome%20in%20ischemic%20stroke&author=TV.%20Arumugam&journal=Nat%20Med&volume=12&pages=621-623&publication_year=2006)

Barretto RPJ, Messerschmidt B, Schnitzer MJ (2009) In vivo fluorescence imaging with high-resolution microlenses. Nat Methods 6:511–512
PubMed (http://www.ncbi.nlm.nih.gov/entrez/query.fcgi?cmd=Retrieve&db=PubMed&dopt=Abstract&list_uids=19525959)
PubMedCentral (http://www.ncbi.nlm.nih.gov/pmc/articles/PMC2849805)
CrossRef (https://doi.org/10.1038/nmeth.1339)
Google Scholar (http://scholar.google.com/scholar_lookup?title=In%20vivo%20fluorescence%20imaging%20with%20high-resolution%20microlenses&author=RPJ.%20Barretto&author=B.%20Messerschmidt&author=MJ.%20Schnitzer&journal=Nat%20Methods&volume=6&pages=511-512&publication_year=2009)

Barretto RPJ et al (2011) Time-lapse imaging of disease progression in deep brain areas using fluorescence microendoscopy. Nat Med 17:223–228
PubMed (http://www.ncbi.nlm.nih.gov/entrez/query.fcgi?cmd=Retrieve&db=PubMed&dopt=Abstract&list_uids=21240263)
PubMedCentral (http://www.ncbi.nlm.nih.gov/pmc/articles/PMC3833825)
CrossRef (https://doi.org/10.1038/nm.2292)
Google Scholar (http://scholar.google.com/scholar_lookup?title=Time-lapse%20imaging%20of%20disease%20progression%20in%20deep%20brain%20areas%20using%20fluorescence%20microendoscopy&author=RPJ.%20Barretto&journal=Nat%20Med&volume=17&pages=223-228&publication_year=2011)

Becker C, Fantini MC, Neurath MF (2007) High resolution colonoscopy in live mice. Nat Protoc 1:2900–2904
CrossRef (https://doi.org/10.1038/nprot.2006.446)
Google Scholar (http://scholar.google.com/scholar_lookup?title=High%20resolution%20colonoscopy%20in%20live%20mice&author=C.%20Becker&author=MC.%20Fantini&author=MF.%20Neurath&journal=Nat%20Protoc&volume=1&pages=2900-2904&publication_year=2007)

Beni-Adani L et al (2001) A peptide derived from activity-dependent neuroprotective protein (ADNP) ameliorates injury response in closed head injury in mice. J Pharmacol Exp Ther 296:57–63
PubMed (http://www.ncbi.nlm.nih.gov/entrez/query.fcgi?cmd=Retrieve&db=PubMed&dopt=Abstract&list_uids=11123362)
PubMedCentral (http://www.ncbi.nlm.nih.gov/pmc/articles/PMC11123362)
Google Scholar (http://scholar.google.com/scholar_lookup?title=A%20peptide%20derived%20from%20activity-dependent%20neuroprotective%20protein%20%28ADNP%29%20ameliorates%20injury%20response%20in%20closed%20head%20injury%20in%20mice&author=L.%20Beni-Adani&journal=J%20Pharmacol%20Exp%20Ther&volume=296&pages=57-63&publication_year=2001)

Birder L, Andersson K-E (2018) Animal modelling of interstitial cystitis/bladder pain syndrome. Int Neurourol J 22:S3–S9
PubMed (http://www.ncbi.nlm.nih.gov/entrez/query.fcgi?cmd=Retrieve&db=PubMed&dopt=Abstract&list_uids=29385788)
PubMedCentral (http://www.ncbi.nlm.nih.gov/pmc/articles/PMC5798638)
CrossRef (https://doi.org/10.5213/inj.1835062.531)
Google Scholar (http://scholar.google.com/scholar_lookup?title=Animal%20modelling%20of%20interstitial%20cystitis%2Fbladder%20pain%20syndrome&author=L.%20Birder&author=K-E.%20Andersson&journal=Int%20Neurourol%20J&volume=22&pages=S3-S9&publication_year=2018)

Bociort F (1994) Imaging properties of gradient-index lenses. Berichte der Technischen Optik, (Koester, 1994)
Google Scholar (https://scholar.google.com/scholar?q=Bociort%20F%20%281994%29%20Imaging%20properties%20of%20gradient-index%20lenses.%20Berichte%20der%20Technischen%20Optik%2C%20%28Koester%2C%201994%29)

Chien KR, Domian IJ, Parker KK (2008) Cardiogenesis and the complex biology of regenerative cardiovascular medicine. Science 322:1494–1497
PubMed (http://www.ncbi.nlm.nih.gov/entrez/query.fcgi?cmd=Retrieve&db=PubMed&dopt=Abstract&list_uids=19056974)
CrossRef (https://doi.org/10.1126/science.1163267)
PubMedCentral (http://www.ncbi.nlm.nih.gov/pmc/articles/PMC19056974)
Google Scholar (http://scholar.google.com/scholar_lookup?title=Cardiogenesis%20and%20the%20complex%20biology%20of%20regenerative%20cardiovascular%20medicine&author=KR.%20Chien&author=IJ.%20Domian&author=KK.%20Parker&journal=Science&volume=322&pages=1494-1497&publication_year=2008)

Chilian WM, Eastham CL, Marcus ML (1986) Microvascular distribution of coronary vascular resistance in beating left ventricle. Am J Physiol-Heart Circ Physiol 251:H779–H788
CrossRef (https://doi.org/10.1152/ajpheart.1986.251.4.H779)
Google Scholar (http://scholar.google.com/scholar_lookup?title=Microvascular%20distribution%20of%20coronary%20vascular%20resistance%20in%20beating%20left%20ventricle&

author=WM.%20Chilian&author=CL.%20Eastham&author=ML.%20Marcus&journal=Am%20J%20Physiol-Heart%20Circ%20Physiol&volume=251&pages=H779-H788&publication_year=1986)

Choi JW, Kim JK, Choi M, Kim YR, Yun SH (2014) In vivo imaging of Lgr5-positive cell populations using confocal laser endomicroscopy during early colon tumorigenesis. Endoscopy 46:1110–1116
PubMed (http://www.ncbi.nlm.nih.gov/entrez/query.fcgi?cmd=Retrieve&db=PubMed&dopt=Abstract&list_uids=25216325)
PubMedCentral (http://www.ncbi.nlm.nih.gov/pmc/articles/PMC4403755)
CrossRef (https://doi.org/10.1055/s-0034-1377631)
Google Scholar (http://scholar.google.com/scholar_lookup?title=In%20vivo%20imaging%20of%20Lgr5-positive%20cell%20populations%20using%20confocal%20laser%20endomicroscopy%20during%20early%20colon%20tumorigenesis&author=JW.%20Choi&author=JK.%20Kim&author=M.%20Choi&author=YR.%20Kim&author=SH.%20Yun&journal=Endoscopy&volume=46&pages=1110-1116&publication_year=2014)

Chudnovsky Y, Khavari PA, Adams AE (2005) Melanoma genetics and the development of rational therapeutics. J Clin Invest 115:813–824
PubMed (http://www.ncbi.nlm.nih.gov/entrez/query.fcgi?cmd=Retrieve&db=PubMed&dopt=Abstract&list_uids=15841168)
PubMedCentral (http://www.ncbi.nlm.nih.gov/pmc/articles/PMC1070435)
CrossRef (https://doi.org/10.1172/JCI24808)
Google Scholar (http://scholar.google.com/scholar_lookup?title=Melanoma%20genetics%20and%20the%20development%20of%20rational%20therapeutics&author=Y.%20Chudnovsky&author=PA.%20Khavari&author=AE.%20Adams&journal=J%20Clin%20Invest&volume=115&pages=813-824&publication_year=2005)

Cortez-Retamozo V et al (2008) Real-time assessment of inflammation and treatment response in a mouse model of allergic airway inflammation. J Clin Invest 118:4058–4066
PubMed (http://www.ncbi.nlm.nih.gov/entrez/query.fcgi?cmd=Retrieve&db=PubMed&dopt=Abstract&list_uids=19033674)
PubMedCentral (http://www.ncbi.nlm.nih.gov/pmc/articles/PMC2579705)
CrossRef (https://doi.org/10.1172/JCI36335)
Google Scholar (http://scholar.google.com/scholar_lookup?title=Real-time%20assessment%20of%20inflammation%20and%20treatment%20response%20in%20a%20mouse%20model%20of%20allergic%20airway%20inflammation&author=V.%20Cortez-Retamozo&journal=J%20Clin%20Invest&volume=118&pages=4058-4066&publication_year=2008)

Cosenza S et al (2018) Mesenchymal stem cells-derived exosomes are more immunosuppressive than microparticles in inflammatory arthritis. Theranostics 8:1399–1410
PubMed (http://www.ncbi.nlm.nih.gov/entrez/query.fcgi?cmd=Retrieve&db=PubMed&dopt=Abstract&list_uids=29507629)
PubMedCentral (http://www.ncbi.nlm.nih.gov/pmc/articles/PMC5835945)
CrossRef (https://doi.org/10.7150/thno.21072)
Google Scholar (http://scholar.google.com/scholar_lookup?title=Mesenchymal%20stem%20cells-derived%20exosomes%20are%20more%20immunosuppressive%20than%20microparticles%20in%20inflammatory%20arthritis&author=S.%20Cosenza&journal=Theranostics&volume=8&pages=1399-1410&publication_year=2018)

del Río AD, Gómez-Reino C, Flores-Arias MT (2015) Third-order aberrations in GRIN crystalline lens: a new method based on axial and field rays. J Optom 8:77–85
PubMed (http://www.ncbi.nlm.nih.gov/entrez/query.fcgi?cmd=Retrieve&db=PubMed&dopt=Abstract&list_uids=25444647)
CrossRef (https://doi.org/10.1016/j.optom.2014.09.003)
PubMedCentral (http://www.ncbi.nlm.nih.gov/pmc/articles/PMC25444647)
Google Scholar (http://scholar.google.com/scholar_lookup?title=Third-order%20aberrations%20in%20GRIN%20crystalline%20lens%3A%20a%20new%20method%20based%20on%20axial%20and%20field%20rays&author=AD.%20R%C3%ADo&author=C.%20G%C3%B3mez-Reino&author=MT.%20Flores-Arias&journal=J%20Optom&volume=8&pages=77-85&publication_year=2015)

Dela Cruz JM, McMullen JD, Williams RM, Zipfel WR (2010) Feasibility of using multiphoton excited tissue autofluorescence for in vivo human histopathology. Biomed Opt Express 1:1320
CrossRef (https://doi.org/10.1364/BOE.1.001320)
Google Scholar (http://scholar.google.com/scholar_lookup?title=Feasibility%20of%20using%20multiphoton%20excited%20tissue%20autofluorescence%20for%20in%20vivo%20human%20histopathology&author=JM.%20Cruz&author=JD.%20McMullen&author=RM.%20Williams&author=WR.%20Zipfel&journal=Biomed%20Opt%20Express&volume=1&pages=1320&publication_year=2010)

Eriksson EE (2011) Intravital microscopy on atherosclerosis in apolipoprotein E-deficient mice establishes microvessels as major entry pathways for leukocytes to advanced lesions. Circulation 124, CIRCULATIONAHA-111
Google Scholar (https://scholar.google.com/scholar?q=Eriksson%20EE%20%282011%29%20Intravital%20microscopy%20on%20atherosclerosis%20in%20apolipoprotein%20E-deficient%20mice%20establishes%20microvessels%20as%20major%20entry%20pathways%20for%20leukocytes%20to%20advanced%20lesions.%20Circulation%20124%2C%20CIRCULATIONAHA-111)

Fan Z et al (2010) In vivo tracking of ‘color-coded’ effector, natural and induced regulatory T cells in the allograft response. Nat Med 16:718–722
PubMed (http://www.ncbi.nlm.nih.gov/entrez/query.fcgi?cmd=Retrieve&db=PubMed&dopt=Abstract&list_uids=20495571)
PubMedCentral (http://www.ncbi.nlm.nih.gov/pmc/articles/PMC2894571)
CrossRef (https://doi.org/10.1038/nm.2155)
Google Scholar (http://scholar.google.com/scholar_lookup?title=In%20vivo%20tracking%20of%20%E2%80%98color-coded%E2%80%99%20effector%2C%20natural%20and%20induced%20regulatory%20T%20cells%20in%20the%20allograft%20response&author=Z.%20Fan&journal=Nat%20Med&volume=16&pages=718-722&publication_year=2010)

Feiden W, Steude U, Bise K, Gündisch O (1991) Accuracy of stereotactic brain tumor biopsy: comparison of the histologic findings in biopsy cylinders and resected tumor tissue. Neurosurg Rev 14:51–56

PubMed (http://www.ncbi.nlm.nih.gov/entrez/query.fcgi?cmd=Retrieve&db=PubMed&dopt=Abstract&list_uids=2030827)
PubMedCentral (http://www.ncbi.nlm.nih.gov/pmc/articles/PMC2030827)
Google Scholar (http://scholar.google.com/scholar_lookup?title=Accuracy%20of%20stereotactic%20brain%20tumor%20biopsy%3A%20comparison%20of%20the%20histologic%20findings%20in%20biopsy%20cylinders%20and%20resected%20tumor%20tissue&author=W.%20Feiden&author=U.%20Steude&author=K.%20Bise&author=O.%20G%C3%BCndisch&journal=Neurosurg%20Rev&volume=14&pages=51-56&publication_year=1991)

Feng Y et al (2016) A comparison of a fully covered and an uncovered segmented biodegradable esophageal stent in a porcine model: preclinical evaluation of degradation, complications, and tissue reactions. Gastroenterol Res Pract 2016:1–7
CrossRef (https://doi.org/10.1155/2016/8690858)
Google Scholar (http://scholar.google.com/scholar_lookup?title=A%20comparison%20of%20a%20fully%20covered%20and%20an%20uncovered%20segmented%20biodegradable%20oesophageal%20stent%20in%20a%20porcine%20model%3A%20preclinical%20evaluation%20of%20degradation%2C%20complications%2C%20and%20tissue%20reactions&author=Y.%20Feng&journal=Gastroenterol%20Res%20Pract&volume=2016&pages=1-7&publication_year=2016)

Flusberg BA et al (2005) Fiber-optic fluorescence imaging. Nat Methods 2:941–950
PubMed (http://www.ncbi.nlm.nih.gov/entrez/query.fcgi?cmd=Retrieve&db=PubMed&dopt=Abstract&list_uids=16299479)
PubMedCentral (http://www.ncbi.nlm.nih.gov/pmc/articles/PMC2849801)
CrossRef (https://doi.org/10.1038/nmeth820)
Google Scholar (http://scholar.google.com/scholar_lookup?title=Fiber-optic%20fluorescence%20imaging&author=BA.%20Flusberg&journal=Nat%20Methods&volume=2&pages=941-950&publication_year=2005)

Frangogiannis N (2006) Targeting the inflammatory response in healing myocardial infarcts. Curr Med Chem 13:1877–1893
PubMed (http://www.ncbi.nlm.nih.gov/entrez/query.fcgi?cmd=Retrieve&db=PubMed&dopt=Abstract&list_uids=16842199)
CrossRef (https://doi.org/10.2174/092986706777585086)
PubMedCentral (http://www.ncbi.nlm.nih.gov/pmc/articles/PMC16842199)
Google Scholar (http://scholar.google.com/scholar_lookup?title=Targeting%20the%20inflammatory%20response%20in%20healing%20myocardial%20infarcts&author=N.%20Frangogiannis&journal=Curr%20Med%20Chem&volume=13&pages=1877-1893&publication_year=2006)

Fuhrmann M et al (2010) Microglial Cx3cr1 knockout prevents neuron loss in a mouse model of Alzheimer's disease. Nat Neurosci 13:411–413
PubMed (http://www.ncbi.nlm.nih.gov/entrez/query.fcgi?cmd=Retrieve&db=PubMed&dopt=Abstract&list_uids=20305648)
PubMedCentral (http://www.ncbi.nlm.nih.gov/pmc/articles/PMC4072212)
CrossRef (https://doi.org/10.1038/nn.2511)
Google Scholar (http://scholar.google.com/scholar_lookup?title=Microglial%20Cx3cr1%20knockout%20prevents%20neuron%20loss%20in%20a%20mouse%20model%20of%20Alzheimer%E2%80%99s%20disease&author=M.%20Fuhrmann&journal=Nat%20Neurosci&volume=13&pages=411-413&publication_year=2010)

Fujisaki J et al (2011) In vivo imaging of Treg cells providing immune privilege to the haematopoietic stem-cell niche. Nature 474:216–219
PubMed (http://www.ncbi.nlm.nih.gov/entrez/query.fcgi?cmd=Retrieve&db=PubMed&dopt=Abstract&list_uids=21654805)
PubMedCentral (http://www.ncbi.nlm.nih.gov/pmc/articles/PMC3725645)
CrossRef (https://doi.org/10.1038/nature10160)
Google Scholar (http://scholar.google.com/scholar_lookup?title=In%20vivo%20imaging%20of%20Treg%20cells%20providing%20immune%20privilege%20to%20the%20haematopoietic%20stem-cell%20niche&author=J.%20Fujisaki&journal=Nature&volume=474&pages=216-219&publication_year=2011)

Gelderblom M et al (2009) Temporal and spatial dynamics of cerebral immune cell accumulation in stroke. Stroke 40:1849–1857
PubMed (http://www.ncbi.nlm.nih.gov/entrez/query.fcgi?cmd=Retrieve&db=PubMed&dopt=Abstract&list_uids=19265055)
CrossRef (https://doi.org/10.1161/STROKEAHA.108.534503)
PubMedCentral (http://www.ncbi.nlm.nih.gov/pmc/articles/PMC19265055)
Google Scholar (http://scholar.google.com/scholar_lookup?title=Temporal%20and%20spatial%20dynamics%20of%20cerebral%20immune%20cell%20accumulation%20in%20stroke&author=M.%20Gelderblom&journal=Stroke&volume=40&pages=1849-1857&publication_year=2009)

Göbel W, Kerr JND, Nimmerjahn A, Helmchen F (2004) Miniaturized two-photon microscope based on a flexible coherent fiber bundle and a gradient-index lens objective. Opt Lett 29:2521
PubMed (http://www.ncbi.nlm.nih.gov/entrez/query.fcgi?cmd=Retrieve&db=PubMed&dopt=Abstract&list_uids=15584281)
CrossRef (https://doi.org/10.1364/OL.29.002521)
PubMedCentral (http://www.ncbi.nlm.nih.gov/pmc/articles/PMC15584281)
Google Scholar (http://scholar.google.com/scholar_lookup?title=Miniaturized%20two-photon%20microscope%20based%20on%20a%20flexible%20coherent%20fiber%20bundle%20and%20a%20gradient-index%20lens%20objective&author=W.%20G%C3%B6bel&author=JND.%20Kerr&author=A.%20Nimmerjahn&author=F.%20Helmchen&journal=Opt%20Lett&volume=29&pages=2521&publication_year=2004)

Greenberg DS, Kerr JND (2009) Automated correction of fast motion artifacts for two-photon imaging of awake animals. J Neurosci Methods 176:1–15
PubMed (http://www.ncbi.nlm.nih.gov/entrez/query.fcgi?cmd=Retrieve&db=PubMed&dopt=Abstract&list_uids=18789968)
CrossRef (https://doi.org/10.1016/j.jneumeth.2008.08.020)

PubMedCentral (http://www.ncbi.nlm.nih.gov/pmc/articles/PMC18789968)
Google Scholar (http://scholar.google.com/scholar_lookup?title=Automated%20correction%20of%20fast%20motion%20artifacts%20for%20two-photon%20imaging%20of%20awake%20animals&author=DS.%20Greenberg&author=JND.%20Kerr&journal=J%20Neurosci%20Methods&volume=176&pages=1-15&publication_year=2009)

Guizar-Sicairos M, Thurman ST, Fienup JR (2008) Efficient subpixel image registration algorithms. Opt Lett 33:156
PubMed (http://www.ncbi.nlm.nih.gov/entrez/query.fcgi?cmd=Retrieve&db=PubMed&dopt=Abstract&list_uids=18197224)
CrossRef (https://doi.org/10.1364/OL.33.000156)
PubMedCentral (http://www.ncbi.nlm.nih.gov/pmc/articles/PMC18197224)
Google Scholar (http://scholar.google.com/scholar_lookup?title=Efficient%20subpixel%20image%20registration%20algorithms&author=M.%20Guizar-Sicairos&author=ST.%20Thurman&author=JR.%20Fienup&journal=Opt%20Lett&volume=33&pages=156&publication_year=2008)

Hara A, Niwa M, Yoshimi N, Mori H (1997) Apoptotic cell death in vulnerable subpopulation of cerebellar granule cells. Acta Neuropathol. (Berl.) 94:517–518
CrossRef (https://doi.org/10.1007/s004010050744)
Google Scholar (http://scholar.google.com/scholar_lookup?title=Apoptotic%20cell%20death%20in%20vulnerable%20subpopulation%20of%20cerebellar%20granule%20cells&author=A.%20Hara&author=M.%20Niwa&author=N.%20Yoshimi&author=H.%20Mori&journal=Acta%20Neuropathol.%20%28Berl.%29&volume=94&pages=517-518&publication_year=1997)

Helmchen F, Denk W (2005) Deep tissue two-photon microscopy. Nat Methods 2:932–940
PubMed (http://www.ncbi.nlm.nih.gov/entrez/query.fcgi?cmd=Retrieve&db=PubMed&dopt=Abstract&list_uids=16299478)
CrossRef (https://doi.org/10.1038/nmeth818)
PubMedCentral (http://www.ncbi.nlm.nih.gov/pmc/articles/PMC16299478)
Google Scholar (http://scholar.google.com/scholar_lookup?title=Deep%20tissue%20two-photon%20microscopy&author=F.%20Helmchen&author=W.%20Denk&journal=Nat%20Methods&volume=2&pages=932-940&publication_year=2005)

Holtmaat A et al (2009) Long-term, high-resolution imaging in the mouse neocortex through a chronic cranial window. Nat Protoc 4:1128–1144
PubMed (http://www.ncbi.nlm.nih.gov/entrez/query.fcgi?cmd=Retrieve&db=PubMed&dopt=Abstract&list_uids=3072839)
PubMedCentral (http://www.ncbi.nlm.nih.gov/pmc/articles/PMC3072839)
CrossRef (https://doi.org/10.1038/nprot.2009.89)
Google Scholar (http://scholar.google.com/scholar_lookup?title=Long-term%2C%20high-resolution%20imaging%20in%20the%20mouse%20neocortex%20through%20a%20chronic%20cranial%20window&author=A.%20Holtmaat&journal=Nat%20Protoc&volume=4&pages=1128-1144&publication_year=2009)

Hong K-S et al (2015) A porous membrane-mediated isolation of mesenchymal stem cells from human embryonic stem cells. Tissue Eng Part C Methods 21:322–329
PubMed (http://www.ncbi.nlm.nih.gov/entrez/query.fcgi?cmd=Retrieve&db=PubMed&dopt=Abstract&list_uids=25190318)
CrossRef (https://doi.org/10.1089/ten.tec.2014.0171)
PubMedCentral (http://www.ncbi.nlm.nih.gov/pmc/articles/PMC25190318)
Google Scholar (http://scholar.google.com/scholar_lookup?title=A%20porous%20membrane-mediated%20isolation%20of%20mesenchymal%20stem%20cells%20from%20human%20embryonic%20stem%20cells&author=K-S.%20Hong&journal=Tissue%20Eng%20Part%20C%20Methods&volume=21&pages=322-329&publication_year=2015)

Hsiung P-L et al (2008) Detection of colonic dysplasia in vivo using a targeted heptapeptide and confocal microendoscopy. Nat Med 14:454–458
PubMed (http://www.ncbi.nlm.nih.gov/entrez/query.fcgi?cmd=Retrieve&db=PubMed&dopt=Abstract&list_uids=18345013)
PubMedCentral (http://www.ncbi.nlm.nih.gov/pmc/articles/PMC3324975)
CrossRef (https://doi.org/10.1038/nm1692)
Google Scholar (http://scholar.google.com/scholar_lookup?title=Detection%20of%20colonic%20dysplasia%20in%20vivo%20using%20a%20targeted%20heptapeptide%20and%20confocal%20microendoscopy&author=P-L.%20Hsiung&journal=Nat%20Med&volume=14&pages=454-458&publication_year=2008)

Ieda M et al (2010) Direct reprogramming of fibroblasts into functional cardiomyocytes by defined factors. Cell 149:375–387
CrossRef (https://doi.org/10.1016/j.cell.2010.07.002)
Google Scholar (http://scholar.google.com/scholar_lookup?title=Direct%20reprogramming%20of%20fibroblasts%20into%20functional%20cardiomyocytes%20by%20defined%20factors&author=M.%20Ieda&journal=Cell&volume=149&pages=375-387&publication_year=2010)

Iwano M et al (2002) Evidence that fibroblasts derive from epithelium during tissue fibrosis. J Clin Invest 110:341–350
PubMed (http://www.ncbi.nlm.nih.gov/entrez/query.fcgi?cmd=Retrieve&db=PubMed&dopt=Abstract&list_uids=12163453)
PubMedCentral (http://www.ncbi.nlm.nih.gov/pmc/articles/PMC151091)
CrossRef (https://doi.org/10.1172/JCI0215518)
Google Scholar (http://scholar.google.com/scholar_lookup?title=Evidence%20that%20fibroblasts%20derive%20from%20epithelium%20during%20tissue%20fibrosis&author=M.%20Iwano&journal=J%20Clin%20Invest&volume=110&pages=341-350&publication_year=2002)

Jun EJ et al (2017) EW-7197, an activin-like kinase 5 inhibitor, suppresses granulation tissue after stent placement in rat esophagus. Gastrointest Endosc 86:219–228
PubMed (http://www.ncbi.nlm.nih.gov/entrez/query.fcgi?cmd=Retrieve&db=PubMed&dopt=Abstract&list_uids=28137596)
CrossRef (https://doi.org/10.1016/j.gie.2017.01.013)

PubMedCentral (http://www.ncbi.nlm.nih.gov/pmc/articles/PMC28137596)
Google Scholar (http://scholar.google.com/scholar_lookup?title=EW-7197%2C%20an%20activin-like%20kinase%205%20inhibitor%2C%20suppresses%20granulation%20tissue%20after%20stent%20placement%20in%20rat%20esophagus&author=EJ.%20Jun&journal=Gastrointest%20Endosc&volume=86&pages=219-228&publication_year=2017)

Jun EJ et al (2018) In vivo fluorescence microendoscopic monitoring of stent-induced fibroblast cell proliferation in an esophageal mouse model. J Vasc Interv Radiol 29:1756–1763
PubMed (http://www.ncbi.nlm.nih.gov/entrez/query.fcgi?cmd=Retrieve&db=PubMed&dopt=Abstract&list_uids=30266211)
CrossRef (https://doi.org/10.1016/j.jvir.2018.06.024)
PubMedCentral (http://www.ncbi.nlm.nih.gov/pmc/articles/PMC30266211)
Google Scholar (http://scholar.google.com/scholar_lookup?title=In%20vivo%20fluorescence%20microendoscopic%20monitoring%20of%20stent-induced%20fibroblast%20cell%20proliferation%20in%20an%20esophageal%20mouse%20model&author=EJ.%20Jun&journal=J%20Vasc%20Interv%20Radiol&volume=29&pages=1756-1763&publication_year=2018)

Jung JC, Schnitzer MJ (2003) Multiphoton endoscopy. Opt Lett 28:902–904
PubMed (http://www.ncbi.nlm.nih.gov/entrez/query.fcgi?cmd=Retrieve&db=PubMed&dopt=Abstract&list_uids=12816240)
CrossRef (https://doi.org/10.1364/OL.28.000902)
PubMedCentral (http://www.ncbi.nlm.nih.gov/pmc/articles/PMC12816240)
Google Scholar (http://scholar.google.com/scholar_lookup?title=Multiphoton%20endoscopy&author=JC.%20Jung&author=MJ.%20Schnitzer&journal=Opt%20Lett&volume=28&pages=902-904&publication_year=2003)

Jung K et al (2013) Endoscopic time-lapse imaging of immune cells in infarcted mouse hearts. Circ Res 112:891–899
PubMed (http://www.ncbi.nlm.nih.gov/entrez/query.fcgi?cmd=Retrieve&db=PubMed&dopt=Abstract&list_uids=23392842)
CrossRef (https://doi.org/10.1161/CIRCRESAHA.111.300484)
PubMedCentral (http://www.ncbi.nlm.nih.gov/pmc/articles/PMC23392842)
Google Scholar (http://scholar.google.com/scholar_lookup?title=Endoscopic%20time-lapse%20imaging%20of%20immune%20cells%20in%20infarcted%20mouse%20hearts&author=K.%20Jung&journal=Circ%20Res&volume=112&pages=891-899&publication_year=2013)

Eric R Kandel (2000) Principles of neural science. McGraw-Hill, Health Professions Division
Google Scholar (https://scholar.google.com/scholar?q=Eric%20R%20Kandel%20%282000%29%20Principles%20of%20neural%20science.%20McGraw-Hill%2C%20Health%20Professions%20Division)

Kavet RI, Brain JD (1974) Minireview reaction of the lung to air pollutant exposure. Life Sci 15:849–861
PubMed (http://www.ncbi.nlm.nih.gov/entrez/query.fcgi?cmd=Retrieve&db=PubMed&dopt=Abstract&list_uids=4620968)
CrossRef (https://doi.org/10.1016/0024-3205(74)90002-2)
PubMedCentral (http://www.ncbi.nlm.nih.gov/pmc/articles/PMC4620968)
Google Scholar (http://scholar.google.com/scholar_lookup?title=Minireview%20reaction%20of%20the%20lung%20to%20air%20pollutant%20exposure&author=RI.%20Kavet&author=JD.%20Brain&journal=Life%20Sci&volume=15&pages=849-861&publication_year=1974)

Kim A, Shin D-M Choo M-S (2016a) Stem cell therapy for interstitial cystitis/bladder pain syndrome. Curr Urol Rep 17
Google Scholar (https://scholar.google.com/scholar?q=Kim%20A%2C%20Shin%20D-M%20Choo%20M-S%20%282016a%29%20Stem%20cell%20therapy%20for%20interstitial%20cystitis%2Fbladder%20pain%20syndrome.%20Curr%20Urol%20Rep%2017)

Kim A et al (2016b) Mesenchymal stem cells protect against the tissue fibrosis of ketamine-induced cystitis in rat bladder. Sci Rep 6:30881
PubMed (http://www.ncbi.nlm.nih.gov/entrez/query.fcgi?cmd=Retrieve&db=PubMed&dopt=Abstract&list_uids=27481042)
PubMedCentral (http://www.ncbi.nlm.nih.gov/pmc/articles/PMC4969614)
CrossRef (https://doi.org/10.1038/srep30881)
Google Scholar (http://scholar.google.com/scholar_lookup?title=Mesenchymal%20stem%20cells%20protect%20against%20the%20tissue%20fibrosis%20of%20ketamine-induced%20cystitis%20in%20rat%20bladder&author=A.%20Kim&journal=Sci%20Rep&volume=6&publication_year=2016)

Kim A et al (2017) Improved efficacy and in vivo cellular properties of human embryonic stem cell derivative in a preclinical model of bladder pain syndrome. Sci Rep 7:8872
PubMed (http://www.ncbi.nlm.nih.gov/entrez/query.fcgi?cmd=Retrieve&db=PubMed&dopt=Abstract&list_uids=28827631)
PubMedCentral (http://www.ncbi.nlm.nih.gov/pmc/articles/PMC5567131)
CrossRef (https://doi.org/10.1038/s41598-017-09330-x)
Google Scholar (http://scholar.google.com/scholar_lookup?title=Improved%20efficacy%20and%20in%20vivo%20cellular%20properties%20of%20human%20embryonic%20stem%20cell%20derivative%20in%20a%20preclinical%20model%20of%20bladder%20pain%20syndrome&author=A.%20Kim&journal=Sci%20Rep&volume=7&pages=8872&publication_year=2017)

Kim DY et al (2019) Lissajous scanning two-photon endomicroscope for in vivo tissue imaging. Sci Rep 9:3560
PubMed (http://www.ncbi.nlm.nih.gov/entrez/query.fcgi?cmd=Retrieve&db=PubMed&dopt=Abstract&list_uids=30837501)
PubMedCentral (http://www.ncbi.nlm.nih.gov/pmc/articles/PMC6401070)
CrossRef (https://doi.org/10.1038/s41598-019-38762-w)
Google Scholar (http://scholar.google.com/scholar_lookup?title=Lissajous%20scanning%20two-photon%20endomicroscope%20for%20in%20vivo%20tissue%20imaging&author=DY.%20Kim&journal=Sci%20Rep&volume=9&pages=3560&publication_year=2019)

Kim E-Y, Shin JH, Jung YY, Shin D-H, Song H-Y (2010b) A rat esophageal model to investigate stent-induced tissue hyperplasia. J Vasc Interv Radiol 21:1287–1291
PubMed (http://www.ncbi.nlm.nih.gov/entrez/query.fcgi?cmd=Retrieve&db=PubMed&dopt=Abstract&list_uids=20656225)
CrossRef (https://doi.org/10.1016/j.jvir.2010.04.023)
PubMedCentral (http://www.ncbi.nlm.nih.gov/pmc/articles/PMC20656225)
Google Scholar (http://scholar.google.com/scholar_lookup?title=A%20rat%20esophageal%20model%20to%20investigate%20stent-induced%20tissue%20hyperplasia&author=E-Y.%20Kim&author=JH.%20Shin&author=YY.%20Jung&author=D-H.%20Shin&author=H-Y.%20Song&journal=J%20Vasc%20Interv%20Radiol&volume=21&pages=1287-1291&publication_year=2010)

Kim E-Y et al (2013a) IN-1233-eluting covered metallic stent to prevent hyperplasia: experimental study in a rabbit esophageal model. Radiology 267:396–404
PubMed (http://www.ncbi.nlm.nih.gov/entrez/query.fcgi?cmd=Retrieve&db=PubMed&dopt=Abstract&list_uids=23315658)
CrossRef (https://doi.org/10.1148/radiol.12120361)
PubMedCentral (http://www.ncbi.nlm.nih.gov/pmc/articles/PMC23315658)
Google Scholar (http://scholar.google.com/scholar_lookup?title=IN-1233-eluting%20covered%20metallic%20stent%20to%20prevent%20hyperplasia%3A%20experimental%20study%20in%20a%20rabbit%20esophageal%20model&author=E-Y.%20Kim&journal=Radiology&volume=267&pages=396-404&publication_year=2013)

Kim JH et al (2007) Benign tracheobronchial strictures: long-term results and factors affecting airway patency after temporary stent placement. Am J Roentgenol 188:1033–1038
CrossRef (https://doi.org/10.2214/AJR.06.0888)
Google Scholar (http://scholar.google.com/scholar_lookup?title=Benign%20tracheobronchial%20strictures%3A%20long-term%20results%20and%20factors%20affecting%20airway%20patency%20after%20temporary%20stent%20placement&author=JH.%20Kim&journal=Am%20J%20Roentgenol&volume=188&pages=1033-1038&publication_year=2007)

Kim JH et al (2009) Temporary metallic stent placement in the treatment of refractory benign esophageal strictures: results and factors associated with outcome in 55 patients. Eur Radiol 19:384–390
PubMed (http://www.ncbi.nlm.nih.gov/entrez/query.fcgi?cmd=Retrieve&db=PubMed&dopt=Abstract&list_uids=18726598)
CrossRef (https://doi.org/10.1007/s00330-008-1151-2)
PubMedCentral (http://www.ncbi.nlm.nih.gov/pmc/articles/PMC18726598)
Google Scholar (http://scholar.google.com/scholar_lookup?title=Temporary%20metallic%20stent%20placement%20in%20the%20treatment%20of%20refractory%20benign%20esophageal%20strictures%3A%20results%20and%20factors%20associated%20with%20outcome%20in%2055%20patients&author=JH.%20Kim&journal=Eur%20Radiol&volume=19&pages=384-390&publication_year=2009)

Kim JK et al (2012a) Fabrication and operation of GRIN probes for in vivo fluorescence cellular imaging of internal organs in small animals. Nat Protoc 7:1456–1469
PubMed (http://www.ncbi.nlm.nih.gov/entrez/query.fcgi?cmd=Retrieve&db=PubMed&dopt=Abstract&list_uids=22767088)
PubMedCentral (http://www.ncbi.nlm.nih.gov/pmc/articles/PMC3707120)
CrossRef (https://doi.org/10.1038/nprot.2012.078)
Google Scholar (http://scholar.google.com/scholar_lookup?title=Fabrication%20and%20operation%20of%20GRIN%20probes%20for%20in%20vivo%20fluorescence%20cellular%20imaging%20of%20internal%20organs%20in%20small%20animals&author=JK.%20Kim&journal=Nat%20Protoc&volume=7&pages=1456-1469&publication_year=2012)

Kim JK et al (2012b) In vivo imaging of tracheal epithelial cells in mice during airway regeneration. Am J Respir Cell Mol Biol 47:864–868
PubMed (http://www.ncbi.nlm.nih.gov/entrez/query.fcgi?cmd=Retrieve&db=PubMed&dopt=Abstract&list_uids=22984086)
PubMedCentral (http://www.ncbi.nlm.nih.gov/pmc/articles/PMC3547097)
CrossRef (https://doi.org/10.1165/rcmb.2012-0164OC)
Google Scholar (http://scholar.google.com/scholar_lookup?title=In%20vivo%20imaging%20of%20tracheal%20epithelial%20cells%20in%20mice%20during%20airway%20regeneration&author=JK.%20Kim&journal=Am%20J%20Respir%20Cell%20Mol%20Biol&volume=47&pages=864-868&publication_year=2012)

Kim JK, Choi JW, Yun SH (2013b) 350-μ m side-view optical probe for imaging the murine brain *in vivo* from the cortex to the hypothalamus. J Biomed Opt 18:050502
CrossRef (https://doi.org/10.1117/1.JBO.18.5.050502)
Google Scholar (http://scholar.google.com/scholar_lookup?title=350-%CE%BC%20m%20side-view%20optical%20probe%20for%20imaging%20the%20murine%20brain%20in%20vivo%20from%20the%20cortex%20to%20the%20hypothalamus&author=JK.%20Kim&author=JW.%20Choi&author=SH.%20Yun&journal=J%20Biomed%20Opt&volume=18&publication_year=2013)

Kim JK, Choi JW, Yun SH (2013c) Optical fine-needle imaging biopsy of the brain. Biomed Opt Express 4:2846
PubMed (http://www.ncbi.nlm.nih.gov/entrez/query.fcgi?cmd=Retrieve&db=PubMed&dopt=Abstract&list_uids=24409385)
PubMedCentral (http://www.ncbi.nlm.nih.gov/pmc/articles/PMC3862157)
CrossRef (https://doi.org/10.1364/BOE.4.002846)
Google Scholar (http://scholar.google.com/scholar_lookup?title=Optical%20fine-needle%20imaging%20biopsy%20of%20the%20brain&author=JK.%20Kim&author=JW.%20Choi&author=SH.%20Yun&journal=Biomed%20Opt%20Express&volume=4&pages=2846&publication_year=2013)

Kim JM et al (2016c) Perivascular progenitor cells derived from human embryonic stem cells exhibit functional characteristics of pericytes and improve the retinal vasculature in a rodent model of diabetic retinopathy: hESC-PVPCs improve the retinal vasculature of DR. Stem Cells Transl Med 5:1268–1276
PubMed (http://www.ncbi.nlm.nih.gov/entrez/query.fcgi?cmd=Retrieve&db=PubMed&dopt=Abstract&list_uids=27388242)

PubMedCentral (http://www.ncbi.nlm.nih.gov/pmc/articles/PMC4996442)
CrossRef (https://doi.org/10.5966/sctm.2015-0342)
Google Scholar (http://scholar.google.com/scholar_lookup?title=Perivascular%20progenitor%20cells%20derived%20from%20human%20embryonic%20stem%20cells%20exhibit%20functional%20characteristics%20of%20pericytes%20and%20improve%20the%20retinal%20vasculature%20in%20a%20rodent%20model%20of%20diabetic%20retinopathy%3A%20hESC-PVPCs%20improve%20the%20retinal%20vasculature%20of%20DR&author=JM.%20Kim&journal=Stem%20Cells%20Transl%20Med&volume=5&pages=1268-1276&publication_year=2016)

Kim P, Puoris'haag M, Côté D, Yun SH (2008) In vivo confocal and multiphoton microendoscopy. J Biomed Opt 13:010501
PubMed (http://www.ncbi.nlm.nih.gov/entrez/query.fcgi?cmd=Retrieve&db=PubMed&dopt=Abstract&list_uids=18315346)
PubMedCentral (http://www.ncbi.nlm.nih.gov/pmc/articles/PMC2752311)
CrossRef (https://doi.org/10.1117/1.2839043)
Google Scholar (http://scholar.google.com/scholar_lookup?title=In%20vivo%20confocal%20and%20multiphoton%20microendoscopy&author=P.%20Kim&author=M.%20Puoris%E2%80%99haag&author=D.%20C%C3%B4t%C3%A9&author=SH.%20Yun&journal=J%20Biomed%20Opt&volume=13&publication_year=2008)

Kim P et al (2010a) In vivo wide-area cellular imaging by side-view endomicroscopy. Nat Methods 7:303–305
PubMed (http://www.ncbi.nlm.nih.gov/entrez/query.fcgi?cmd=Retrieve&db=PubMed&dopt=Abstract&list_uids=20228814)
PubMedCentral (http://www.ncbi.nlm.nih.gov/pmc/articles/PMC2849759)
CrossRef (https://doi.org/10.1038/nmeth.1440)
Google Scholar (http://scholar.google.com/scholar_lookup?title=In%20vivo%20wide-area%20cellular%20imaging%20by%20side-view%20endomicroscopy&author=P.%20Kim&journal=Nat%20Methods&volume=7&pages=303-305&publication_year=2010)

Kim Y et al (2018) Small hypoxia-primed mesenchymal stem cells attenuate graft-versus-host disease. Leukemia 32:2672–2684
PubMed (http://www.ncbi.nlm.nih.gov/entrez/query.fcgi?cmd=Retrieve&db=PubMed&dopt=Abstract&list_uids=29789652)
PubMedCentral (http://www.ncbi.nlm.nih.gov/pmc/articles/PMC6286327)
CrossRef (https://doi.org/10.1038/s41375-018-0151-8)
Google Scholar (http://scholar.google.com/scholar_lookup?title=Small%20hypoxia-primed%20mesenchymal%20stem%20cells%20attenuate%20graft-versus-host%20disease&author=Y.%20Kim&journal=Leukemia&volume=32&pages=2672-2684&publication_year=2018)

Kimura H et al (2009) Real-time imaging of single cancer-cell dynamics of lung metastasis. J Cell Biochem. n/a–n/a. https://doi.org/10.1002/jcb.22379 (https://doi.org/10.1002/jcb.22379)

Kleinfeld D, Mitra PP, Helmchen F, Denk W (1998) Fluctuations and stimulus-induced changes in blood flow observed in individual capillaries in layers 2 through 4 of rat neocortex. Proc Natl Acad Sci 95:15741–15746
PubMed (http://www.ncbi.nlm.nih.gov/entrez/query.fcgi?cmd=Retrieve&db=PubMed&dopt=Abstract&list_uids=9861040)
CrossRef (https://doi.org/10.1073/pnas.95.26.15741)
PubMedCentral (http://www.ncbi.nlm.nih.gov/pmc/articles/PMC9861040)
Google Scholar (http://scholar.google.com/scholar_lookup?title=Fluctuations%20and%20stimulus-induced%20changes%20in%20blood%20flow%20observed%20in%20individual%20capillaries%20in%20layers%202%20through%204%20of%20rat%20neocortex&author=D.%20Kleinfeld&author=PP.%20Mitra&author=F.%20Helmchen&author=W.%20Denk&journal=Proc%20Natl%20Acad%20Sci&volume=95&pages=15741-15746&publication_year=1998)

Kobat D, Horton NG, Xu C (2011) In vivo two-photon microscopy to 1.6-mm depth in mouse cortex. J Biomed Opt 16:106014
PubMed (http://www.ncbi.nlm.nih.gov/entrez/query.fcgi?cmd=Retrieve&db=PubMed&dopt=Abstract&list_uids=22029361)
CrossRef (https://doi.org/10.1117/1.3646209)
PubMedCentral (http://www.ncbi.nlm.nih.gov/pmc/articles/PMC22029361)
Google Scholar (http://scholar.google.com/scholar_lookup?title=In%20vivo%20two-photon%20microscopy%20to%201.6-mm%20depth%20in%20mouse%20cortex&author=D.%20Kobat&author=NG.%20Horton&author=C.%20Xu&journal=J%20Biomed%20Opt&volume=16&publication_year=2011)

Kohler A et al (2008) Estimating and correcting Mie scattering in synchrotron-based microscopic Fourier transform infrared spectra by extended multiplicative signal correction. Appl Spectrosc 62:259–266
PubMed (http://www.ncbi.nlm.nih.gov/entrez/query.fcgi?cmd=Retrieve&db=PubMed&dopt=Abstract&list_uids=18339231)
CrossRef (https://doi.org/10.1366/000370208783759669)
PubMedCentral (http://www.ncbi.nlm.nih.gov/pmc/articles/PMC18339231)
Google Scholar (http://scholar.google.com/scholar_lookup?title=Estimating%20and%20correcting%20Mie%20scattering%20in%20synchrotron-based%20microscopic%20Fourier%20transform%20infrared%20spectra%20by%20extended%20multiplicative%20signal%20correction&author=A.%20Kohler&journal=Appl%20Spectrosc&volume=62&pages=259-266&publication_year=2008)

Köhler M et al (2018) Integrative micro-endoscopic system combined with conventional microscope for live animal tissue imaging. J Biophotonics 11:e201800206
PubMed (http://www.ncbi.nlm.nih.gov/entrez/query.fcgi?cmd=Retrieve&db=PubMed&dopt=Abstract&list_uids=30079609)
CrossRef (https://doi.org/10.1002/jbio.201800206)
PubMedCentral (http://www.ncbi.nlm.nih.gov/pmc/articles/PMC30079609)
Google Scholar (http://scholar.google.com/scholar_lookup?title=Integrative%20micro-endoscopic%20system%20combined%20with%20conventional%20microscope%20for%20live%20animal%20tissue%20imaging&author=M.%20K%C3%B6hler&journal=J%20Biophotonics&volume=11&publication_year=2018)

Krishna KSR, Sharma A (1996) Chromatic aberrations of radial gradient-index lenses I Theory. Appl Opt 35:1032

PubMed (http://www.ncbi.nlm.nih.gov/entrez/query.fcgi?cmd=Retrieve&db=PubMed&dopt=Abstract&list_uids=21085210)
CrossRef (https://doi.org/10.1364/AO.35.001032)
PubMedCentral (http://www.ncbi.nlm.nih.gov/pmc/articles/PMC21085210)
Google Scholar (http://scholar.google.com/scholar_lookup?title=Chromatic%20aberrations%20of%20radial%20gradient-index%20lenses%20I%20Theory&author=KSR.%20Krishna&author=A.%20Sharma&journal=Appl%20Opt&volume=35&pages=1032&publication_year=1996)

Leask A, Abraham DJ (2004) TGF-β signaling and the fibrotic response. FASEB J 18:816–827
PubMed (http://www.ncbi.nlm.nih.gov/entrez/query.fcgi?cmd=Retrieve&db=PubMed&dopt=Abstract&list_uids=15117886)
CrossRef (https://doi.org/10.1096/fj.03-1273rev)
PubMedCentral (http://www.ncbi.nlm.nih.gov/pmc/articles/PMC15117886)
Google Scholar (http://scholar.google.com/scholar_lookup?title=TGF-%CE%B2%20signaling%20and%20the%20fibrotic%20response&author=A.%20Leask&author=DJ.%20Abraham&journal=FASEB%20J&volume=18&pages=816-827&publication_year=2004)

Lee CM, Engelbrecht CJ, Soper TD, Helmchen F, Seibel EJ (2010) Scanning fiber endoscopy with highly flexible, 1 mm catheterscopes for wide-field, full-color imaging. J Biophotonics 3:385–407
PubMed (http://www.ncbi.nlm.nih.gov/entrez/query.fcgi?cmd=Retrieve&db=PubMed&dopt=Abstract&list_uids=20336702)
PubMedCentral (http://www.ncbi.nlm.nih.gov/pmc/articles/PMC3163080)
CrossRef (https://doi.org/10.1002/jbio.200900087)
Google Scholar (http://scholar.google.com/scholar_lookup?title=Scanning%20fiber%20endoscopy%20with%20highly%20flexible%2C%201%20mm%20catheterscopes%20for%20wide-field%2C%20full-color%20imaging&author=CM.%20Lee&author=CJ.%20Engelbrecht&author=TD.%20Soper&author=F.%20Helmchen&author=EJ.%20Seibel&journal=J%20Biophotonics&volume=3&pages=385-407&publication_year=2010)

Lee S et al (2012) Real-time in vivo imaging of the beating mouse heart at microscopic resolution. Nat Commun 3:1054
PubMed (http://www.ncbi.nlm.nih.gov/entrez/query.fcgi?cmd=Retrieve&db=PubMed&dopt=Abstract&list_uids=22968700)
PubMedCentral (http://www.ncbi.nlm.nih.gov/pmc/articles/PMC3622400)
CrossRef (https://doi.org/10.1038/ncomms2060)
Google Scholar (http://scholar.google.com/scholar_lookup?title=Real-time%20in%20vivo%20imaging%20of%20the%20beating%20mouse%20heart%20at%20microscopic%20resolution&author=S.%20Lee&journal=Nat%20Commun&volume=3&pages=1054&publication_year=2012)

Li W et al (2012) Intravital 2-photon imaging of leukocyte trafficking in beating heart. J Clin Invest 122:2499–2508
PubMed (http://www.ncbi.nlm.nih.gov/entrez/query.fcgi?cmd=Retrieve&db=PubMed&dopt=Abstract&list_uids=22706307)
PubMedCentral (http://www.ncbi.nlm.nih.gov/pmc/articles/PMC3386827)
CrossRef (https://doi.org/10.1172/JCI62970)
Google Scholar (http://scholar.google.com/scholar_lookup?title=Intravital%202-photon%20imaging%20of%20leukocyte%20trafficking%20in%20beating%20heart&author=W.%20Li&journal=J%20Clin%20Invest&volume=122&pages=2499-2508&publication_year=2012)

Liang X, Ding Y, Zhang Y, Tse H-F, Lian Q (2014) Paracrine mechanisms of mesenchymal stem cell-based therapy: current status and perspectives. Cell Transplant 23:1045–1059
PubMed (http://www.ncbi.nlm.nih.gov/entrez/query.fcgi?cmd=Retrieve&db=PubMed&dopt=Abstract&list_uids=23676629)
CrossRef (https://doi.org/10.3727/096368913X667709)
PubMedCentral (http://www.ncbi.nlm.nih.gov/pmc/articles/PMC23676629)
Google Scholar (http://scholar.google.com/scholar_lookup?title=Paracrine%20mechanisms%20of%20mesenchymal%20stem%20cell-based%20therapy%3A%20current%20status%20and%20perspectives&author=X.%20Liang&author=Y.%20Ding&author=Y.%20Zhang&author=H-F.%20Tse&author=Q.%20Lian&journal=Cell%20Transplant&volume=23&pages=1045-1059&publication_year=2014)

Lindley LE, Briegel KJ (2010) Molecular characterization of TGFβ-induced epithelial-mesenchymal transition in normal finite lifespan human mammary epithelial cells. Biochem Biophys Res Commun 399:659–664
PubMed (http://www.ncbi.nlm.nih.gov/entrez/query.fcgi?cmd=Retrieve&db=PubMed&dopt=Abstract&list_uids=20691661)
CrossRef (https://doi.org/10.1016/j.bbrc.2010.07.138)
PubMedCentral (http://www.ncbi.nlm.nih.gov/pmc/articles/PMC20691661)
Google Scholar (http://scholar.google.com/scholar_lookup?title=Molecular%20characterization%20of%20TGF%CE%B2-induced%20epithelial-mesenchymal%20transition%20in%20normal%20finite%20lifespan%20human%20mammary%20epithelial%20cells&author=LE.%20Lindley&author=KJ.%20Briegel&journal=Biochem%20Biophys%20Res%20Commun&volume=399&pages=659-664&publication_year=2010)

Looney MR et al (2011) Stabilized imaging of immune surveillance in the mouse lung. Nat Methods 8:91–96
PubMed (http://www.ncbi.nlm.nih.gov/entrez/query.fcgi?cmd=Retrieve&db=PubMed&dopt=Abstract&list_uids=21151136)
CrossRef (https://doi.org/10.1038/nmeth.1543)
PubMedCentral (http://www.ncbi.nlm.nih.gov/pmc/articles/PMC21151136)
Google Scholar (http://scholar.google.com/scholar_lookup?title=Stabilized%20imaging%20of%20immune%20surveillance%20in%20the%20mouse%20lung&author=MR.%20Looney&journal=Nat%20Methods&volume=8&pages=91-96&publication_year=2011)

Lucitti JL et al (2007) Vascular remodeling of the mouse yolk sac requires hemodynamic force. Development 134:3317–3326
PubMed (http://www.ncbi.nlm.nih.gov/entrez/query.fcgi?cmd=Retrieve&db=PubMed&dopt=Abstract&list_uids=17720695)
PubMedCentral (http://www.ncbi.nlm.nih.gov/pmc/articles/PMC4260474)

CrossRef (https://doi.org/10.1242/dev.02883)
Google Scholar (http://scholar.google.com/scholar_lookup?title=Vascular%20remodeling%20of%20the%20mouse%20yolk%20sac%20requires%20hemodynamic%20force&author=JL.%20Lucitti&journal=Development&volume=134&pages=3317-3326&publication_year=2007)

Matz G et al (2017) Chip-on-the-tip compact flexible endoscopic epifluorescence video-microscope for in-vivo imaging in medicine and biomedical research. Biomed Opt Express 8:3329
PubMed (http://www.ncbi.nlm.nih.gov/entrez/query.fcgi?cmd=Retrieve&db=PubMed&dopt=Abstract&list_uids=28717570)
PubMedCentral (http://www.ncbi.nlm.nih.gov/pmc/articles/PMC5508831)
CrossRef (https://doi.org/10.1364/BOE.8.003329)
Google Scholar (http://scholar.google.com/scholar_lookup?title=Chip-on-the-tip%20compact%20flexible%20endoscopic%20epifluorescence%20video-microscope%20for%20in-vivo%20imaging%20in%20medicine%20and%20biomedical%20research&author=G.%20Matz&journal=Biomed%20Opt%20Express&volume=8&pages=3329&publication_year=2017)

Miller MJ (2002) Two-photon imaging of lymphocyte motility and antigen response in intact lymph node. Science 296:1869–1873
CrossRef (https://doi.org/10.1126/science.1070051)
Google Scholar (http://scholar.google.com/scholar_lookup?title=Two-photon%20imaging%20of%20lymphocyte%20motility%20and%20antigen%20response%20in%20intact%20lymph%20node&author=MJ.%20Miller&journal=Science&volume=296&pages=1869-1873&publication_year=2002)

Miyajima M et al (2011) Early acceptance of renal allografts in mice is dependent on Foxp3+ cells. Am J Pathol 178:1635–1645
PubMed (http://www.ncbi.nlm.nih.gov/entrez/query.fcgi?cmd=Retrieve&db=PubMed&dopt=Abstract&list_uids=21435448)
PubMedCentral (http://www.ncbi.nlm.nih.gov/pmc/articles/PMC3078464)
CrossRef (https://doi.org/10.1016/j.ajpath.2010.12.024)
Google Scholar (http://scholar.google.com/scholar_lookup?title=Early%20acceptance%20of%20renal%20allografts%20in%20mice%20is%20dependent%20on%20Foxp3%2B%20cells&author=M.%20Miyajima&journal=Am%20J%20Pathol&volume=178&pages=1635-1645&publication_year=2011)

Nagashima K et al (1995) Apoptotic process of cerebellar degeneration in experimental methylmercury intoxication of rats. Acta Neuropathol (Berl) 91:72–77
CrossRef (https://doi.org/10.1007/s004010050394)
Google Scholar (http://scholar.google.com/scholar_lookup?title=Apoptotic%20process%20of%20cerebellar%20degeneration%20in%20experimental%20methylmercury%20intoxication%20of%20rats&author=K.%20Nagashima&journal=Acta%20Neuropathol%20%28Berl%29&volume=91&pages=72-77&publication_year=1995)

Nahrendorf M, Pittet MJ, Swirski FK (2010) Monocytes: protagonists of infarct inflammation and repair after myocardial infarction. Circulation 121:2437–2445
PubMed (http://www.ncbi.nlm.nih.gov/entrez/query.fcgi?cmd=Retrieve&db=PubMed&dopt=Abstract&list_uids=20530020)
PubMedCentral (http://www.ncbi.nlm.nih.gov/pmc/articles/PMC2892474)
CrossRef (https://doi.org/10.1161/CIRCULATIONAHA.109.916346)
Google Scholar (http://scholar.google.com/scholar_lookup?title=Monocytes%3A%20protagonists%20of%20infarct%20inflammation%20and%20repair%20after%20myocardial%20infarction&author=M.%20Nahrendorf&author=MJ.%20Pittet&author=FK.%20Swirski&journal=Circulation&volume=121&pages=2437-2445&publication_year=2010)

Okada H, Danoff TM, Kalluri R, Neilson EG (1997) Early role of Fsp1 in epithelial-mesenchymal transformation. Am J Physiol-Ren Physiol 273:F563–F574
CrossRef (https://doi.org/10.1152/ajprenal.1997.273.4.F563)
Google Scholar (http://scholar.google.com/scholar_lookup?title=Early%20role%20of%20Fsp1%20in%20epithelial-mesenchymal%20transformation&author=H.%20Okada&author=TM.%20Danoff&author=R.%20Kalluri&author=EG.%20Neilson&journal=Am%20J%20Physiol-Ren%20Physiol&volume=273&pages=F563-F574&publication_year=1997)

Oravisto KJ (1975) Epidemiology of interstitial cystitis. Ann Chir Gynaecol Fenn 64:75–77
PubMed (http://www.ncbi.nlm.nih.gov/entrez/query.fcgi?cmd=Retrieve&db=PubMed&dopt=Abstract&list_uids=1137336)
PubMedCentral (http://www.ncbi.nlm.nih.gov/pmc/articles/PMC1137336)
Google Scholar (http://scholar.google.com/scholar_lookup?title=Epidemiology%20of%20interstitial%20cystitis&author=KJ.%20Oravisto&journal=Ann%20Chir%20Gynaecol%20Fenn&volume=64&pages=75-77&publication_year=1975)

Park J-H et al (2012) Polytetrafluoroethylene-covered retrievable expandable nitinol stents for malignant esophageal obstructions: factors influencing the outcome of 270 patients. Am J Roentgenol 199:1380–1386
CrossRef (https://doi.org/10.2214/AJR.10.6306)
Google Scholar (http://scholar.google.com/scholar_lookup?title=Polytetrafluoroethylene-covered%20retrievable%20expandable%20nitinol%20stents%20for%20malignant%20esophageal%20obstructions%3A%20ofactors%20influencing%20the%20outcome%20of%20270%20patients&author=J-H.%20Park&journal=Am%20J%20Roentgenol&volume=199&pages=1380-1386&publication_year=2012)

Park J-H et al (2014) Bioreducible polymer–delivered siRNA targeting MMP-9: suppression of granulation tissue formation after bare metallic stent placement in a rat urethral model. Radiology 271:87–95
PubMed (http://www.ncbi.nlm.nih.gov/entrez/query.fcgi?cmd=Retrieve&db=PubMed&dopt=Abstract&list_uids=24475825)
CrossRef (https://doi.org/10.1148/radiol.13130980)
PubMedCentral (http://www.ncbi.nlm.nih.gov/pmc/articles/PMC24475825)
Google Scholar (http://scholar.google.com/scholar_lookup?title=Bioreducible%20polymer%E2%80%93delivered%20siRNA%20targeting%20MMP-9%3A%20suppression%20of%20granulation%20tissue%20formation%20after%20bare%20metallic%20stent%20placemen

t%20in%20a%20rat%20urethral%20model&author=J-H.%20Park&journal=Radiology&volume=271&pages=87-95&publication_year=2014)

Pittet MJ, Weissleder R (2011) Intravital imaging. Cell 147:983–991
PubMed (http://www.ncbi.nlm.nih.gov/entrez/query.fcgi?cmd=Retrieve&db=PubMed&dopt=Abstract&list_uids=22118457)
CrossRef (https://doi.org/10.1016/j.cell.2011.11.004)
PubMedCentral (http://www.ncbi.nlm.nih.gov/pmc/articles/PMC22118457)
Google Scholar (http://scholar.google.com/scholar_lookup?title=Intravital%20imaging&author=MJ.%20Pittet&author=R.%20Weissleder&journal=Cell&volume=147&pages=983-991&publication_year=2011)

Polyak K, Weinberg RA (2009) Transitions between epithelial and mesenchymal states: acquisition of malignant and stem cell traits. Nat Rev Cancer 9:265–273
PubMed (http://www.ncbi.nlm.nih.gov/entrez/query.fcgi?cmd=Retrieve&db=PubMed&dopt=Abstract&list_uids=19262571)
CrossRef (https://doi.org/10.1038/nrc2620)
PubMedCentral (http://www.ncbi.nlm.nih.gov/pmc/articles/PMC19262571)
Google Scholar (http://scholar.google.com/scholar_lookup?title=Transitions%20between%20epithelial%20and%20mesenchymal%20states%3A%20acquisition%20of%20malignant%20and%20stem%20cell%20traits&author=K.%20Polyak&author=RA.%20Weinberg&journal=Nat%20Rev%20Cancer&volume=9&pages=265-273&publication_year=2009)

Propert KJ et al (2000) A prospective study of interstitial cystitis: results of longitudinal followup of the interstitial cystitis data base cohort. J Urol 163:1434–1439
PubMed (http://www.ncbi.nlm.nih.gov/entrez/query.fcgi?cmd=Retrieve&db=PubMed&dopt=Abstract&list_uids=10751852)
CrossRef (https://doi.org/10.1016/S0022-5347(05)67637-9)
PubMedCentral (http://www.ncbi.nlm.nih.gov/pmc/articles/PMC10751852)
Google Scholar (http://scholar.google.com/scholar_lookup?title=A%20prospective%20study%20of%20interstitial%20cystitis%3A%20results%20of%20longitudinal%20followup%20of%20the%20interstitial%20cystitis%20data%20base%20cohort&author=KJ.%20Propert&journal=J%20Urol&volume=163&pages=1434-1439&publication_year=2000)

Rawlins EL et al (2009) The role of Scgb1a1+ Clara cells in the long-term maintenance and repair of lung airway, but not alveolar, epithelium. Cell Stem Cell 4:525–534
PubMed (http://www.ncbi.nlm.nih.gov/entrez/query.fcgi?cmd=Retrieve&db=PubMed&dopt=Abstract&list_uids=19497281)
PubMedCentral (http://www.ncbi.nlm.nih.gov/pmc/articles/PMC2730729)
CrossRef (https://doi.org/10.1016/j.stem.2009.04.002)
Google Scholar (http://scholar.google.com/scholar_lookup?title=The%20role%20of%20Scgb1a1%2B%20Clara%20cells%20in%20the%20long-term%20maintenance%20and%20repair%20of%20lung%20airway%2C%20but%20not%20alveolar%2C%20epithelium&author=EL.%20Rawlins&journal=Cell%20Stem%20Cell&volume=4&pages=525-534&publication_year=2009)

Rock JR et al (2009) Basal cells as stem cells of the mouse trachea and human airway epithelium. Proc Natl Acad Sci 106:12771–12775
PubMed (http://www.ncbi.nlm.nih.gov/entrez/query.fcgi?cmd=Retrieve&db=PubMed&dopt=Abstract&list_uids=19625615)
CrossRef (https://doi.org/10.1073/pnas.0906850106)
PubMedCentral (http://www.ncbi.nlm.nih.gov/pmc/articles/PMC19625615)
Google Scholar (http://scholar.google.com/scholar_lookup?title=Basal%20cells%20as%20stem%20cells%20of%20the%20mouse%20trachea%20and%20human%20airway%20epithelium&author=JR.%20Rock&journal=Proc%20Natl%20Acad%20Sci&volume=106&pages=12771-12775&publication_year=2009)

Rock JR, Randell SH, Hogan BLM (2010) Airway basal stem cells: a perspective on their roles in epithelial homeostasis and remodeling. Dis Model Mech 3:545–556
PubMed (http://www.ncbi.nlm.nih.gov/entrez/query.fcgi?cmd=Retrieve&db=PubMed&dopt=Abstract&list_uids=20699479)
PubMedCentral (http://www.ncbi.nlm.nih.gov/pmc/articles/PMC2931533)
CrossRef (https://doi.org/10.1242/dmm.006031)
Google Scholar (http://scholar.google.com/scholar_lookup?title=Airway%20basal%20stem%20cells%3A%20a%20perspective%20on%20their%20roles%20in%20epithelial%20homeostasis%20and%20remodeling&author=JR.%20Rock&author=SH.%20Randell&author=BLM.%20Hogan&journal=Dis%20Model%20Mech&volume=3&pages=545-556&publication_year=2010)

Ryu C-M et al (2018) Longitudinal intravital imaging of transplanted mesenchymal stem cells elucidates their functional integration and therapeutic potency in an animal model of interstitial cystitis/bladder pain syndrome. Theranostics 8:5610–5624
PubMed (http://www.ncbi.nlm.nih.gov/entrez/query.fcgi?cmd=Retrieve&db=PubMed&dopt=Abstract&list_uids=30555567)
PubMedCentral (http://www.ncbi.nlm.nih.gov/pmc/articles/PMC6276303)
CrossRef (https://doi.org/10.7150/thno.27559)
Google Scholar (http://scholar.google.com/scholar_lookup?title=Longitudinal%20intravital%20imaging%20of%20transplanted%20mesenchymal%20stem%20cells%20elucidates%20their%20functional%20integration%20and%20therapeutic%20potency%20in%20an%20animal%20model%20of%20interstitial%20cystitis%2Fbladder%20pain%20syndrome&author=C-M.%20Ryu&journal=Theranostics&volume=8&pages=5610-5624&publication_year=2018)

Schroeder JL et al (2010) Short communication: subcellular motion compensation for minimally invasive microscopy, in vivo: evidence for oxygen gradients in resting muscle. Circ Res 106:1129–1133
PubMed (http://www.ncbi.nlm.nih.gov/entrez/query.fcgi?cmd=Retrieve&db=PubMed&dopt=Abstract&list_uids=20167928)

PubMedCentral (http://www.ncbi.nlm.nih.gov/pmc/articles/PMC3209509)
CrossRef (https://doi.org/10.1161/CIRCRESAHA.109.211946)
Google Scholar (http://scholar.google.com/scholar_lookup?title=Short%20communication%3A%20subcellular%20motion%20compensation%20for%20minimally%20invasive%20microscopy%2C%20in%20vivo%3A%20evidence%20for%20oxygen%20gradients%20in%20resting%20muscle&author=JL.%20Schroeder&journal=Circ%20Res&volume=106&pages=1129-1133&publication_year=2010)

Smith AM, Mancini MC, Nie S (2009) Bioimaging: second window for in vivo imaging. Nat Nanotechnol 4:710–711
PubMed (http://www.ncbi.nlm.nih.gov/entrez/query.fcgi?cmd=Retrieve&db=PubMed&dopt=Abstract&list_uids=19898521)
PubMedCentral (http://www.ncbi.nlm.nih.gov/pmc/articles/PMC2862008)
CrossRef (https://doi.org/10.1038/nnano.2009.326)
Google Scholar (http://scholar.google.com/scholar_lookup?title=Bioimaging%3A%20second%20window%20for%20in%20vivo%20imaging&author=AM.%20Smith&author=MC.%20Mancini&author=S.%20Nie&journal=Nat%20Nanotechnol&volume=4&pages=710-711&publication_year=2009)

Song H-Y et al (2003) Recurrent traumatic urethral strictures near the external sphincter: treatment with a covered, retrievable, expandable nitinol stent—initial results. Radiology 226:433–440
PubMed (http://www.ncbi.nlm.nih.gov/entrez/query.fcgi?cmd=Retrieve&db=PubMed&dopt=Abstract&list_uids=12563137)
CrossRef (https://doi.org/10.1148/radiol.2262012160)
PubMedCentral (http://www.ncbi.nlm.nih.gov/pmc/articles/PMC12563137)
Google Scholar (http://scholar.google.com/scholar_lookup?title=Recurrent%20traumatic%20urethral%20strictures%20near%20the%20external%20sphincter%3A%20treatment%20with%20a%20covered%2C%20retrievable%2C%20expandable%20nitinol%20stent%E2%80%94initial%20results&author=H-Y.%20Song&journal=Radiology&volume=226&pages=433-440&publication_year=2003)

Song M et al (2014) The paracrine effects of mesenchymal stem cells stimulate the regeneration capacity of endogenous stem cells in the repair of a bladder-outlet-obstruction-induced overactive bladder. Stem Cells Dev 23:654–663
PubMed (http://www.ncbi.nlm.nih.gov/entrez/query.fcgi?cmd=Retrieve&db=PubMed&dopt=Abstract&list_uids=24192209)
CrossRef (https://doi.org/10.1089/scd.2013.0277)
PubMedCentral (http://www.ncbi.nlm.nih.gov/pmc/articles/PMC24192209)
Google Scholar (http://scholar.google.com/scholar_lookup?title=The%20paracrine%20effects%20of%20mesenchymal%20stem%20cells%20stimulate%20the%20regeneration%20capacity%20of%20endogenous%20stem%20cells%20in%20the%20repair%20of%20a%20bladder-outlet-obstruction-induced%20overactive%20bladder&author=M.%20Song&journal=Stem%20Cells%20Dev&volume=23&pages=654-663&publication_year=2014)

Song M et al (2015) Mesenchymal stem cell therapy alleviates interstitial cystitis by activating Wnt signaling pathway. Stem Cells Dev 24:1648–1657
PubMed (http://www.ncbi.nlm.nih.gov/entrez/query.fcgi?cmd=Retrieve&db=PubMed&dopt=Abstract&list_uids=25745847)
PubMedCentral (http://www.ncbi.nlm.nih.gov/pmc/articles/PMC4499842)
CrossRef (https://doi.org/10.1089/scd.2014.0459)
Google Scholar (http://scholar.google.com/scholar_lookup?title=Mesenchymal%20stem%20cell%20therapy%20alleviates%20interstitial%20cystitis%20by%20activating%20Wnt%20signaling%20pathway&author=M.%20Song&journal=Stem%20Cells%20Dev&volume=24&pages=1648-1657&publication_year=2015)

Stein PC, Pham H, Ito T, Parsons CL (1996) Bladder injury model induced in rats by exposure to protamine sulfate followed by bacterial endotoxin. J Urol 155:1133–1138
PubMed (http://www.ncbi.nlm.nih.gov/entrez/query.fcgi?cmd=Retrieve&db=PubMed&dopt=Abstract&list_uids=8583579)
CrossRef (https://doi.org/10.1016/S0022-5347(01)66406-1)
PubMedCentral (http://www.ncbi.nlm.nih.gov/pmc/articles/PMC8583579)
Google Scholar (http://scholar.google.com/scholar_lookup?title=Bladder%20injury%20model%20induced%20in%20rats%20by%20exposure%20to%20protamine%20sulfate%20followed%20by%20bacterial%20endotoxin&author=PC.%20Stein&author=H.%20Pham&author=T.%20Ito&author=CL.%20Parsons&journal=J%20Urol&volume=155&pages=1133-1138&publication_year=1996)

Storkebaum E, Quaegebeur A, Vikkula M, Carmeliet P (2011) Cerebrovascular disorders: molecular insights and therapeutic opportunities. Nat Neurosci 14:1390–1397
PubMed (http://www.ncbi.nlm.nih.gov/entrez/query.fcgi?cmd=Retrieve&db=PubMed&dopt=Abstract&list_uids=22030550)
CrossRef (https://doi.org/10.1038/nn.2947)
PubMedCentral (http://www.ncbi.nlm.nih.gov/pmc/articles/PMC22030550)
Google Scholar (http://scholar.google.com/scholar_lookup?title=Cerebrovascular%20disorders%3A%20molecular%20insights%20and%20therapeutic%20opportunities&author=E.%20Storkebaum&author=A.%20Quaegebeur&author=M.%20Vikkula&author=P.%20Carmeliet&journal=Nat%20Neurosci&volume=14&pages=1390-1397&publication_year=2011)

Swirski FK et al (2009) Identification of splenic reservoir monocytes and their deployment to inflammatory sites. Science 325:612–616
PubMed (http://www.ncbi.nlm.nih.gov/entrez/query.fcgi?cmd=Retrieve&db=PubMed&dopt=Abstract&list_uids=19644120)
PubMedCentral (http://www.ncbi.nlm.nih.gov/pmc/articles/PMC2803111)
CrossRef (https://doi.org/10.1126/science.1175202)
Google Scholar (http://scholar.google.com/scholar_lookup?title=Identification%20of%20splenic%20reservoir%20monocytes%20and%20their%20deployment%20to%20inflammatory%20sites&author=FK.%20Swirski&journal=Science&volume=325&pages=612-616&publication_year=2009)

Taylor MA, Parvani JG, Schiemann WP (2010) The pathophysiology of epithelial-mesenchymal transition induced by transforming growth factor-β in normal and malignant mammary epithelial cells. J Mammary Gland Biol Neoplasia 15:169–

190
PubMed (http://www.ncbi.nlm.nih.gov/entrez/query.fcgi?cmd=Retrieve&db=PubMed&dopt=Abstract&list_uids=20467795)
PubMedCentral (http://www.ncbi.nlm.nih.gov/pmc/articles/PMC3721368)
CrossRef (https://doi.org/10.1007/s10911-010-9181-1)
Google Scholar (http://scholar.google.com/scholar_lookup?title=The%20pathophysiology%20of%20epithelial-mesenchymal%20transition%20induced%20by%20transforming%20growth%20factor-%CE%B2%20in%20normal%20and%20malignant%20mammary%20epithelial%20cells&author=MA.%20Taylor&author=JG.%20Parvani&author=WP.%20Schiemann&journal=J%20Mammary%20Gland%20Biol%20Neoplasia&volume=15&pages=169-190&publication_year=2010)

Thiberville L et al (2007) In vivo imaging of the bronchial wall microstructure using fibered confocal fluorescence microscopy. Am J Respir Crit Care Med 175:22–31
PubMed (http://www.ncbi.nlm.nih.gov/entrez/query.fcgi?cmd=Retrieve&db=PubMed&dopt=Abstract&list_uids=17023733)
CrossRef (https://doi.org/10.1164/rccm.200605-684OC)
PubMedCentral (http://www.ncbi.nlm.nih.gov/pmc/articles/PMC17023733)
Google Scholar (http://scholar.google.com/scholar_lookup?title=In%20vivo%20imaging%20of%20the%20bronchial%20wall%20microstructure%20using%20fibered%20confocal%20fluorescence%20microscopy&author=L.%20Thiberville&journal=Am%20J%20Respir%20Crit%20Care%20Med&volume=175&pages=22-31&publication_year=2007)

Tilgner J, Herr M, Ostertag C, Volk B (2005) Validation of intraoperative diagnoses using smear preparations from stereotactic brain biopsies: intraoperative versus final diagnosis—influence of clinical factors. Neurosurgery 56:257–265
PubMed (http://www.ncbi.nlm.nih.gov/entrez/query.fcgi?cmd=Retrieve&db=PubMed&dopt=Abstract&list_uids=15670374)
CrossRef (https://doi.org/10.1227/01.NEU.0000148899.39020.87)
PubMedCentral (http://www.ncbi.nlm.nih.gov/pmc/articles/PMC15670374)
Google Scholar (http://scholar.google.com/scholar_lookup?title=Validation%20of%20intraoperative%20diagnoses%20using%20smear%20preparations%20from%20stereotactic%20brain%20biopsies%3A%20intraoperative%20versus%20final%20diagnosis%E2%80%94influence%20of%20clinical%20factors&author=J.%20Tilgner&author=M.%20Herr&author=C.%20Ostertag&author=B.%20Volk&journal=Neurosurgery&volume=56&pages=257-265&publication_year=2005)

Tyack PL, Calambokidis J, Friedlaender A, Goldbogen J, Southall B, Formal Comment on Schorr GS, Falcone EA, Moretti DJ, Andrews RD (2014) First long-term behavioral records from Cuvier's beaked whales (*Ziphius cavirostris*) reveal record-breaking dives. PLoS ONE 9(3):e92633. https://doi.org/10.1371/journal.pone.0092633 (https://doi.org/10.1371/journal.pone.0092633). PLoS ONE 10, e0142287 (2015)

Veilleux I, Spencer JA, Biss DP, Cote D, Lin CP (2008) *In vivo* cell tracking with video rate multimodality laser scanning microscopy. IEEE J Sel Top Quantum Electron 14:10–18
CrossRef (https://doi.org/10.1109/JSTQE.2007.912751)
Google Scholar (http://scholar.google.com/scholar_lookup?title=In%20vivo%20cell%20tracking%20with%20video%20rate%20multimodality%20laser%20scanning%20microscopy&author=I.%20Veilleux&author=JA.%20Spencer&author=DP.%20Biss&author=D.%20Cote&author=CP.%20Lin&journal=IEEE%20J%20Sel%20Top%20Quantum%20Electron&volume=14&pages=10-18&publication_year=2008)

Vonk LA et al (2018) Mesenchymal stromal/stem cell-derived extracellular vesicles promote human cartilage regeneration *in vitro*. Theranostics 8:906–920
PubMed (http://www.ncbi.nlm.nih.gov/entrez/query.fcgi?cmd=Retrieve&db=PubMed&dopt=Abstract&list_uids=29463990)
PubMedCentral (http://www.ncbi.nlm.nih.gov/pmc/articles/PMC5817101)
CrossRef (https://doi.org/10.7150/thno.20746)
Google Scholar (http://scholar.google.com/scholar_lookup?title=Mesenchymal%20stromal%2Fstem%20cell-derived%20extracellular%20vesicles%20promote%20human%20cartilage%20regeneration%20in%20vitro&author=LA.%20Vonk&journal=Theranostics&volume=8&pages=906-920&publication_year=2018)

Wang Y, Chen X, Cao W, Shi Y (2014) Plasticity of mesenchymal stem cells in immunomodulation: pathological and therapeutic implications. Nat Immunol 15:1009–1016
PubMed (http://www.ncbi.nlm.nih.gov/entrez/query.fcgi?cmd=Retrieve&db=PubMed&dopt=Abstract&list_uids=25329189)
CrossRef (https://doi.org/10.1038/ni.3002)
PubMedCentral (http://www.ncbi.nlm.nih.gov/pmc/articles/PMC25329189)
Google Scholar (http://scholar.google.com/scholar_lookup?title=Plasticity%20of%20mesenchymal%20stem%20cells%20in%20immunomodulation%3A%20pathological%20and%20therapeutic%20implications&author=Y.%20Wang&author=X.%20Chen&author=W.%20Cao&author=Y.%20Shi&journal=Nat%20Immunol&volume=15&pages=1009-1016&publication_year=2014)

Wang Z et al (2015) Nitinol stents loaded with a high dose of antitumor 5-fluorouracil or paclitaxel: esophageal tissue responses in a porcine model. Gastrointest Endosc 82:153.e1–160.e1
Google Scholar (http://scholar.google.com/scholar_lookup?title=Nitinol%20stents%20loaded%20with%20a%20high%20dose%20of%20antitumor%205-fluorouracil%20or%20paclitaxel%3A%20esophageal%20tissue%20responses%20in%20a%20porcine%20model&author=Z.%20Wang&journal=Gastrointest%20Endosc&volume=82&pages=153.e1-160.e1&publication_year=2015)

Werner S, Krieg T, Smola H (2007) Keratinocyte–fibroblast interactions in wound healing. J Invest Dermatol 127:998–1008
PubMed (http://www.ncbi.nlm.nih.gov/entrez/query.fcgi?cmd=Retrieve&db=PubMed&dopt=Abstract&list_uids=17435785)
CrossRef (https://doi.org/10.1038/sj.jid.5700786)
PubMedCentral (http://www.ncbi.nlm.nih.gov/pmc/articles/PMC17435785)
Google Scholar (http://scholar.google.com/scholar_lookup?title=Keratinocyte%E2%80%93fibroblast%20interactions%20in%20wound%20healing&author=S.%20Werner&author=T.%20Krieg&author=H.%20Smola&journal=J%20Invest%20Dermatol&volume=127&pages=998-1008&publication_year=2007)

Wiesmann F et al (2003) High-resolution MRI with cardiac and respiratory gating allows for accurate in vivo atherosclerotic plaque visualization in the murine aortic arch. Magn Reson Med 50:69–74
PubMed (http://www.ncbi.nlm.nih.gov/entrez/query.fcgi?cmd=Retrieve&db=PubMed&dopt=Abstract&list_uids=12815680)
CrossRef (https://doi.org/10.1002/mrm.10500)
PubMedCentral (http://www.ncbi.nlm.nih.gov/pmc/articles/PMC12815680)
Google Scholar (http://scholar.google.com/scholar_lookup?title=High-resolution%20MRI%20with%20cardiac%20and%20respiratory%20gating%20allows%20for%20accurate%20in%20vivo%20atherosclerotic%20plaque%20visualization%20in%20the%20murine%20aortic%20arch&author=F.%20Wiesmann&journal=Magn%20Reson%20Med&volume=50&pages=69-74&publication_year=2003)

Woollard KJ, Geissmann F (2010) Monocytes in atherosclerosis: subsets and functions. Nat Rev Cardiol 7:77–86
PubMed (http://www.ncbi.nlm.nih.gov/entrez/query.fcgi?cmd=Retrieve&db=PubMed&dopt=Abstract&list_uids=20065951)
PubMedCentral (http://www.ncbi.nlm.nih.gov/pmc/articles/PMC2813241)
CrossRef (https://doi.org/10.1038/nrcardio.2009.228)
Google Scholar (http://scholar.google.com/scholar_lookup?title=Monocytes%20in%20atherosclerosis%3A%20subsets%20and%20functions&author=KJ.%20Woollard&author=F.%20Geissmann&journal=Nat%20Rev%20Cardiol&volume=7&pages=77-86&publication_year=2010)

Wu Y, Leng Y, Xi J, Li X (2009) Scanning all-fiber-optic endomicroscopy system for 3D nonlinear optical imaging of biological tissues. Opt Express 17:7907–7915
PubMed (http://www.ncbi.nlm.nih.gov/entrez/query.fcgi?cmd=Retrieve&db=PubMed&dopt=Abstract&list_uids=19434122)
PubMedCentral (http://www.ncbi.nlm.nih.gov/pmc/articles/PMC2696815)
CrossRef (https://doi.org/10.1364/OE.17.007907)
Google Scholar (http://scholar.google.com/scholar_lookup?title=Scanning%20all-fiber-optic%20endomicroscopy%20system%20for%203D%20nonlinear%20optical%20imaging%20of%20biological%20tissues&author=Y.%20Wu&author=Y.%20Leng&author=J.%20Xi&author=X.%20Li&journal=Opt%20Express&volume=17&pages=7907-7915&publication_year=2009)

Yang G, Pan F, Parkhurst CN, Grutzendler J, Gan W-B (2010) Thinned-skull cranial window technique for long-term imaging of the cortex in live mice. Nat Protoc 5:201–208
PubMed (http://www.ncbi.nlm.nih.gov/entrez/query.fcgi?cmd=Retrieve&db=PubMed&dopt=Abstract&list_uids=4690457)
PubMedCentral (http://www.ncbi.nlm.nih.gov/pmc/articles/PMC4690457)
CrossRef (https://doi.org/10.1038/nprot.2009.222)
Google Scholar (http://scholar.google.com/scholar_lookup?title=Thinned-skull%20cranial%20window%20technique%20for%20long-term%20imaging%20of%20the%20cortex%20in%20live%20mice&author=G.%20Yang&author=F.%20Pan&author=CN.%20Parkhurst&author=J.%20Grutzendler&author=W-B.%20Gan&journal=Nat%20Protoc&volume=5&pages=201-208&publication_year=2010)

Yang L, Mac Raighne A, McCabe EM, Dunbar LA, Scharf T (2005) Confocal microscopy using variable-focal-length microlenses and an optical fiber bundle. Appl Opt 44:5928–5936
PubMed (http://www.ncbi.nlm.nih.gov/entrez/query.fcgi?cmd=Retrieve&db=PubMed&dopt=Abstract&list_uids=16231800)
CrossRef (https://doi.org/10.1364/AO.44.005928)
PubMedCentral (http://www.ncbi.nlm.nih.gov/pmc/articles/PMC16231800)
Google Scholar (http://scholar.google.com/scholar_lookup?title=Confocal%20microscopy%20using%20variable-focal-length%20microlenses%20and%20an%20optical%20fiber%20bundle&author=L.%20Yang&author=A.%20Mac%20Raighne&author=EM.%20McCabe&author=LA.%20Dunbar&author=T.%20Scharf&journal=Appl%20Opt&volume=44&pages=5928-5936&publication_year=2005)

You Y, Richer EJ, Huang T, Brody SL (2002) Growth and differentiation of mouse tracheal epithelial cells: selection of a proliferative population. Am J Physiol-Lung Cell Mol Physiol 283:L1315–L1321
PubMed (http://www.ncbi.nlm.nih.gov/entrez/query.fcgi?cmd=Retrieve&db=PubMed&dopt=Abstract&list_uids=12388377)
CrossRef (https://doi.org/10.1152/ajplung.00169.2002)
PubMedCentral (http://www.ncbi.nlm.nih.gov/pmc/articles/PMC12388377)
Google Scholar (http://scholar.google.com/scholar_lookup?title=Growth%20and%20differentiation%20of%20mouse%20tracheal%20epithelial%20cells%3A%20selection%20of%20a%20proliferative%20population&author=Y.%20You&author=EJ.%20Richer&author=T.%20Huang&author=SL.%20Brody&journal=Am%20J%20Physiol-Lung%20Cell%20Mol%20Physiol&volume=283&pages=L1315-L1321&publication_year=2002)

Zhu Y-Q et al (2017) Technical feasibility and tissue reaction after silicone-covered biodegradable magnesium stent insertion in the oesophagus: a primary study in vitro and in vivo. Eur Radiol 27:2546–2553
PubMed (http://www.ncbi.nlm.nih.gov/entrez/query.fcgi?cmd=Retrieve&db=PubMed&dopt=Abstract&list_uids=27704201)
CrossRef (https://doi.org/10.1007/s00330-016-4602-1)
PubMedCentral (http://www.ncbi.nlm.nih.gov/pmc/articles/PMC27704201)
Google Scholar (http://scholar.google.com/scholar_lookup?title=Technical%20feasibility%20and%20tissue%20reaction%20after%20silicone-covered%20biodegradable%20magnesium%20stent%20insertion%20in%20the%20oesophagus%3A%20a%20primary%20study%20in%20vitro%20and%20in%20vivo&author=Y-Q.%20Zhu&journal=Eur%20Radiol&volume=27&pages=2546-2553&publication_year=2017)

Zitová B, Flusser J (2003) Image registration methods: a survey. Image Vis Comput 21:977–1000
CrossRef (https://doi.org/10.1016/S0262-8856(03)00137-9)
Google Scholar (http://scholar.google.com/scholar_lookup?title=Image%20registration%20methods%3A%20a%20survey&author=B.%20Zitov%C3%A1&author=J.%20Flusser&journal=Image%20Vis%20Comput&volume=21&pages=977-1000&publication_year=2003)

Copyright information

© Springer Nature Singapore Pte Ltd. 2021

About this chapter

Cite this chapter as:

Paulson B., Kim J.K. (2021) Micro-endoscopy for Live Small Animal Fluorescent Imaging. In: Kim J.K., Kim J.K., Pack CG. (eds) Advanced Imaging and Bio Techniques for Convergence Science. Advances in Experimental Medicine and Biology, vol 1310. Springer, Singapore. https://doi.org/10.1007/978-981-33-6064-8_8

- First Online 09 April 2021
- DOI https://doi.org/10.1007/978-981-33-6064-8_8
- Publisher Name Springer, Singapore
- Print ISBN 978-981-33-6063-1
- Online ISBN 978-981-33-6064-8
- eBook Packages Biomedical and Life Sciences Biomedical and Life Sciences (R0)

- Buy this book on publisher's site
- Reprints and Permissions

Personalised recommendations

SPRINGER NATURE

© 2020 Springer Nature Switzerland AG. Part of Springer Nature.